The PHILOSOPHICAL MAGAZINE

FIRST PUBLISHED IN 1798

L. 43 SEVENTH SERIES No. 345 October, 1952

A Journal of Theoretical Experimental and Applied Physics

PRICE 15s. 0d.
Annual Subscription £8 0s. 0d. payable in advance

D AND PUBLISHED BY TAYLOR & FRANCIS LTD., RED LION COURT, FLEET ST., LONDON, E.C.4.

ADVANCES IN PHYSICS

A QUARTERLY SUPPLEMENT OF THE PHILOSOPHICAL MAGAZINE

On 1st January, 1952, the first number of this new Quarterly Supplement to the Philosophical Magazine was published. The aim of this Supplement will be to give those interested in physics comprehensive and authoritative accounts of recent important developments. It is felt by the Editor that in view of the rapid advances in many branches of physics, scientists will welcome a journal devoted to articles of this type.

VOLUME 1 OCTOBER 1952 NUMBER 4

PRICE *per part* 15/- *plus postage* **PRICE** *per annum* £2 15s. 0d. *post free*

Printed and Published by
TAYLOR & FRANCIS, LTD., RED LION COURT, FLEET ST., LONDON, E.C.4

CI. *The Effect of a Finite Nucleus on Beta-Decay*

By I. Malcolm
Department of Natural Philosophy, Aberdeen University*

[Received June 6, revised July 18, 1952]

Abstract

Relativistic wave functions are derived for the electron in a potential field which is constant within the nucleus and Coulombian outside. The relative values of the cut-off wave-functions and the pure Coulomb wave-functions are calculated both for the discrete and continuous spectrum. The changes thereby produced in the probability of orbital electron-capture, in the continuous Beta-spectrum and in the ratio of probabilities of K-capture to positron emission are examined. It is concluded that for the heavier nuclei the probability of K-capture and the ratio of the probabilities of K-capture to positron emission are appreciably affected. The modifications produced in the continuous spectrum are greatest for spin change equal to n where $n(n>1)$ is the degree of forbiddenness of the transition. In this case the coefficients of the squares and products of matrix elements given in the correction factors of Konopinski and Uhlenbeck are appreciably changed. Therefore for given values of the matrix elements the spectrum is modified.

§ 1. Introduction

In a previous paper by Malcolm and Strachan (1951), an investigation was made into changes produced by a cut-off field in the relativistic wave functions of the bound electron. Results were computed only for the case of the K-electron. The calculations have since been extended by the present author and, in table 1, for the K, L_{I} and L_{II} electrons, and for different values of the atomic number Z, are given the values of the ratios $|f/f^c|^2$, $|g/g^c|^2$ and $\chi=\{(|f|^2+|g|^2)/(|f^c|^2+|g^c|^2)\}$ evaluated at the nuclear radius where f, g, f^c, g^c are the radial wave functions for the cut-off field and the pure Coulomb field respectively.

From examination of table 1 we find, as we would expect, that $|g_{L_{\mathrm{I}}}|^2$ is affected slightly less than $|g_K|^2$. However, it is interesting to note that, although $|f_K|^2$ and $|f_{L_{\mathrm{I}}}|^2$ are very much affected by the cut-off field, $|f_{L_{\mathrm{II}}}|^2$, contrary to expectations, is not, its decrease being just slightly less than that of $|g_{L_{\mathrm{I}}}|^2$. We can therefore conclude that the cut-off field has most effect on K-capture and that its influence on orbital decay becomes progressively less for succeeding orbits. For L-capture no comparison with experimental results is made here. However, it is to be

* Communicated by C. Strachan.

noted that, for the heavier nuclei, the effect of the cut-off field on the probability of L-capture will be greater than the order of magnitude of the change we would expect from screening (Slater 1930). The value of the ratio of L to K-capture for any nucleus will be changed only slightly by use of the cut-off functions for, as one can see from table 1, their probabilities have approximately the same decrease.

The components of the Dirac wave function which are affected most do not occur in the calculation of orbital electron capture. Those components are the third and fourth when κ is negative and the first and

Table 1

$Z, \mathscr{A}$	40, 89	48, 107	50, 113	60, 146	70, 170	80, 204
$\lvert f_K/f_K^c\rvert_R^2$		0·400		0·383	0·376	0·326
$\lvert f_{L_I}/f_{L_I}^c\rvert_R^2$	0·418		0·405	0·387	0·364	0·333
$\lvert f_{L_{II}}/f_{L_{II}}^c\rvert_R^2$	0·980		0·968	0·952	0·931	0·902
$\lvert g_K/g_K^c\rvert_R^2$		0·952		0·930	0·904	0·863
$\lvert g_{L_I}/g_{L_I}^c\rvert_R^2$	0·976		0·963	0·944	0·920	0·887
$\lvert g_{L_{II}}/g_{L_{II}}^c\rvert_R^2$	0·451		0·433	0·414	0·390	0·358
χ_K		0·935		0·903	0·868	0·812
χ_{L_I}	0·964		0·943	0·916	0·875	0·834
$\chi_{L_{II}}$	0·966		0·947	0·922	0·884	0·846

second when κ is positive ; $\kappa=-(l+1)$ or l according as the total angular momentum quantum number j is equal to $l+\frac{1}{2}$, $l-\frac{1}{2}$ respectively. However, for the continuum all components of the electron wave-function may play an important part in the determination of the energy distribution of forbidden transitions. We therefore determine the cut-off wave functions of the electron for the continuous spectrum.

§ 2. Wave-Functions

Energy, momentum and length are measured in units mc^2, mc, $\hbar/mc$ respectively. The equations to be solved are

$$\frac{df}{dr}+(1-\kappa)f/r+(W-1-V)g=0, \quad . \quad . \quad . \quad . \quad . \quad (1)$$

$$\frac{dg}{dr}+(1+\kappa)g/r-(W+1-V)f=0, \quad . \quad . \quad . \quad . \quad (2)$$

where

$$V=\begin{cases} -Z\alpha/R \ (0\leqslant r<R : \text{ Region I}), \\ -Z\alpha/r \ (R\leqslant r : \text{ Region II}), \end{cases} \quad . \quad . \quad . \quad (3)$$

$$\alpha=e^2/\hbar c.$$

Here the signs are in accordance with Rose's (1937) definition of the spherical harmonics which give the angular dependence of the wave

functions. In Region I the solutions which behave suitably at $r=0$ are formally the same as those obtained for the discrete spectrum, viz.,

$$\left.\begin{aligned} f&=A_1 f_{\mathrm{I}}=A_1 r^{-\frac{1}{2}} J_{|\kappa-\frac{1}{2}|}(p'r), \\ g&=A_1 g_{\mathrm{I}}=\mp \frac{p' A_1}{W'-1} r^{-\frac{1}{2}} J_{|\kappa+\frac{1}{2}|}(p'r), \end{aligned}\right\} \quad . \quad . \quad . \quad . \quad (4)$$

where $$p'=\sqrt{(W'^2-1)} \text{ and } W'=W+\frac{Z\alpha}{R}. \quad . \quad . \quad . \quad . \quad (5)$$

The general solutions in Region II can be written as

$$\left.\begin{aligned} f&=A(f_{\mathrm{II}}+kF_{\mathrm{II}}), \\ g&=A\,(g_{\mathrm{II}}+kG_{\mathrm{II}}), \end{aligned}\right\} \quad . \quad . \quad . \quad . \quad . \quad . \quad . \quad (6)$$

where f_{II}, g_{II}, F_{II}, G_{II}, are defined as follows :

$$\left.\begin{matrix} f_{\mathrm{II}} \\ g_{\mathrm{II}} \end{matrix}\right\} =(1\mp W)^{1/2}(2ipr)^{\gamma-1} \{[\exp(-ipr+i\eta)](\gamma-\delta)F(1+\gamma-\delta,\ 1+2\gamma,\ 2ipr)\mp\text{c.c.}\}, \quad . \quad (7)$$

$$\left.\begin{matrix} F_{\mathrm{II}} \\ G_{\mathrm{II}} \end{matrix}\right\} =(1\mp W)^{1/2}(2ipr)^{-\gamma-1}(\gamma-\delta) \{[\exp(-ipr+i\eta)]F(1-\gamma-\delta,\ 1-2\gamma,\ 2ipr)\pm\text{c.c.}\} \quad . \quad . \quad . \quad . \quad (8)$$

where c.c. stands for the complex conjugate and F is used for the hypergeometric function ${}_1F_1$ in the notation of Pochammer and Barnes (Watson 1944). Also

$$p=\sqrt{(W^2-1)},\ \delta=\frac{iZ\alpha W}{p},\ \delta'=\frac{iZ\alpha}{p},\ \gamma=\sqrt{(\kappa^2-Z^2\alpha^2)} \quad . \quad . \quad (9)$$

and $$\exp(2i\eta)=(-\kappa+\delta')/(\gamma-\delta).$$

We note that, apart from the normalization constant, f_{II} and g_{II} are the solutions as given by Rose of the Dirac wave-equation for a pure Coulomb field. When normalized our wave functions in Region II may be written

$$\left.\begin{aligned} f&=(N_C S)(f_{\mathrm{II}}+kF_{\mathrm{II}}), \\ g&=(N_C S)(g_{\mathrm{II}}+kG_{\mathrm{II}}), \end{aligned}\right\} \quad . \quad . \quad . \quad . \quad . \quad . \quad (10)$$

where $(N_C S)$ is the normalization for the cut-off potential and N_C is the usual Coulomb normalization factor. Since $(N_C f_{\mathrm{II}})$, $(N_C g_{\mathrm{II}})$ are the normalized pure Coulomb wave-functions, say f^c, g^c respectively, we obtain

$$\left.\begin{aligned} f&=(f^c)S\left(1+k\frac{F_{\mathrm{II}}}{f_{\mathrm{II}}}\right), \\ g&=(g^c)S\left(1+k\frac{G_{\mathrm{II}}}{g_{\mathrm{II}}}\right). \end{aligned}\right\} \quad . \quad . \quad . \quad . \quad . \quad . \quad . \quad (11)$$

The boundary condition at $r=R$, the nuclear radius, gives

$$k=-\left(\frac{g_{\mathrm{I}}f_{\mathrm{II}}-f_{\mathrm{I}}g_{\mathrm{II}}}{g_{\mathrm{I}}F_{\mathrm{II}}-f\,G_{\mathrm{II}}}\right)_R. \quad . \quad . \quad . \quad . \quad . \quad . \quad (12)$$

Using this substitution for k in (11) gives for the value of our wave-function at the nuclear radius

$$\left.\begin{aligned}(f)_R&=(f^c)_R S\left(1-\frac{1-Q}{1-T}\right),\\(g)_R&=(g^c)_R S\left(1-\frac{1-Q^{-1}}{1-T^{-1}}\right),\end{aligned}\right\} \quad . \quad . \quad . \quad . \quad . \quad (13)$$

where $$Q=(f_{\mathrm{I}}\, g_{\mathrm{II}}/g_{\mathrm{I}}\, f_{\mathrm{II}})_R,\ T=(f_{\mathrm{I}}\, G_{\mathrm{II}}/g_{\mathrm{I}}\, F_{\mathrm{II}})_R. \quad . \quad . \quad . \quad . \quad (14)$$

Hereafter the suffices $\pm$ affixed to Q and T will mean the values of these quantities for κ positive and κ negative, respectively. Analytical expressions for $Q_\pm$ and $T_\pm$ are given in Appendix I.

§ 3. Normalization

For normalization of the continuous wave-function we arrange that

$$\int_0^\infty r^2\, dr(g^*_{\kappa,W'}\, g_{\kappa,W}+f_{\kappa,W}\, f^*_{\kappa,W'})=N'\,\delta(W'-W), \quad . \quad . \quad . \quad (15)$$

where $\delta(x)$ is the Dirac delta function. Along with eqns. (1) and (2) this requires

$$N'=\int_{W-\Delta W}^{W+\Delta W} dW' \lim_{r\to\infty}\frac{r^2}{W'-W}(g^*_{\kappa,W'}f_{\kappa,W}-f^*_{\kappa,W'}\, g_{\kappa,W}) \quad . \quad . \quad (16)$$

where A of equation (7) satisfies $A=1/\sqrt{N'}$.
Evaluation of the integral (16) gives

$$(N')_{\text{cut-off}}=(1+kD)(1+k^*D^*)(N')_{\text{Coulomb}} \quad . \quad . \quad . \quad . \quad (17)$$

where $$D=\frac{\Gamma(1+\gamma-\delta)}{\Gamma(1+2\gamma)}\frac{\Gamma(1-2\gamma)}{\Gamma(1-\gamma-\delta)}. \quad . \quad . \quad . \quad . \quad . \quad (18)$$

Therefore, for the cut-off field, A is given by

$$A=N_C S=N_C[(1+kD)(1+k^*D^*)]^{-1/2} \quad . \quad . \quad . \quad . \quad (19)$$

where N_C is the pure Coulomb normalization factor. Expanding by the binomial theorem and dropping the term $|kD|^2/2$ which will be very small we have

$$S=[1-\mathscr{R}\{kD\}] \quad . \quad . \quad . \quad . \quad . \quad . \quad . \quad . \quad (20)$$

where $\mathscr{R}\{kD\}$ stands for the real part of the argument.

The above method gives the normalization factor for solutions normalized per unit energy interval. To obtain solutions normalized to one particle in a sphere of unit radius one must multiply the above solutions by $(\pi p/W)^{1/2}$. We shall assume that this has been done and that the extra factor has been absorbed into the pure Coulomb normalization factor N_C. Formulae for $k_\pm$ and $\mathscr{R}\{k_\pm D\}$ are given in the Appendix. Calculations were carried out for $|\kappa|>1$, but the resulting change in the normalization factor was found to be negligible. Computation of the values of $[1-\mathscr{R}\{kD\}]^2$ (over the appropriate energy ranges for the disintegration) was carried out for $Z=44$, 51, 70 and 84 and $|\kappa|=1$. It was found that even for $|\kappa|=1$ and high Z the change in the normalization factor squared is very small, being at most about 1%.

§4. Results of Computation

Using Rose's suffix notation for f and g, we obtain from eqns. (13) the following relations between the cut-off wave functions and the Coulomb wave-functions evaluated at $r=R$:—

For κ negative,

$$\left.\begin{aligned}(f_l)_R&=C_l^f(f_l^c)_R \text{ where } C_l^f=S_l\left(1-\frac{1-Q_-}{1-T_-}\right),\\ (g_l)_R&=C_l^g(g_l^c)_R \text{ where } C_l^g=S_l\left(1-\frac{1-Q_-^{-1}}{1-T_-^{-1}}\right).\end{aligned}\right\} \quad . \quad . \quad . \quad (21)$$

For κ positive,

$$\left.\begin{aligned}(f_{-l-1})_R&=C^f_{-l-1}(f^c_{-l-1})_R \text{ where } C^f_{-l-1}=S_{-l-1}\left(1-\frac{1-Q_+}{1-T_+}\right),\\ (g_{-l-1})_R&=C^g_{-l-1}(g^c_{-l-1})_R \text{ where } C^g_{-l-1}=S_{-l-1}\left(1-\frac{1-Q_+^{-1}}{1-T_+^{-1}}\right).\end{aligned}\right\} \quad . \quad (22)$$

Also $$S_l=(1-\mathscr{R}\{k_-D\}),\ S_{-l-1}=(1-\mathscr{R}\{k_+D\}) \quad . \quad . \quad . \quad (23)$$

where k_-, k_+ and D are defined by eqns. (A1), (A2) and (18) respectively.

For four values of Z, calculations were made of the values of $(C_l^f)^2$, $(C^f_{-l-1})^2$, $(C_l^g)^2$ and $(C^g_{-l-1})^2$ for $l=0$, 1, 2. The values of Z chosen give a reasonable distribution in Z; other reasons for this choice will be discussed below. In table 2 the results of these calculations are given in full for the case $Z=84$. For the other values of Z we quote in table 3 only the mean values of the above quantities over the energy range considered, since in all cases it was found that the C^f and C^g are almost independent of the energy.

Table 2

W (mc^2)	$(C_0^f)^2$	$(C^g_{-2})^2$	$(C_1^f)^2$	$(C^g_{-3})^2$	$(C_0^g)^2$	$(C^f_{-2})^2$	$(C_1^g)^2$	$(C^f_{-3})^2$
1·25	0·3274	0·3529	0·6170	0·6350	0·8796	0·8969	0·9882	0·9892
1·50	0·3295	0·3534	0·6189	0·6367	0·8776	0·8934	0·9880	0·9890
1·75	0·3301	0·3536	0·6210	0·6385	0·8751	0·8911	0·9878	0·9889
2·00	0·3307	0·3538	0·6228	0·6401	0·8727	0·8883	0·9877	0·9887
2·25	0·3313	0·3542	0·6247	0·6419	0·8704	0·8856	0·9875	0·9886
2·50	0·3319	0·3545	0·6265	0·6437	0·8682	0·8830	0·9874	0·9884
2·75	0·3326	0·3549	0·6283	0·6454	0·8662	0·8805	0·9872	0·9883
3·00	0·3333	0·3553	0·6302	0·6471	0·8642	0·8782	0·9870	0·9881

From examination of tables 2 and 3 we can therefore draw the following conclusions :

(*a*) f_l, the small component when κ is negative, and g_{-l-1}, the large component when κ is positive, are very much affected by the deviation from the Coulomb field. This effect is appreciable even for a nucleus

whose value of Z is as small as 43 (see table 3). The other components are much less affected, but it is interesting to notice that for Z as high as 83 (see table 2) even $|g_0|^2$ has been reduced by about 12%.

Table 3

Decaying nucleus	$(C^f_0)^2$	$(C^g_{-2})^2$	$(C^f_1)^2$	$(C^g_{-3})^2$	$(C^g_0)^2$	$(C^f_{-2})^2$	$(C^g_1)^2$	$(C^f_{-3})^2$
^{99}Tc	0·4200	0·4494	0·6370	0·6620	0·9763	0·9799	0·9969	0·9973
^{125}Sn	0·4314	0·4575	0·6530	0·6718	0·9641	0·9952	0·9681	0·9957
^{170}Tm	0·3761	0·4059	0·6320	0·6512	0·9261	0·9359	0·9916	0·9925

(*b*) As one would expect, the effect of the cut-off field on the components of the wave-functions decreases as the angular momentum increases.

(*c*) The values of the C^f and C^g as defined by eqns. (21) and (22) are almost independent of the energy over the ranges considered.

§ 5. Modification of the Formulae of Konopinski and Uhlenbeck (1941)

We first consider the effect which the above results will have on the L, M, and N, as defined by Konopinski and Uhlenbeck. Their formulae, expressed in terms of the Coulomb functions, become for the cut-off function,

$$\left.\begin{aligned} L'_l &= v(Z, W)(C^g_l)^2 \{(g^c_l)^2 + \alpha_1 (f^c_{-l-1})^2\}_R, \\ M'_l &= v(Z, W)(C^f_l)^2 \{(f^c_l)^2 + \alpha_2 (g^c_{-l-1})^2\}_R, \\ N'_l &= v(Z, W)\, C^f_l C^g_l \{f^c_l g^c_l - \alpha_3 f^c_{-l-1} g^c_{-l-1}\}_R, \end{aligned}\right\} \quad . \quad . \quad . \quad (24)$$

where $$v(Z, W) = \left(\frac{p^2}{2\pi} F(Z, W)\right)^{-1} \frac{1}{4\pi}, \alpha_1 = (C^f_{-l-1}/C^g_l)^2, \alpha_2 = (C^g_{-l-1}/C^f_l)^2,$$

$$\alpha_3 = (C^f_{-l-1} C^g_{-l-1}/C^f_l C^g_l).$$

Examination of tables 2 and 3 shows that α_1, α_2 and α_3 are approximately equal to unity and that they vary only very little with energy. Therefore, since the C^g and C^f have also only a slight energy dependence, the major effect of the cut-off field on the L, M, and N is to multiply them by a factor which is approximately constant over the energy range.

We represent the forbidden correction factors given explicitly by Konopinski and Uhlenbeck in the following manner:

$$C_n = \sum_r A^n_r (A^n_r \text{ shape}) \quad . \quad . \quad . \quad . \quad . \quad . \quad . \quad (25)$$

where the index n denotes the order of forbiddenness and the $\sum_r$ represents a summation over the various squares and products (A_r^n) of the matrix elements which occur. In (25) we have not used an index to denote the

type of interaction, since, whenever we need to particularize in the text, this will be made clear.

For allowed transitions $\Sigma_r A_r^0$ (A_r^0 shape) reduces to one term, say A_1^0 (A_1^0 shape), where (A_1^0 shape)$=L_0$. For first forbidden transitions the (A_r^1 shape) can contain only sums of L_0, L_1, N_0 and M_0. Also for heavy nuclei the M are the largest terms ; for example,

$$M_0 : L_0 : N_0 = \left(\frac{Z\alpha}{2R}\right)^2 : \frac{Z\alpha}{2R} : 1.$$

If we let q denote the neutrino energy, we can write the different types of (A_r^1 shape) that occur as follows :

(*a*) (A_r^1 shape)$=M_0+\frac{2}{3}qN_0+$terms in L_0, L_1,

(*b*) (A_r^1 shape)$=-N_0+\frac{1}{3}qL_0$,

(*c*) (A_r^1 shape)$=L_0$,

(*d*) (A_r^1 shape)$=\frac{1}{12}q^2L_0+\frac{3}{4}L_1=\alpha$ factor.

We can therefore deduce that (A_1^0 shape) and (A_r^1 shape) type (*c*) will not be affected appreciably by our modification since they depend on a

Fig. 1

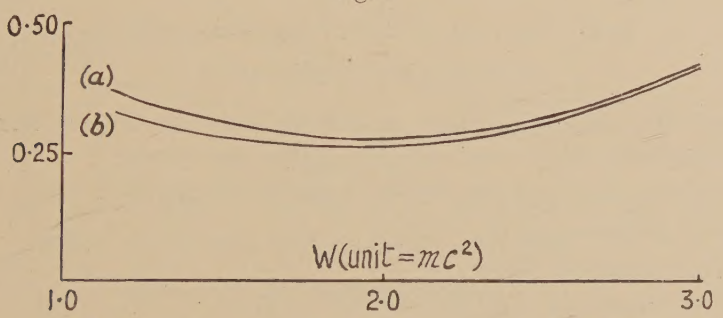

RaE. Curve (*a*) is the α factor curve unmodified ; curve (*b*) is the modified α factor curve.

single term which, when corrected for the influence of the cut-off field, is virtually multiplied by a factor independent of the energy. However, A_r^1 shape type (*d*) contains two terms one of which ($\frac{1}{12}q^2L_0$) is dominant at low energies and the other ($\frac{3}{4}L_1$) dominant at high energies. Therefore, if the reductions in L_0 and L_1 are appreciably different, (A_r^1 shape) for this type of transition will be modified. This is true for $Z=84$ and for $Z=71$ although for the latter the effect will be much smaller. Since $(C_1^q)^2>(C_0^q)^2$ the corrected (A_r^1 shape) will have a relatively greater depression at the low energy end as compared to the high energy region. This is shown in fig. 1 where for $Z=84$ we have drawn the modified and unmodified α factor curves. The above argument applies in a lesser degree to (A_r^1 shape) types (*a*) and (*b*). Here, although the leading terms are largest at all energies, the effect of the second terms may be appreciable at low energies or more especially at high values of q. We would therefore

expect that, for moderate values of the end point energy, the effect of the cut-off field on the actual shapes of the (A_r^1 shape) types (*a*) and (*b*) will be intermediate between that produced on types (*c*) and (*d*); however, the (A_r^1 shape) types (*a*) and (*b*) will be reduced by approximately constant multipliers which deviate more from unity than those for types (*c*) and (*d*).

The modification of the (A_r^1 shape) type (*d*) depends on the changes produced in the L which are the least affected by the cut-off field. Therefore for the maximum effect of the cut-off field we must examine the second forbidden transitions or higher. For second forbidden transitions the (A_r^2 shape) can contain only sums of L_0, L_1, L_2, N_0, N_1,

Fig. 2

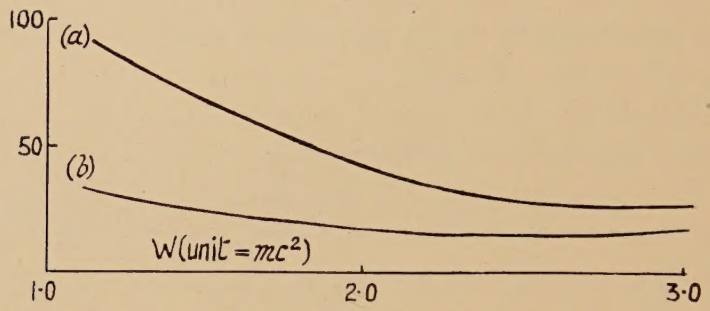

RaE. Curve (*a*) is ($\sum_{ij}|T_{ij}|^2$ shape) unmodified; curve (*b*) is the modified curve.

M_0 and M_1. We write them as follows, only the largest terms being given explicitly when much smaller terms also occur.

(*a*) (A_r^2 shape)$=\frac{1}{72}(\frac{1}{15}q^4L_0+2q^2L_1+15L_2)=D_2$ factor,

(*b*) (A_r^2 shape)$=\frac{1}{12}(q^2M_0+9M_1+\ldots.)$,

(*c*) (A_r^2 shape)$=\alpha$ factor,

(*d*) (A_r^2 shape)$=\frac{1}{4}(-\frac{1}{3}q^2N_0-3N_1+\ldots.)$,

(*e*) (A_r^2 shape)$=(M_0+\frac{2}{3}qN_0+\ldots.)$.

We have already considered the change in types (*c*) and (*e*). Type (*a*) is somewhat similar to the α factor and for Z as low as 44 and 51 the modification produced in it is negligible. The maximum influence of the cut-off field on the (A_r^2 shape) is exhibited by terms of types (*b*) and (*d*), especially type (*b*). These are the coefficients which occur for $n=2$ and spin change of 2 (i.e. unfavourable parity change in the case of Gamow–Teller interactions). In types (*b*) and (*d*) the (A_r^2 shape) are dominated by q^2M_0, $-\frac{1}{3}q^2N_0$ respectively at low energies and by $9M_1$, $-3N_1$ respectively at high energies. Since C_1^f and C_0^f are appreciably different and $C_1^f>C_0^f$ it is evident that these (A_r^2 shape) will be affected in the same manner as the α factor though to a much greater extent, i.e. there will again be a relatively greater depression at the low energy end as compared with the high energy end and the change will be the more obvious the higher the maximum energy W_0. This is illustrated in figs. 2, 3, 4 and 5, where, for $Z=51$ and 84, the (A_r^2 shape)

Fig. 3

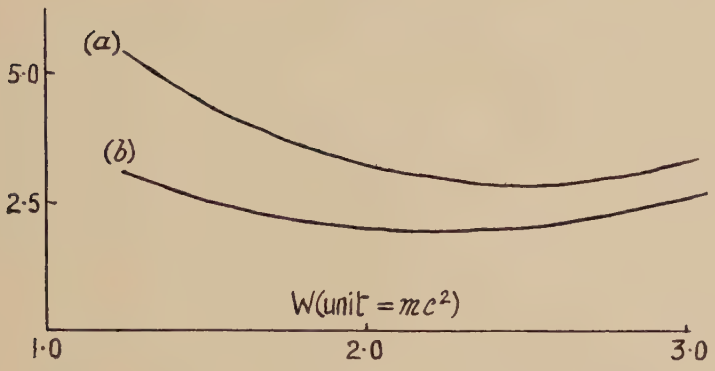

RaE. Curve (*a*) is ($\sum_{ij}(T_{ij}A^*_{ij}+$ c.c.) shape) unmodified ; curve (*b*) is the modified curve.

Fig. 4

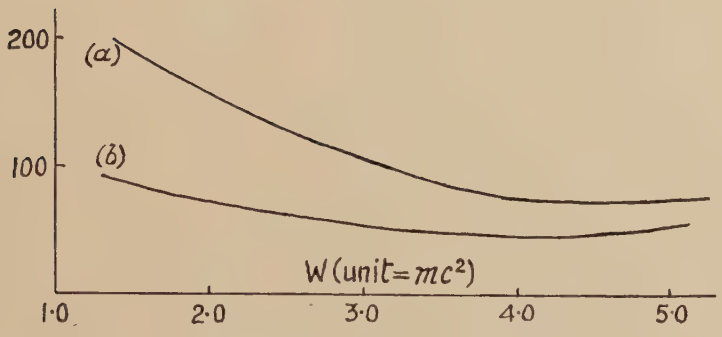

^{125}Sn. Curve (*a*) is ($\sum_{ij}|T_{ij}|^2$ shape) unmodified ; curve (*b*) is the modified curve.

Fig. 5

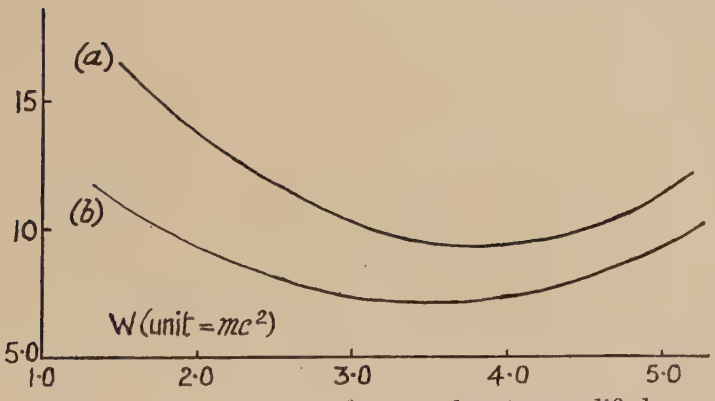

^{125}Sn. Curve (*a*) is ($\sum_{ij}(T_{ij}A^*_{ij}+$c.c.) shape) unmodified ; curve (*b*) is the modified curve.

types (*b*) and (*d*) have been drawn for the modified and unmodified functions. The type of change of shape shown there would seem to hold good for any (A_r^n shape) which is appreciably modified by the cut-off field.

However, we can draw no general conclusion as to the manner of the change in shape of the total correction factors which include the (A_r^2 shape) types (*b*) and (*d*) since the coefficient of the (A_r^2 shape) type (*d*) may be either positive or negative. The resultant change of shape will therefore depend on the size of the matrix elements. However, we can conclude with certainty that, for a fixed set of matrix elements, the second forbidden correction factor with spin change 2 should give very appreciably different curves for the modified and unmodified functions, as well as a change in the *ft* value. This statement is also true for any forbidden transition of degree n ($n>1$) and spin change n. It should be noted that even in the cases where the shapes are not modified the *ft* values will be changed.

While the work described above was being used for comparison with experimental spectra (see § 6), a letter by Rose and Holmes (1951) was published which gave the results of their consideration of the same problem. The conclusions they reach are in the main in agreement with those stated above. However, we can see no reason for the general statement made at the top of p. 91, column 2, that ' a relatively greater depression of the spectrum is to be expected at the low energy end as compared with the high energy region '. For the orders of forbiddenness which Rose and Holmes consider this seems to the author, as stated above, to depend on whether the cross term is negative or positive and on the order of magnitude of the different matrix elements.

Rose and Holmes used approximately a uniform charge distribution within the nucleus (actually they include a term representing charge distortion but find their results insensitive to this) in place of the charged shell at the nuclear radius considered here. This means that within the nuclear radius their potential well is approximately half as deep again as that used here. This difference affects some results considerably. For example, for $Z=83$ (RaE) Rose and Holmes calculate that $(C'_0{}')^2 \doteqdot 0{\cdot}47$ while for the constant potential inside the nucleus we find $(C'_0{}')^2 \doteqdot 0{\cdot}33$; similarly for $(C'_1{}')^2$ Rose and Holmes calculate $(C'_1{}')^2 \doteqdot 0{\cdot}8$ against our value of $(C'_1{}')^2 \doteqdot 0{\cdot}62$. (The approximation signs have been used because a rough mean value over the energy range has been quoted.) However, since the ratio $(C'_0{}')^2/(C'_1{}')^2$ is approximately the same in both cases, little change in the shape of the spectrum for the two cases will result though the *ft* values will be different. Rose and Holmes point out that their modification may only be important for $Z \gtrsim 60$. However, because of the shallower well employed above, lighter nuclei will be affected more in our calculations, and this is one reason those calculations were made for Z with as low a value as 44.

§ 6. Application to Spectra

We have already shown that the cut-off field has an important influence on certain types of Beta-transitions. The difficulty is to illustrate it by application to particular cases. The surest way would be to calculate the matrix elements for a particular transition on the basis of some nuclear model, although this would be very difficult for some of the heavy nuclei with which we are dealing. Another method, which was the one decided upon, is to attempt to fit the modified and unmodified correction factor curves to correction factor curves derived from experimental results. This method seemed to be the better because (*a*) one could compare the two best fits so obtained and (*b*) even although there may be little choice between these best fits (as might easily happen since we are allowing the matrix elements to vary), the values of the matrix elements so derived would illustrate the difference produced by consideration of the finite nucleus. They could also be compared with theoretically derived values of the matrix elements if so desired.

The values of Z used for the calculations of § 4 were chosen because those values of Z belong to the product nuclei of disintegrations with reasonably reliable experimental spectra whose shapes have so far, in our view, not been adequately explained and which might be explicable by applying the modified correction factor for second forbidden transitions with unfavourable parity change under Gamow-Teller rules. It was decided to use the pure tensor form of the interaction in the fitting because evidence indicates that the tensor interaction must be at least part, if not all, of the interaction necessary for the explanation of Beta-decay. The attempt was therefore made to fit our theoretical correction factors for ^{99}Tc, ^{125}Sn, ^{170}Tm and ^{210}RaE to those derived from experiment (see the Appendix); the correction factors were calculated on the assumption that all decays were second forbidden with spin change 2. (Evidence for the order of forbiddenness is given below.)

Using the A_r^2 as unknown constants, the method of least squares was used for fitting $\sum_r A_r^2$ (A_r^2 shape) to the experimental curve. Here a difficulty arose which the author has never seen mentioned elsewhere. It was found in all cases that, on reduction, the matrix of the equations proved to be singular within the accuracy of the calculations; that is, in each case there was virtually a linear relationship between the different (A_r^2 shape). This is rather surprising, since we are using only three or four curves in the fitting. However, it is due to the different (A_r^2 shape) having somewhat similar shapes. This singularity of the matrix means, of course, that fitting the experimental curve will not determine the ratio of the matrix elements uniquely. Whether the shapes of the correction factors for the cut-off and pure Coulomb fields are appreciably different or not, the ratio of the matrix elements derived from the fitting will certainly be much affected. However, comparison of these ratios with each other

and with an independent estimate of the matrix elements (say from a single particle model) now becomes impossible because of their lack of uniqueness.

In the forbidden correction factors certain inequalities hold between some (A_r^n shape); in particular for the second forbidden factor

$$4\{\sum_{ij}|T_{ij}|^2\}\{\sum_{ij}|A_{ij}|^2\}\geqslant\{\sum_{ij}T_{ij}A_{ij}^*+\text{c.c.}\}^2. \quad . \quad . \quad . \quad (26)$$

Some authors quote the values of their matrix elements, derived from curve fitting, with the subsidiary condition

$$4\{\sum_{ij}|T_{ij}|^2\}\{\sum_{ij}|A_{ij}|^2\}=\{\sum_{ij}T_{ij}A_{ij}^*+\text{c.c.}\}^2 \quad . \quad . \quad . \quad . \quad (27)$$

which may or may not be true. This condition would, of course, overcome the lack of uniqueness in the matrix elements. As an example, in the case of RaE, we have also made our fitting subject to (27) rather than (26) and quote the ratios of the squares of the matrix elements so derived. However, one should not forget that, for fixed values of the matrix elements, the actual correction factor curves for the modified and unmodified field will be different.

Technetium ($^{99}_{43}$Tc)

The energy spectrum of ^{99}Tc was measured by Taimuty (1951) using fairly thin sources which varied in thickness from 0·17 mg/cm^2 to 1·3 mg/cm^2. He determined the end point energy to be $0{\cdot}292\pm0{\cdot}003$ Mev and using this value of W_0 and a half-life of $2{\cdot}12\times10^5$ years he obtained an *ft* value of $2{\cdot}3\times10^{12}$ for this decay. Empirically this value would make the transition about second forbidden, which is very satisfactory from the point of view of applying our modifications.

Taimuty attempted to fit his spectra by applying second and first forbidden correction factors which contained only single matrix elements by Gamow-Teller rules. The fits which he obtains are not very satisfactory. On the other hand, examination of fig. 6 shows that a very good fit has been obtained both for the modified and unmodified C_{2T} correction factor with spin change 2. Hereafter the modified factor will be denoted by $(C_{2T})'$. Of the two, $(C_{2T})'$ gives the better fit, the ordinary correction factor falling away slightly at low energies. This slight rising of the $(C_{2T})'$ curve with respect to the C_{2T} curve at low energies occurs also for the other nuclei (except in the case of RaE, where both curves are the same). It is interesting to note that this deviation is in the same direction as that which would be produced by source thickness distortion.

Tin ($^{125}_{50}$Sn)

This nucleus has an *ft* value of $3{\cdot}7\times10^8$ which suggests that it decays by a second forbidden transition. Its energy spectrum has been measured by Hayward (1950). From the shape of his Fermi plot Hayward considers that the transition is complex and attempts to fit the high energy component by the α correction factor. Hayward concludes that the fit is satisfactory, but an examination of his figure 2 shows that, in fact, the corrected points lie on a smooth curve other than a straight line.

For this nucleus also, we have obtained a better fit, with both $(C_{2T})'$ and C_{2T}, than has hitherto been achieved. Here, however, both C_{2T} and $(C_{2T})'$ lay within the experimental limits.

Fig. 6

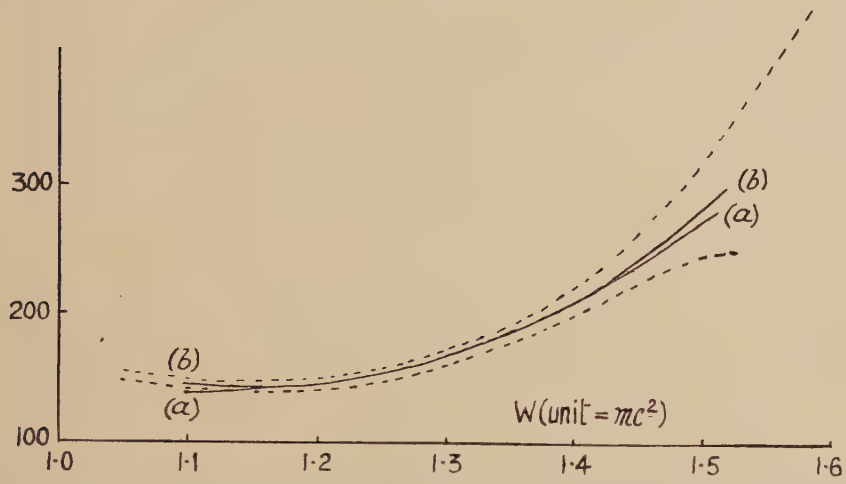

^{99}Tc. Dashed curves are the correction factor curves derived from experiment. Curve (*a*) is the best fit for the unmodified C_{2T} curve ; curve (*b*) is the best fit for the modified C_{2T} curve.

Fig. 7

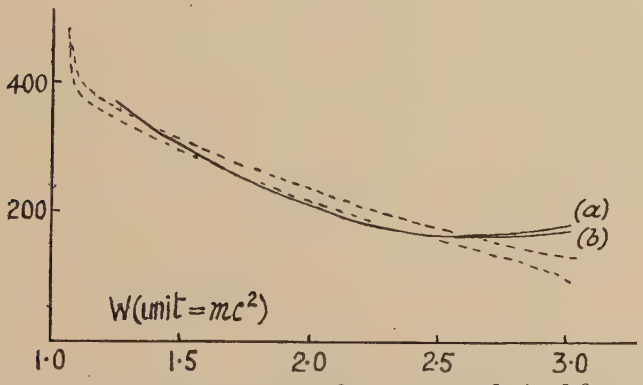

RaE. Dashed curves are the correction factor curves derived from experiment. Curve (*a*) is the best fit for the unmodified C_{2T} curve ; curve (*b*) is the best fit for the modified C_{2T} curve.

Radium E

The first attempt to fit the RaE spectrum was made by Konopinski and Uhlenbeck (1941). By use of the C_{2T} factor for spin change $2 \rightarrow 0$ they obtained quite a good fit with the experimental spectrum as measured by Flammersfeld, but not such a good fit with the spectrum as measured by Neary. Later work, however, by Langer and Price (1949) has confirmed the experimental work of Neary. This, therefore, seemed an interesting case for the application of our modifications. Figure 7

shows the fit obtained with the factors C_{2T} and $(C_{2T})'$ (for spin change $2 \rightarrow 0$) using the results of Langer and Price. Both fits are practically the same and could be classed as quite good, though perhaps not really as satisfactory as we should like. We obtain for the ratios of $\sum_{ij}|A_{ij}|^2/\sum_{ij}|T_{ij}|^2$ the values 2·9 and 19·7 for the cut-off and pure Coulomb fields respectively. Konopinski and Uhlenbeck obtained a value of 33·6 from their fit. Rose applied his nuclear field modifications (see § 5) in an attempt to explain the RaE spectrum. He, also, failed to obtain a satisfactory fit for any of the pure invariant forms of the interaction. However, he states in his letter that S. Moszkowski communicated to him privately more recent evidence which points to a complex spectrum in this case.

§ 7. Ratio of K-Capture to Positron Emission

We find that for $Z=50$, L_0 is reduced by a factor 0·94 (a value which is almost independent of energy release) for negatron emission. We may therefore expect that for positron emission L_0 will be increased by a factor of approximately 1·06. It was pointed out by Malcolm and Strachan (1951) that the experimental value of the ratio of the probabilities of K-capture to positron emission for ^{107}Cd is 320 ± 30, whereas Bouchez, de Groot, Nataf and Tolhoek (1950) calculate it to be 360. Taking into account only the modifications of the discrete spectrum, our wave functions give 343, a value within the experimental limits of accuracy. Modification of the wave-function of the positron can only place this value more securely within the experimental limits and, if we assume that L_0 is increased by a factor 1·06, the value 324 replaces 343. As was pointed out before, the nucleus ^{107}Cd is the only one considered by Bouchez *et al.* which has Z large enough to be affected by our modifications, and it is also interesting to note that it is the only nucleus for which they found the theoretical ratio of the probabilities of K-capture to positron emission greater than the experimental ratio.

§ 8. Further Work in Progress

Very recently, evidence has been accumulating (Horie and Umezawa 1951, Tolhoek and de Groot 1951, Pursey 1951) in favour of using a combination of interactions, and in this connection cut-off wave-functions for the electrons are now being applied by the author, especially to the work of Smith (1952).

Acknowledgments

I owe much to Dr. C. Strachan for suggesting this research problem and for many helpful discussions. I am indebted to Aberdeen University for a grant of money for computational assistance and to the Mathematics Department for the use of their calculating machines. I must also thank Dr. F. H. C. Marriott for his advice on curve fitting.

APPENDIX

Analytical Expressions for $Q_{\pm}$, $T_{\pm}$, $k_{\pm}$ and $k_{\pm}D$.

If we let $$\psi_{\pm}(W)=\left(\frac{f_{\mathrm{I}}}{g_{\mathrm{I}}}\right)_{\pm,R}\left(\frac{W+1}{W-1}\right)^{1/2},$$

we can derive the following formulae for $Q_{\pm}$ and $T_{\pm}$ by expansion of the confluent hypergeometric functions occurring in the wave functions. We obtain

$$Q_{-}=-\psi_{-}(W)\left\{\frac{a\cos\alpha-b\sin\alpha}{a\sin\alpha+b\cos\alpha}\right\},$$

$$Q_{+}=-\psi_{+}(W)\left\{\frac{-a\sin\beta-b\cos\beta}{a\cos\beta-b\sin\beta}\right\},$$

$$T_{-}=\psi_{-}(W)\left\{\frac{-a'\sin\beta+b'\cos\beta}{a'\cos\beta+b'\sin\beta}\right\},$$

$$T_{+}=\psi_{+}(W)\left\{\frac{a'\cos\alpha+b'\sin\alpha}{a'\sin\alpha-b'\cos\alpha}\right\},$$

where

$$a=1-\frac{2Z\alpha RW}{1+2\gamma}-\frac{(1+\gamma)(2+\gamma)-(Z^2\alpha^2W^2/p^2)}{(1+2\gamma)(2+2\gamma)}2(pR)^2,$$

$$b=pR\left\{\frac{2(1+\gamma)}{1+2\gamma}-\frac{2Z\alpha RW(3+2\gamma)}{(1+2\gamma)(2+2\gamma)}\right.$$
$$\left.-\frac{(1+\gamma)(2+\gamma)(3+\gamma)-(Z^2\alpha^2W^2/p^2)}{(1+2\gamma)(2+2\gamma)(3+2\gamma)}\frac{4}{3}(pR)^2\right\},$$

$$a'=1-\frac{2Z\alpha RW}{1-2\gamma}-\frac{(1-\gamma)(2-\gamma)-(Z^2\alpha^2W^2/p^2)}{(1-2\gamma)(2-2\gamma)}2(pR)^2,$$

$$b'=pR\left\{\frac{2(1-\gamma)}{1-2\gamma}-\frac{2Z\alpha RW(3-2\gamma)}{(1-2\gamma)(2-2\gamma)}\right.$$
$$\left.-\frac{(1-\gamma)(2-\gamma)(3-\gamma)-(Z^2\alpha^2W^2/p^2)}{(1-2\gamma)(2-2\gamma)(3-2\gamma)}\frac{4}{3}(pR)^2\right\}.$$

Also $$\alpha=\tfrac{1}{2}(\theta_2+\theta_1-2pR),\quad \beta=\tfrac{1}{2}(\theta_2-\theta_1-2pR),$$

where $$\theta_2=\tan^{-1}\frac{Z\alpha W}{p\gamma},\quad \theta_1=\tan^{-1}\frac{Z\alpha}{p|\kappa|}.$$

Since $\gamma=\sqrt{(\kappa^2-Z^2\alpha^2)}$, $\sin\beta$ is usually small. We have therefore included a further term in the expansions of b and b' for use when a and a' are multiplied by $\sin\beta$ (i.e. in the numerators of Q_{+} and T_{-}, respectively).

From eqns. (12) and (14) $k_{\pm}$ may be written in either of the equivalent forms

$$k_{\pm}=-\left(\frac{1-Q_{\pm}}{1-T_{\pm}}\right)\left(\frac{f_{\mathrm{II}}}{F^s_{\mathrm{II}}}\right)_{\pm,R}\left(\frac{(2ipR)^{2\gamma}}{\gamma-\delta}\right), \quad \ldots \quad \text{(A1)}$$

$$k_{\pm}=-\left(\frac{1-Q_{\pm}^{-1}}{1-T_{\pm}^{-1}}\right)\left(\frac{g_{\mathrm{II}}}{G^s_{\mathrm{II}}}\right)_{\pm,R}\left(\frac{(2ipR)^{2\gamma}}{\gamma-\delta}\right), \quad \ldots \quad \text{(A2)}$$

where
$$\left.\begin{aligned}(F_{\text{II}})_R&=(F^s_{\text{II}})_R(\gamma-\delta)(2ipR)^{-2\gamma},\\ (G_{\text{II}})_R&=(G^s_{\text{II}})_R(\gamma-\delta)(2ipR)^{-2\gamma}.\end{aligned}\right\}$$

To the same order of approximation as was used for $Q_\pm$ we obtain for $(g_{\text{II}}/G^s_{\text{II}})_{\pm,R}$, $(f_{\text{II}}/F^s_{\text{II}})_{\pm,R}$ respectively, the following formulae :—

$$\left(\frac{g_{\text{II}}}{G^s_{\text{II}}}\right)_+ =ir_2\left\{\frac{a\sin\beta+b\cos\beta}{a'\cos\alpha+b'\sin\alpha}\right\},$$

$$\left(\frac{g_{\text{II}}}{G^s_{\text{II}}}\right)_- =ir_2\left\{\frac{a\cos\alpha-b\sin\alpha}{a'\sin\beta-b'\cos\beta}\right\},$$

$$\left(\frac{f_{\text{II}}}{F^s_{\text{II}}}\right)_+ =ir_2\left\{\frac{a\cos\beta-b\sin\beta}{a'\sin\alpha-b'\cos\alpha}\right\},$$

$$\left(\frac{f_{\text{II}}}{F^s_{\text{II}}}\right)_- =ir_2\left\{\frac{a\sin\alpha+b\cos\alpha}{a'\cos\beta+b'\sin\beta}\right\},$$

where $r_2{}^2=\gamma^2+\dfrac{Z^2\alpha^2W^2}{p^2}$.

Except for $\Gamma(\gamma-\delta)/\Gamma(1-\gamma-\delta)$ we have all the explicit formulae required for the complete evaluation of the $\mathscr{R}\{k_\pm D\}$ and therefore of the normalization factor S.

For $|\kappa|=1$

$$\frac{\Gamma(\gamma-\delta)}{\Gamma(1-\gamma-\delta)}=\frac{\Gamma(\overline{\gamma-1}-\overline{\delta-1})}{\Gamma(\overline{1-\gamma}-\overline{\delta-1})}(1-\gamma-\delta)$$

$$\doteq(1-\gamma-\delta)\frac{\Gamma(-\delta+1)}{\Gamma(-\delta+1)}\left\{\frac{1+\overline{\gamma-1}\psi(-\delta)}{(1+\overline{1-\gamma}\psi(-\delta)}\right\},$$

by application of Taylor's expansion to the Γ functions. $\psi(-\delta)$ is the logarithmic derivative of the Γ function and may be expressed as

$$\psi(z)=-C+\sum_{n=1}^{\infty}\frac{z}{n(n+z)},$$

where $C=0{\cdot}57722$ (Jahnke and Emde 1945). Therefore

$$\frac{\Gamma(\gamma-\delta)}{\Gamma(1-\gamma-\delta)}\doteq(1-\gamma-\delta)\{1-2(1-\gamma)\psi(-\delta)\}.$$

For $|\kappa|>1$ one obtains slightly more complicated expressions because the Γ functions have to be reduced till they are amenable to expansion by Taylor's Theorem (i.e. until the Γ functions can be expanded in powers of $|\kappa|-\gamma$). Calculations were carried out for $|\kappa|>1$ but the resultant change in the Coulomb normalization factor was found to be negligible.

References

Bouchez, R., de Groot, S. R., Nataf, R., and Tolhoek, H. A., 1950, *J. Phys. Radium*, **11,** 105.
Hayward, R. W., 1950, *Phys. Rev.* [2], **79,** 409.
Horie, H., and Umezawa, M., 1951, *Phys. Rev.* [2], **83,** 1253.
Konopinski, E. J., and Uhlenbeck, G. E., 1941, *Phys. Rev.* [2], **60,** 308.
Langer, L. M., and Price, H. C., 1949, *Phys. Rev.* [2], **76,** 641.
Malcolm, I., and Strachan, C., 1951, *Proc. Camb. Phil. Soc.*, **47,** 610.
Pursey, D. L., 1951, *Phil. Mag.* [7], **42,** 1193.
Rose, M. E., 1937, *Phys. Rev.* [2], **51,** 484.
Rose, M. E., and Holmes, D. K., 1951, *Phys. Rev.* [2], **83,** 190.
Slater, J. C., 1930, *Phys. Rev.* [2], **36,** 57.
Smith, A. M., 1952, *Thesis*, Aberdeen.
Taimuty, S. I., 1951, *Phys. Rev.* [2], **81,** 461.
Tolhoek, H. A., and de Groot, S. R., 1951, *Phys. Rev.* [2], **84,** 150.
Watson, G. N., 1944, *Theory of Bessel Functions* (Cambridge : University Press).

CII. *The Decomposition of Thin Oriented Silver Halide Layers*

By D. W. Pashley
Imperial College, London*

[Received August 1, 1952]

Abstract

Thin layers of oriented silver halides (AgCl, AgBr and AgI) have been prepared in various ways, and their stability to electron (30–60 kv) bombardment has been investigated. Unstable specimens are found to decompose to give highly oriented silver, in the case of silver chloride and silver bromide, but to give mainly randomly oriented silver in the case of silver iodide. Silver chloride also gives rise to highly oriented silver during ultra-violet irradiation.

Chemical development of the halides produced randomly oriented silver, except when the halide was supported on a metallic silver crystal substrate. In this latter case the developed silver formed in an oriented fashion on the silver substrate.

Diffuse streak patterns were observed from the silver halides and their origin is discussed.

§1. Introduction

The first definite evidence that the metallic silver lattice, formed during the decomposition of silver halide, can be oriented in a definite way relative to the halide lattice was obtained by Kooy and Burgers (1948). They studied, by means of x-rays, the silver formed during the photolysis of silver chloride, and obtained arc ring patterns indicating some preferred orientation of silver; this orientation was not identified. More recently, Berry (1949) and Berry and Griffith (1950) have studied in greater detail the effect of ultra-violet radiation on single crystals of silver bromide. They concluded that silver grows in a parallel orientation (two parallel cubic lattices) well inside the silver bromide, but that it has other orientations at the surface. Simultaneously with this work, the decomposition of oriented silver halide layers during electron bombardment has been independently studied. Preliminary accounts of some of the results have already been given (Pashley 1950, 1951). The latter paper described how certain silver chloride specimens decompose to give metallic silver in an orientation parallel to that of the silver chloride; prominent twinning of the silver on its (111) planes was also observed.

The work has since been extended, and this paper describes a study of the decomposition of the three halides (silver chloride, silver bromide and

* Communicated by Sir George Thomson, F.R.S.

silver iodide). Thin halide layers have been prepared in various ways, and their behaviour to electron bombardment examined by electron diffraction. It is found that some specimens decompose, and that others are quite stable. Some of the stable films have been decomposed by chemical means. A few specimens have also been reduced by ultra-violet irradiation.

§2. Experimental Procedure and Apparatus

The silver halide layers were mostly prepared in one of the two following ways: (1) by evaporating the silver halide (in vacuo) on to various substrates, as described elsewhere (Pashley 1951, 1952 b); (2) by growing the halide by direct halogen attack of single crystals of silver (Pashley 1952 a). The substrates used for the evaporated layers included mica, rocksalt, potassium bromide, magnesium oxide and metallic silver, all in single crystal form.

The specimens were always examined in the electron diffraction camera by the reflection technique; by studying the diffraction patterns after various periods of electron bombardment (by the beam used to form the diffraction pattern), it could be ascertained whether the specimens were stable or unstable to the electrons. The unstable specimens were examined in detail, patterns being obtained and recorded at various stages of the bombardment, varying from about one minute to three hours.

Some of the specimens were immersed in a dilute solution of a photographic developer (metol-hydroquinone), and the growth of silver studied. No intermediate stages of growth could be recorded by this method, because the decomposition occurred too rapidly.

The electron diffraction camera used was of a conventional type, employing a hot filament electron gun and magnetic focusing. The electron accelerating potentials were in the range 30–60 kv, and the camera length was 35 cm.

§3. Decomposition of Chemically Grown Layers on Silver Crystals

Silver chloride, silver bromide and silver iodide films formed by direct halogen attack of single crystals of silver were completely stable to electron bombardment. These layers were usually highly oriented on the silver crystals (Pashley 1952 a), and have been decomposed by immersion in a chemical developer. It was found that the silver so produced was mostly oriented parallel to the substrate silver crystal, and was twinned on its (111) planes. There was also some randomly oriented silver. This type of silver formation was observed with layers of all three halides. The general features of the silver formation were independent of which lattice plane of the substrate silver was parallel to the surface (experiments were performed with (111), (100), (110) and (311) silver surfaces), and of the orientation of the halide layer. The extent of the twinning did vary from specimen to specimen. When the silver crystal had a surface containing many atomically flat patches, very prominent twinning occurred on (111)

planes parallel to the surface, but only relatively small amounts of silver were twinned on the other (111) type planes. In other cases, twinning was equally prominent on all four type (111) planes. It appears that the twinning occurred very readily on (111) planes which were parallel to facets bounding the substrate surface, but much less readily on other (111) type planes. Presumably the twinning does not occur until the particular (111) facets are developed.

These effects show that the formation of silver occurs by deposition on to the substrate silver, either at the silver–silver halide interface, or via ionic conduction through the solution. This conclusion is supported by the fact that electrolytic deposition of silver on to the silver crystals gives rise to similar twinning effects.

§ 4. Decomposition of Evaporated Layers of Silver Bromide and Silver Chloride

In order to eliminate the effect of the substrate silver, films of silver halides (thickness varying from 10 Å to 1 000 Å) were prepared by evaporation on to cleavage surfaces of mica, rocksalt, potassium bromide and magnesium oxide. These layers were highly oriented (Pashley 1952 b), and were found to reduce to silver slowly during electron bombardment in the diffraction camera. Their decomposition could therefore be studied very conveniently without the need for any chemical developer.

(a) *Orientations during Electron Bombardment*

The electron beam was allowed to impinge on a certain spot of the specimen, and the growth of silver on this patch of the surface was studied as a function of time. The rate of decomposition varied markedly from specimen to specimen, and although thicker films decomposed more slowly than thinner films, the correlation between rate of decomposition and thickness was not as marked as was indicated by the first few experiments (Pashley 1950).

The decomposition of silver chloride and of silver bromide occurred in very similar ways. A series of diffraction photographs showing the growth of silver during electron bombardment of silver chloride layers on mica has already been published (Pashley 1951). The main effects illustrated were that the silver chloride gradually decomposes to give a parallel orientation (two cubic lattices parallel) of silver, with prominent (111) twinning of the silver. Figure 1 (figs. 1–3, 6–8, Plate LXVIII) shows the pattern from a silver bromide layer on potassium bromide, after fifteen minutes bombardment. The smaller square pattern of very elongated spots is due to the silver bromide crystallites, which have fairly smooth tops. The larger square pattern of spots, which appears only after a few minutes bombardment, is due to the growth of a parallel orientation of silver. As the growth is continued, these latter spots split up into groups of four subsidiary spots, and the silver bromide pattern is reduced in intensity.

After ninety minutes bombardment, the silver bromide on the patch of specimen under bombardment had been almost completely decomposed, and the pattern of fig. 2 was obtained. The strongest pattern arises from the parallel orientation of silver, and forms a square pattern of spots. These spots are split into groups of four subsidiary spots; this splitting is explained in terms of the intersection of the Ewald sphere with the diffuse rods of intensity along all of the (111) type directions in the reciprocal lattice, and passing through all of the reciprocal lattice points. The pattern of subsidiary spots is identical with that obtained by Kirchner and Lassen (1935) from a layer of silver condensed on to rocksalt. These diffuse reciprocal lattice rods are due either to the presence of prominent (111) boundary planes, or to effects arising from repeated twinning on

Fig. 4

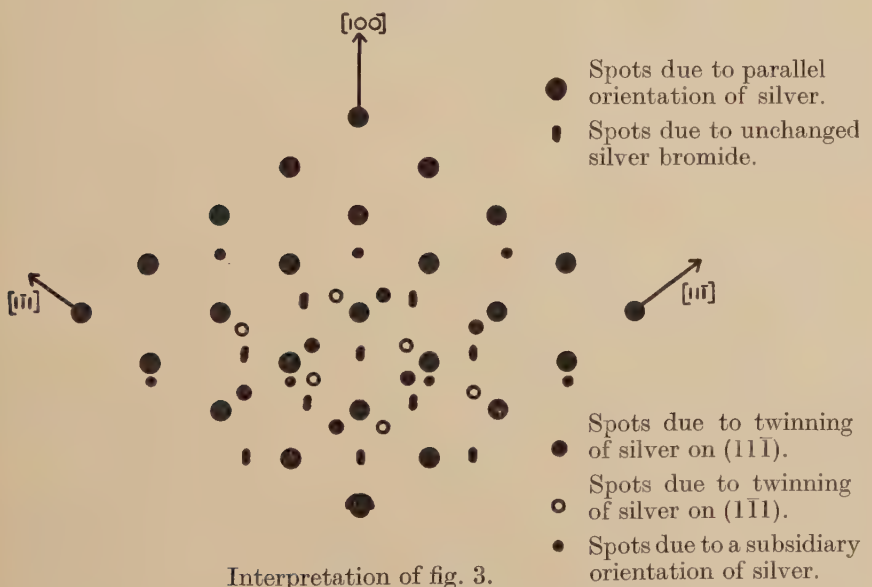

Interpretation of fig. 3.

(111) planes. Since the twinning probably only occurs after (111) facets are developed on the growing silver, it is likely that both effects (facets and twinning) are involved in the appearance of the subsidiary spots. The rings on fig. 2 are due to randomly oriented silver, which formed to a greater extent in silver bromide than in silver chloride.

The occurrence of twinning was conclusively revealed when other azimuthal settings of the substrates were used. Figure 3 shows the pattern obtained from a silver bromide layer on rocksalt, after thirty minutes of electron bombardment. The interpretation of the pattern is given in fig. 4, there being five component patterns. The (111) twinning was a general characteristic of the silver growths which occurred during the decomposition of all of the specimens. In the very early stages of the growth the twin spots were either very weak, or absent altogether.

The subsidiary orientation which is listed in fig. 4 may be expressed as : (211) silver parallel to (100) silver halide, with [01$\bar{1}$] silver parallel to [01$\bar{1}$] silver halide. Again, this subsidiary orientation occurred for both silver bromide and silver chloride, when mica, rocksalt, and potassium bromide were used as substrates. It is therefore reasonable to assume that this orientation is not influenced by the substrate, but is a characteristic of the decomposition process. Although the (211) silver planes and the (100) silver halide planes are parallel for this orientation, it does not necessarily follow that these are the contact planes between the two lattices. Table 1 lists the low-indexed halide planes which have a low-indexed parallel lattice plane in the silver. All these pairs of planes are possible contact planes. There are twelve orientations which are equivalent, as

Table 1. Parallel Lattice Planes for the Subsidiary Orientation

Halide Plane	(100)	(011)	(01$\bar{1}$)	(111)	(211)	(2$\bar{1}\bar{1}$)	(1$\bar{2}\bar{2}$)
Parallel Silver Plane	(211)	(1$\bar{1}\bar{1}$)	(01$\bar{1}$)	(011)	(122)	(100)	(2$\bar{1}\bar{1}$)

Fig. 5

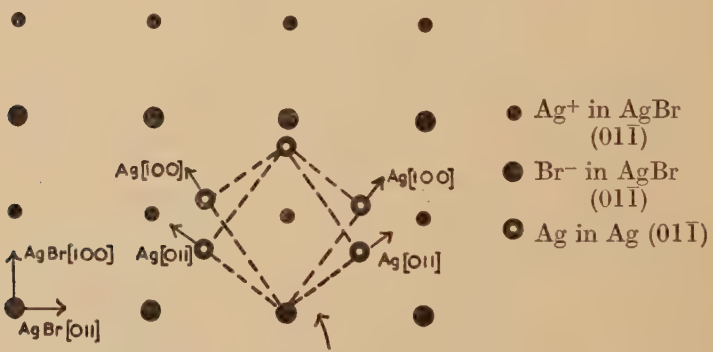

Two rectangles represent two equivalent ways for Ag (01$\bar{1}$) to fit on AgBr (01$\bar{1}$).

Fit of silver on silver bromide for subsidiary orientation, if (01$\bar{1}$) planes are contact planes.

regards the fit between the two lattices, to this subsidiary orientation. For example, if the (01$\bar{1}$) planes are regarded as the contact planes, there are two equivalent ways in which the (01$\bar{1}$) silver plane can fit on the (01$\bar{1}$) halide plane (see fig. 5). Since there are six non-parallel (01$\bar{1}$) type halide planes on which to fit, this makes twelve possibilities in all. Diffraction patterns from these equivalent orientations did not always occur when they would be expected, since a given one of the equivalent orientations only gave a strong pattern when the electron beam was set along a direction perpendicular to the parallel silver (1$\bar{1}\bar{1}$) and halide (011) type planes. At other settings, a given one of the equivalent orientations gave either no pattern (when one would be expected) or only a very weak pattern. This is not entirely understood, but possibly means that the silver which is in

the subsidiary orientation grows in the form of (111) plates (several layers thick) parallel to the silver halide (110) type planes, so that strong patterns will be obtained only when the plates present large areas to the electron beam. This is a possible explanation, since more electrons will impinge on a given plate when the electron beam is set perpendicular to it, than at any other setting.

It is also interesting to note that no disorientation of the silver halide was observed during any stages of the decomposition.

Several weak spots on the diffraction patterns were not interpreted.

(b) *The Influence of the Substrate*

In order to determine whether the substrate upon which the halide is deposited influences the occurrence of oriented silver, several different substrates have been used (see § 2). The results of the decomposition on all the substrates were entirely consistent, in that the observed orientations of silver were always the same relative to those of the parent silver halide (see § 4 (a)). In particular, the silver halide was in a ' fibrous ' orientation on magnesium oxide, and the silver formed during decomposition was in the same ' fibrous ' orientation.

A further experiment was carried out in order to obtain conclusive results on the influence of the substrate. Silver bromide could be oriented on potassium bromide in one of two ways, by changing the temperature of the substrate during deposition (Pashley 1952 b); (*a*) a parallel orientation; (*b*) an orientation with (111) silver bromide planes parallel to the potassium bromide (100) surface. In both cases decomposition occurred such that the silver formed in the same orientations relative to those of the silver bromide parent crystal; the orientations of the silver relative to that of the potassium bromide substrate were therefore different in the two cases. There can thus be no doubt that the growth of silver described in § 4 (a) is characteristic of decomposition of the silver halide, and that the substrate does not initiate the orientation of the silver.

Trillat (1951, 1952) has recently studied the decomposition (by electron bombardment) of oriented layers of silver bromide which were stripped from rocksalt substrates, and examined by the transmission method. He found non-oriented growth of silver. Similar transmission specimens have been examined by the author, with both silver bromide (stripped from potassium bromide substrates) and with silver chloride (stripped from rocksalt substrates). It was found that although much of the silver formed during bombardment was randomly oriented, there was also some parallel oriented silver, particularly in the case of silver chloride. Slight parallel orientation of silver has since been obtained by Trillat with his silver bromide specimens (private communication). This result adds further confirmation to the conclusion that the parallel orientation of silver is a characteristic of the decomposition process, and is not just a substrate effect. A further important effect (discussed in § 8) was that the silver halide recrystallized during electron bombardment, so that some of it became randomly oriented before being decomposed.

(c) *Decomposition by Ultra-violet Irradiation*

Preliminary experiments have been carried out on the decomposition of evaporated silver halide layers during ultra-violet irradiation. Silver chloride was evaporated on to some mica and rocksalt specimens, and two of the specimens were used to check that the chloride had oriented on the substrates in the usual manner. The other specimens were then placed in an evacuated quartz tube, and irradiated by means of an ultra-violet lamp for eight hours. These specimens were not subjected to electron bombardment before the irradiation. After irradiation, the specimens were examined in the electron diffraction camera ; the pattern obtained immediately the electron beam was switched on indicated that much decomposition had occurred during the ultra-violet irradiation. The pattern from such a decomposed layer on rocksalt is shown in fig. 6. The growth is identical to that which occurred during electron bombardment (the larger square pattern of fig. 6 indicating the parallel orientation of silver), except that rather more randomly oriented silver is formed than in the electron case. The study of the layers on mica confirmed that the decomposition of silver chloride under ultra-violet irradiation occurs in a manner which is not significantly different from that occurring during electron bombardment.

Some further experiments, in particular with silver bromide, have indicated that more complicated effects can occur, but since some of these effects might be influenced by reactions with the substrate, they will not be reported at present. It is worthy of note, however, that in none of these experiments have the non-parallel orientations of silver reported by Berry and Griffith (1950) been observed.

(d) *Chemical Development*

Specimens prepared on magnesium oxide substrates have been decomposed by treatment with a dilute chemical developer (metol-hydroquinone), without subjecting the specimens to any previous electron bombardment. Subsequent electron diffraction examination of these specimens has in all cases revealed the formation of randomly oriented silver.

§ 5. Decomposition of Evaporated Layers of Silver Iodide

Silver iodide layers have also been prepared by evaporation on to various substrates. Although the molten bead of silver iodide, from which the evaporation was effected, gradually decomposed, the diffraction patterns from the freshly prepared specimens were due entirely to silver iodide. There are two common forms of silver iodide, a cubic (zinc-blende type) structure and a hexagonal (zincite type) structure. Both modifications often occur together. It was found, however, that a layer consisting of only one modification could be formed. Such layers were highly oriented.

Figure 7 shows a pattern from an oriented layer of hexagonal silver iodide on mica, after twenty minutes exposure to the electron beam. Most

of the silver formed has grown in a random orientation, giving rise to the ring pattern. The spot pattern arises from the oriented silver iodide. With continued bombardment, the silver pattern becomes stronger, and many weak arcs can be distinguished on the silver rings. Two distinct patterns have been identified, indicating the orientations given in table 2.

Table 2. Silver Orientations in Silver Iodide

	Orientation	(1)	(2)
Hexagonal Iodide.	Silver plane parallel to silver iodide (001).	(110)	(110)
	Silver axis parallel to silver iodide [100].	[1$\bar{1}$0]	[1$\bar{1}$2]
Cubic Iodide.	Silver plane parallel to silver iodide (111).	(110)	(110)
	Silver axis parallel to silver iodide [1$\bar{1}$0].	[1$\bar{1}$0]	[1$\bar{1}$2]

We can therefore say that the decomposition of silver iodide, both cubic and hexagonal, leads mainly to randomly oriented silver. It is not yet certain whether the weak orientations observed are influenced by the substrate, or not, but it seems probable that they are not.

§ 6. The Stability of Silver Halides to Electron Bombardment

A point of interest that arises from the present work concerns the stability of silver halides to electron bombardment. The only specimens which are found to be unstable are: (1) evaporated layers of halide on rocksalt, potassium bromide, magnesium oxide and mica substrates; (2) stripped layers from rocksalt and potassium bromide substrates. The following specimens showed no indication of decomposition after two hours' bombardment in the diffraction camera: (1) chemically grown layers on silver; (2) evaporated layers of halide on metallic silver. Layers formed by evaporating silver halide on to a formvar film were found to decompose slightly during a two-hour bombardment (by transmission). Several other workers have found that various kinds of silver halide specimens are completely stable to electron bombardment. A summary of these results has already been given (Pashley 1951).

§ 7. Diffuse Background Patterns from the Silver Halides

Burgers and Tan Koen Hiok (1946) have studied silver chloride crystals by x-ray diffraction, and have observed the presence of diffuse streaks on their diffraction patterns. Similar streaks are also found on the electron diffraction patterns from some of the silver chloride and silver bromide specimens used in the present work. The streaks were more prominent with silver bromide specimens than with those of silver chloride. The streak patterns correspond to the presence of diffuse rods of intensity passing through all the 'strong' reciprocal lattice points (allowed points with even indices) along the three cube

directions. The occurrence of the streaks on patterns from chemically grown layers on silver crystals is well illustrated on a photograph published previously (Pashley 1952 a, fig. 13). The streaks from an evaporated layer are shown in fig. 8. None of the diffuse reciprocal lattice rods lies in the $(21\bar{1})$ reciprocal lattice plane, which is perpendicular to the electron beam, but some are inclined to it at only a small angle. The disposition of the diffuse rods just in front of the $(2\bar{1}\bar{1})$ reciprocal lattice plane (a similar set is also behind) is indicated in fig. 9. There are two orientations of the bromide, each of which gives the same spot pattern; the

Fig. 9

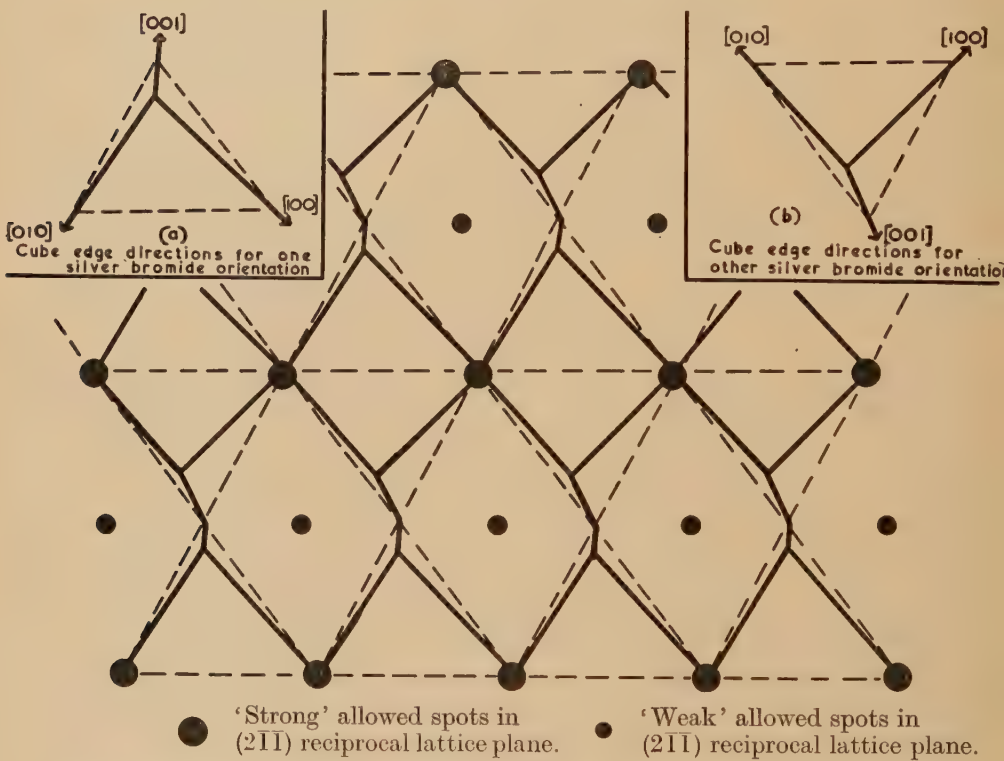

Disposition of diffuse rods in front of $(2\bar{1}\bar{1})$ reciprocal lattice plane, for two orientations.

diffuse streak patterns from the two orientations are not coincident, the two components being indicated in figs. 9(*a*) and 9(*b*). When the electron beam is set nearly perpendicular to the $(2\bar{1}\bar{1})$ reciprocal lattice plane, the Ewald sphere intersects these broad diffuse rods to give the pattern plotted in fig. 10. This is identical with the diffuse pattern in fig. 8.

Such diffuse streaks were observed quite frequently, but varied in intensity from specimen to specimen. It is considered that the reason for this variation is due to the variation in general background intensity

from specimen to specimen, since even quite a low background is sufficient to mask the diffuse streaks.

Similar diffuse streaks were also found with evaporated thallium chloride layers (Pashley 1952 b), and can also be seen on an electron diffraction photograph published by Yamaguti (1935). These latter streaks were obtained from a cleavage surface of zinc-blende from which a previously grown oxide layer had been removed. Yamaguti did not comment on the streaks ; these streaks can also be explained in terms of the presence of broad diffuse rods of intensity along the cube directions of the zinc blende reciprocal lattice.

Burgers and Tan Koen Hiok (1946) suggested that the streaks which they observed could be explained by supposing that various cube planes of their crystals had slipped, so that they were not phase linked with the rest of the crystal. Mitchell (1949) has suggested that the presence

Fig. 10

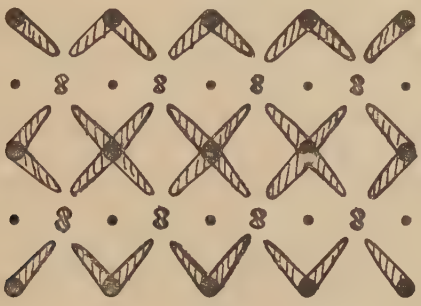

Diffuse streak pattern of fig. 8.

of F-centres could explain the streaks. The streaks observed on the electron diffraction patterns from the thin silver halide layers cannot be due to F-centre aggregates. A (100) plane of the halide, with its halide ions replaced by F-centres over a small area, would give rise to diffuse rods of intensity along [100] directions in the reciprocal lattice, and these rods would pass through all allowed halide reciprocal lattice points (points with indices all even or all odd). ' Weak ' reciprocal lattice points (allowed points with odd indices) should therefore have rods passing through them of the same intensity as those passing through the ' strong ' points. Streaks through the ' weak ' points were never observed. Since Burgers and Tan Koen Hiok found that their diffuse x-ray patterns were present even with the chloride at liquid air temperature, it seems unlikely that the streaks are of thermal origin.

It is thus considered that the possible explanations of the streaks are : (1) the slipping of various cube planes, as suggested by Burgers and Tan Koen Hiok ; (2) the presence of numerous small cavities in the crystals, consisting of missing cube planes (both silver and halide ions) of small area, and one layer in thickness ; (3) some distortion involving the cube planes.

The presence, or otherwise, of the diffuse streaks on the electron diffraction patterns showed no correlation with the stability of the halide to electron bombardment. The streaks do not, therefore, indicate the early stages of the silver growth, or the property of a particular specimen which controls its stability to electrons. It is possible, however, that the property which gives rise to the streaks does play some vital part in the decomposition process.

§ 8. Summary and Discussion

The main results presented above may be summarized as follows:

(1) The decomposition, during electron bombardment, of thin layers of oriented silver bromide and silver chloride gives rise to a parallel orientation of silver, with prominent (111) twinning. Other weak orientations also occur.

(2) Silver chloride behaves in the same way during ultra-violet irradiation.

(3) Silver iodide decomposes during electron bombardment to give mainly randomly oriented silver.

(4) Diffuse streak patterns are obtained from silver bromide and silver chloride; they do not appear to be linked with the early stages of nucleation of silver.

(5) Chemical development of oriented layers of silver bromide and silver chloride gives randomly oriented silver except when a single crystal of silver is used as substrate; then the silver which is formed by development continues the structure of the substrate, and twins on (111) planes.

The orientation of silver produced during electron bombardment of silver halides has been shown (see § 4 (b)) to be a characteristic of the decomposition process, and is not a substrate effect. The apparent discrepancy between the results of transmission experiments (which indicate only slight orientation of silver) and the reflection experiments is considered to be a due to a combination of the following: (1) the silver halide crystallites on the substrates are rigidly held, whereas the silver halide crystallites in the stripped films are not; (2) recrystallization of the halide occurs with the stripped films (giving randomly oriented silver halide), but no disorientation occurs with the halides on the substrates. This recrystallization is possibly due to thermal effects of the electron beam, for although transmission specimens might be appreciably heated (cooling conditions are poor), crystallites on a massive substrate will not be appreciably heated because of the conduction losses via the substrate. Thus the role of the substrate in the above experiments is to orient the silver halide crystallites rigidly, and to provide a means of keeping them cool, without appreciably influencing the orientation of silver produced during decomposition.

Berry and Griffith (1950) find that, during the ultra-violet irradiation of a single of silver bromide, parallel oriented silver grows inside

the crystal, and that other orientations occur at the surface. The evaporated layers of halide which have been used in the present work have a very high surface to volume ratio, and it would be expected that orientations characteristic of surface growth would predominate. Instead, the observed orientations of silver in these layers agree with the orientations which Berry and Griffith find inside their crystals. The relation between these two sets of results is not clear.

It is of interest to consider how the above results fit in with mechanisms suggested for photographic latent image formation. Although the original growth centres of the silver have not been detected by electron diffraction, the fact that highly oriented growth of silver occurs during electron bombardment of silver chloride and silver bromide shows that the growth centres themselves must be well oriented inside the silver halide lattice. In this connection, a latent image theory proposed by Huggins (1943) is of interest. Huggins suggests that the normal rocksalt structure of silver bromide might be converted to a zinc-blende type of structure when photoelectrons are released inside the crystal. The zinc-blende structure is then supposed to break down to form metallic silver. If such a mechanism were to occur, then electron diffraction would be expected to reveal the presence of the abnormal structure. No evidence of this structure was ever observed.

The mechanism by which the decomposition takes place must be such that : (1) oriented silver nuclei are formed ; (2) these nuclei can continue to grow, with the orientation of the silver and the unchanged halide maintained ; (3) the liberated halogen atoms can freely escape ; (4) twinning of the silver can occur ; (5) almost complete decomposition can be achieved, without destroying the orientation. It is difficult to see how such conditions of growth can be maintained unless either (*a*) the reaction takes place at the substrate-halide interface, or (*b*) a certain amount of silver halide remains unchanged, and acts as a support for the oriented silver. Since it has been shown that the substrate is not responsible for the initiation of the orientation, (*b*) seems the more likely. Further, there were always at least small traces of silver halide indicated on the diffraction photographs, and in most cases (except for very thin layers) unchanged silver halide very close to the interface with the substrate would not be detected in the electron diffraction pattern.

Whether the nucleation of the silver occurs at the surface, or inside the crystallites, cannot be determined directly. If, however, nucleation started at the surface, it might be expected that the orientation of the silver would be dependent on the crystal facet upon which nucleation took place, just as in the case for the growth of silver halides on silver (Pashley 1952 a). No variation in orientation from specimen to specimen was found, despite the fact that the halide layers on rocksalt and mica almost certainly had different facet structures. It therefore seems more likely that the nucleation was not a predominantly surface phenomenon,

and that much of the growth started inside the halide crystallites. This is, at least, in partial agreement with the results of Berry and Griffith (1950), who find that the parallel growth occurs inside a massive silver bromide crystal.

It would be of interest if any distinction could be made between the original Gurney and Mott (1938) theory of latent image (involving growth of silver on to 'sensitivity specks', via motion of interstitial silver ions) and the modification of this theory proposed by Mitchell (1949). Mitchell suggests that a latent image in a silver bromide grain could be an aggregate of F-centres; this aggregate can grow to a certain size, and then collapses to form a metallic silver nucleus. A mechanism of this kind might well be expected to form a parallel orientation of silver, since the face-centred silver ion lattice in the halide structure would then have to contract, without change of orientation, to form the face-centred cubic lattice of metallic silver. However, this is not a unique interpretation, and the occurrence of twinned silver definitely indicates that motion of silver ions, either as a surface mobility or as a mobility of interstitial ions, does occur after a certain stage of the process.

It is thus clear that there is not sufficient evidence available at present to decide on the detailed mechanism whereby oriented silver occurs in silver chloride and silver bromide (with hardly any orientation in silver iodide). However, the experiments described here have given a set of results which must be explained by any comprehensive theory of latent image formation.

Acknowledgments

I should like to express my gratitude to Professor Sir George Thomson, F.R.S., and to Dr. M. Blackman for valuable discussions. I am also indebted to The Department of Scientific and Industrial Research for a senior research award, during the tenure of which part of this work has been carried out.

References

Berry, C. R., 1949, *Acta. Cryst.*, **2**, 393.
Berry, C. R., and Griffith, R. L., 1950, *Acta Cryst.*, **3**, 219.
Burgers, W. G., and Tan Koen Hiok, 1946, *Physica*, **11**, 353.
Gurney, R. W., and Mott, N. F., 1938, *Proc. Roy. Soc.* A, **164**, 151.
Huggins, M. L., 1943, *J. Chem. Phys.*, **11**, 9.
Kirchner, F., and Lassen, H., 1935, *Ann. d. Phys.*, **24**, 173.
Kooy, J. N., and Burgers, W. G., 1948, *Rec. Trav. Chim. Pays-Bas*, **67**, 21.
Mitchell, J. W., 1949, *Phil. Mag.*, **40**, 667.
Pashley, D. W., 1950, *Acta. Cryst.*, **3**, 163; 1951, *Fundamental Mechanisms of Photographic Sensitivity* (London: Butterworth), p. 39; 1952 a, *Proc. Roy. Soc.* A, **210**, 354; 1952 b, *Proc. Phys. Soc.* A, **55**, 33.
Trillat, J. J., 1951, *C. R. Acad. Sci.* (Paris), **233**, 1188; 1952, *Acta. Cryst.*, **5**, 471.
Yamaguti, T., 1935, *Proc. Phys-Math. Soc. Jap.*, **17**, 443.

EXPLANATION OF THE PLATE

Fig. 1

Silver bromide layer on potassium bromide, after 15 minutes electron bombardment. Bromide [001] azimuth of (100) surface.

Fig. 2

As for fig. 1, except 90 minutes electron bombardment.

Fig. 3

Silver bromide layer on rocksalt, after 30 minutes electron bombardment. Bromide [011] azimuth of (100) surface.

Fig. 6

Silver chloride layer on rocksalt, after ultra-violet irradiation for 8 hours. Chloride [001] azimuth of (100) surface.

Fig. 7

Hexagonal silver iodide layer on mica, after 20 minutes electron bombardment. Iodide [100] azimuth of (001) surface.

Fig. 8

Silver bromide layer on mica, after 5 minutes electron bombardment. Bromide [$2\bar{1}\bar{1}$] azimuth of (111) surface.

CIII. *The Virial Theorem in the Thomas–Fermi Theory*

By N. H. March*
Wheatstone Physics Laboratory, King's College, London†

[Received July 18, 1952]

Abstract

A discussion of the virial theorem for both Thomas–Fermi and Thomas–Fermi–Dirac systems is given, the results being more general than have hitherto been obtained.

Finally the particular case of a homonuclear diatomic molecule is briefly considered.

§ 1. Introduction

The virial theorem, as is well known, holds in classical and quantum mechanics and in both theories it has had useful applications.

However it is by no means obvious that the theorem will remain valid in the Thomas–Fermi (T.F.) theory in view of the simplifying assumptions involved. Fock (1932) made the first investigation on the subject. He considered a T.F. system of many electrons and nuclei, and using a variational method he derived the form of the virial theorem for such systems. His proof was however later shown by Jensen (1933) to be valid only for the case of a single centre, on account of the improper variations employed. Jensen attempted to avoid the difficulties of Fock's treatment but in doing so made some restrictive assumptions which subsequently proved to be unjustified. Duffin (1935) gave the first satisfactory derivation of the theorem for T.F. systems of many electrons and nuclei.

The proofs mentioned previously all deal with the original T.F. theory in which exchange is neglected. However Jensen (1934) has shown how the theorem is modified by the exchange term for the case of a single nucleus, using Fock's method.

As was first pointed out by Slater and Krutter (1935) the T.F. method is of considerable value for discussion of the behaviour of material under high pressure. Hence it is of interest to investigate the form of the virial theorem when the systems considered are not free, but have a pressure on the boundary. For the case of a single nucleus such an investigation has been carried out by Slater and Krutter (1935) and Jensen (1939).

Recently, an ingenious discussion of the virial theorem based on similarity considerations has been given by Feynman, Metropolis and Teller (1949).

However, no unified and general proof of the theorem has yet been given, and indeed in the Thomas–Fermi–Dirac case the form of the theorem

* Communicated by Professor C. A. Coulson, F.R.S.

† Now at Department of Physics, The University, Sheffield.

in the many nuclei problem has not been established. The purpose of this work is to supply such a general treatment from which all existing results can be obtained immediately as particular cases.

§2. The Unmodified Thomas–Fermi Method

The treatment that we shall adopt follows that given by Duffin (1935), and hence we shall outline his method here. We shall see that we can immediately obtain the required generalization to systems which are not free, simply by retaining a surface integral which Duffin quite justifiably dropped for the free systems that he was considering.

We take as starting point in all cases the expression for the kinetic energy T. In the original T.F. method this may be written in terms of the total electrostatic potential V as

$$T=\frac{3\mu}{20\pi}\int_\tau (V-V_0)^{5/2}\,d\tau., \qquad (1)$$

where

$$\mu=\frac{32\pi^2 e}{3h^3}(2me)^{3/2}$$

and $-eV_0$ is the maximum energy of an electron.

We now use the relation

$$3\int_\tau (V-V_0)^{5/2}\,d\tau=\int_s (V-V_0)^{5/2}\,\mathbf{r}\,.\,\mathbf{ds}-\int_\tau \tfrac{5}{2}(V-V_0)^{3/2}\,\mathbf{r}\,.\,\mathrm{grad}\,V\,d\tau. \qquad (2)$$

Duffin now drops the first term since for free systems $V-V_0=0$ on the boundary. This is not true however for systems in which there is a pressure on the boundary, and hence we retain the term here. Using the usual T.F. expression for the charge density ρ in (2) and then substituting in (1) we obtain

$$2T=\frac{\mu}{10\pi}\int_s (V-V_0)^{5/2}\,\mathbf{r}\,.\,\mathbf{ds}+\int \rho\mathbf{r}\,.\,\mathrm{grad}\,V\,d\tau \qquad (3)$$

If e_k and $\mathbf{r}_k$ are the charge and position vector of the kth nucleus, and V_e is the potential due to the electrons, then we can write

$$V=V_e+\sum_k \frac{e_k}{|\mathbf{r}-\mathbf{r}_k|}. \qquad (4)$$

Also Duffin has proved the following lemma :

$$\int \rho\,\mathbf{r}\,.\,\mathrm{grad}\,V_e\,d\tau=-\tfrac{1}{2}\int \rho\,V_e\,d\tau. \qquad (5)$$

and hence

$$2T=\frac{\mu}{10\pi}\int_s (V-V_0)^{5/2}\,\mathbf{r}\,.\,\mathbf{ds}-\tfrac{1}{2}\int \rho V_e\,d\tau+\sum_k \int \rho\,\mathbf{r}\,.\,\mathrm{grad}\,\frac{e_k}{|\mathbf{r}-\mathbf{r}_k|}\,d\tau. \qquad (6)$$

We now use the identity

$$\mathbf{r}\,.\,\mathrm{grad}\,|\mathbf{r}-\mathbf{r}_k|^{-1}=-|\mathbf{r}-\mathbf{r}_k|^{-1}-\mathbf{r}_k\,.\,\mathrm{grad}_k\,|\mathbf{r}-\mathbf{r}_k|^{-1} \qquad (7)$$

and proceeding exactly as Duffin has done we arrive at the result

$$2T+U=\frac{\mu}{10\pi}\int_s (V-V_0)^{5/2}\,\mathbf{r}\,.\,\mathbf{ds}+\operatorname*{Lim}_{a=0}\sum_k e_k\,\mathbf{r}_k\,.\,\epsilon_a(\mathbf{r}_k), \qquad (8)$$

where U is the potential energy of the electrons and ϵ_a is the electric field produced by all charges outside small spheres of radius a surrounding the nuclei.

Evidently this is the general form of the theorem, the first term on the right arising from the fact that the system considered is not free, in other words it is to be interpreted as the virial of the forces acting on the boundary, whilst the second term can be interpreted as arising from the forces required to hold fast the nuclei.

The various forms of the theorem obtained hitherto follow immediately from (8). Duffin's form is obtained as we have said, by putting the first term on the right equal to zero. Further, for the case of one centre the second term on the right is obviously zero.

For free atoms and ions $(V-V_0)=0$

on the boundary, and hence $2T+U=0.$

For non-free atoms we have

$$2T+U=\frac{\mu}{10\pi}\int_s (V-V_0)^{5/2}\,\mathbf{r}\,.\,\mathbf{ds}$$

$$=\frac{\mu}{10\pi}\left[(V-V_0)^{5/2}\right]_{\text{boundary}}\cdot 3v,$$

where v is the volume.

But Slater and Krutter and Jensen have shown that the pressure p is simply given by

$$p=\frac{\mu}{10\pi}\left[(V-V_0)^{5/2}\right]_{\text{boundary}}$$

and hence $$2T+U=3pv.$$

§3. The Thomas–Fermi–Dirac Method

The preceding proof will now be generalized to apply to the Thomas–Fermi–Dirac (T.F.D.) method in which exchange is included. The only discussions given hitherto (Jensen 1934, Feynman, Metropolis and Teller 1949) are limited to the case of a single centre.

As before, we take as starting-point the expression for the kinetic energy T.

$$T=c_k\int n^{5/3}\,d\tau, \qquad \ldots\ldots\ldots \quad (9)$$

where $$c_k=\frac{3h^2}{10m}\left(\frac{3}{8\pi}\right)^{2/3}$$

and n is the number of electrons per unit volume. For T.F.D. systems, n is related to the total electrostatic potential V by

$$n=\frac{\mu}{4\pi e}\left[a+(V-V_0+a^2)^{1/2}\right]^3, \qquad \ldots\ldots \quad (10)$$

where $$a=\frac{(2me^3)^{1/2}}{h}.$$

It is convenient to introduce the abbreviation

$$\mathcal{V}=[a+(V-V_0+a^2)^{1/2}]^2 \quad . \quad . \quad . \quad . \quad . \quad . \quad . \quad (11)$$

and then from (9)

$$T=\frac{3\mu}{20\pi}\int \mathcal{V}^{5/2}\,d\tau. \quad . \quad . \quad . \quad . \quad . \quad . \quad . \quad . \quad (12)$$

Using Gauss' theorem this can be written

$$2T=\frac{\mu}{10\pi}\int \mathcal{V}^{5/2}\,\mathbf{r}\,.\,\mathbf{ds}+\int \rho\,\mathbf{r}\,.\,\text{grad}\,\mathcal{V}\,d\tau. \quad . \quad . \quad . \quad (13)$$

Now $\text{grad}\,\mathcal{V}=\text{grad}\,V+2a\,\text{grad}\,\mathcal{V}^{1/2}$ . . . . . (14)

and hence

$$2T=\frac{\mu}{10\pi}\int \mathcal{V}^{5/2}\,\mathbf{r}\,.\,\mathbf{ds}+\int \rho\,\mathbf{r}\,.\,\text{grad}\,V\,d\tau-\frac{a\mu}{2\pi}\int \mathcal{V}^{3/2}\,\mathbf{r}\,.\,\text{grad}\,\mathcal{V}^{1/2}\,d\tau.$$

The last term can evidently be written as

$$-\frac{a\mu}{8\pi}\int \mathbf{r}\,.\,\text{grad}\,\mathcal{V}^2\,d\tau,$$

and using Gauss' theorem this becomes

$$-\frac{a\mu}{8\pi}\left(\int \mathcal{V}^2\,\mathbf{r}\,.\,\mathbf{ds}-3\int \mathcal{V}^2\,d\tau\right).$$

The term involving the volume integral can be shown immediately to equal the negative of the exchange energy A,

where $$A=-c_e\int n^{4/3}\,d\tau$$

and $$c_e=\frac{e^2\,3^{1/3}}{4\pi^{1/3}}.$$

Proceeding entirely as before we obtain

$$2T+U+A=\frac{\mu}{10\pi}\int\left(\mathcal{V}^{5/2}-\frac{5a}{4}\,\mathcal{V}^2\right)\mathbf{r}\,.\,\mathbf{ds}+\operatorname*{Lim}_{a=0}\sum_k e_k\,\mathbf{r}_k\,.\,\epsilon_a(\mathbf{r}_k) \quad . \quad . \quad (15)$$

or writing the first integral in terms of n

$$2T+U+A=\int(\tfrac{2}{3}c_k n^{5/3}-\tfrac{1}{3}c_e n^{4/3})\,\mathbf{r}\,.\,\mathbf{ds}+\operatorname*{Lim}_{a=0}\sum_k e_k\,\mathbf{r}_k\,.\,\epsilon_a(\mathbf{r}_k). \quad . \quad (16)$$

This is evidently then the general form of the virial theorem for T.F.D. systems.

As before we can immediately obtain all previous results as special cases. For the case of a single centre the second term on the right is zero. Also Jensen has shown that in this case, the pressure p defined by

$$p=-\frac{dE}{dv}$$

is given by $$p=(\tfrac{2}{3}c_k n^{5/3}-\tfrac{1}{3}c_e n^{4/3})_{\text{boundary}}$$

and hence $$2T+U+A=3pv. \quad . \quad . \quad . \quad . \quad . \quad . \quad . \quad (17)$$

This is the result first obtained by Jensen.

§4. Case of a Free Homonuclear Diatomic Molecule

The results obtained previously are of course quite general, applying to any molecule or crystal. In concluding the discussion, we wish to point out that the theorem in the special case of a homonuclear diatomic molecule described by the original T.F. theory can be put into the more usual form*

$$2T+U=-R\frac{dE}{dR}, \qquad \ldots\ldots\ldots \quad (18)$$

where R is the internuclear distance.

This result, first given by Slater (1933), has not hitherto been proved to hold in the T.F. theory as far as the writer is aware.

All that is necessary is to discuss the last term in (6), that is

$$-\sum_k \int ne\left(\mathbf{r}\,.\,\mathrm{grad}\,\frac{e_k}{|\mathbf{r}-\mathbf{r}_k|}\right)d\tau.$$

In the case we are considering this can be written in the form

$$\int neV_N d\tau+\int neR\frac{dV_N}{dR}\,d\tau,$$

where V_N is the potential due to the nuclei. We have now to set up the energy expression and differentiate it with respect to R to obtain

$$\frac{dE}{dR}=-e\int n\frac{dV_N}{dR}\,d\tau.$$

Hence eqn. (18) is established. It can be shown, after some manipulation, that in this case the kinetic energy T and the potential energy U can be written in the form

$$\left.\begin{aligned} T&=-\frac{6}{7}Ze(V_e)_N-\frac{6}{7}R\frac{dE}{dR},\\ U&=\frac{12}{7}Ze(V_e)_N+\frac{5}{7}R\frac{dE}{dR}, \end{aligned}\right\} \qquad \ldots\ldots \quad (19)$$

where $(V_e)_N$ is the potential at either nucleus due to the electrons.

Acknowledgments

The writer wishes to thank Professor C. A. Coulson, F.R.S., for his valuable comments and encouragement during the course of this work, and to acknowledge a grant from the Department of Scientific and Industrial Research.

References

Duffin, R. J., 1935, *Phys. Rev.*, **47**, 421.
Feynman, R. P., Metropolis, N., and Teller, E., 1949, *Phys. Rev.*, **75**, 1561.
Fock, V., 1932, *Physik. Zeits. Sowjet.*, **1**, 747.
Jensen, H., 1933, *Z. Physik*, **81**, 611 ; 1934, *Ibid.*, **89**, 713 ; 1939, *Ibid.*, **111**, 373.
Slater, J. C., 1933, *J. Chem. Phys.*, **1**, 687.
Slater, J. C., and Krutter, H. M., 1935, *Phys. Rev.*, **47**, 559.

* It should be noted that, as throughout this paper, U does not include the nuclear–nuclear interaction energy U_N, and neither does E (equal to $T+U$). Obviously, (18) is still true if U_N is added to both U and E.

CIV. *On the Latent Heat and Vapour Density of Helium*

By R. Berman and J. Poulter
The Clarendon Laboratory, Oxford*

[Received July 19, 1952]

Abstract

The volume of vapour evolved from liquid helium by known amounts of heat has been measured at temperatures between 2·9 and 4·5° K. The derivation of latent heat values from these results is discussed, and it is shown that the existing experimentally determined values of the saturated vapour density are not sufficiently reliable for this purpose. The probable true values of the vapour density are considered.

§ 1. Introduction

We have constructed an apparatus for measuring very small heat capacities and small differences of heat capacity. In order to avoid errors caused by the heat capacity of the calorimeter in the conventional type of apparatus we use an improved version of Dewar's apparatus (1905) in which the heat content of the sample is measured by determining the volume of vapour driven off by this heat from a low boiling liquid. From this a mean specific heat can be derived.

In our experiments we measure the increase in volume of the liquid–vapour system at constant pressure ; but this increase in volume represents a smaller mass of gas than is produced from the liquid. Suppose 1 g of the liquid to be evaporated ; the gramme of vapour produced can be considered in two parts : (1) the vapour which replaces the liquid evaporated, and is of mass ρ_V/ρ_L g and (2) the vapour of which the volume at room temperature is actually measured and is of mass $(1-\rho_V/\rho_L)$ g. ρ_L and ρ_V are the liquid and vapour densities.

In order to calculate the number of moles of liquid evaporated we must divide the measured volume of gas by $(1-\rho_V/\rho_L)$. In the case of helium above 3° K this factor is appreciably less than unity ($\sim$0·86 at 4·2° K) and cannot be calculated accurately owing to uncertainty as to the density of the saturated vapour. This uncertainty is due to the great deviation from ideality of the vapour and there are few direct measurements of the density at saturation.

As the only measurements of the latent heat of helium at different temperatures are those of Dana and Kamerlingh Onnes (1926), in which the volume of liquid evaporated was determined, we have measured directly the apparent latent heat, L_a, in terms of gas evolved, which is the quantity actually required for our specific heat experiments. This is related to the true latent heat, L, by the equation $L=L_a(1-\rho_V/\rho_L)$.

* Communicated by Professor F. Simon, F.R.S.

§ 2. Experimental

2.1. *Apparatus*

The apparatus used was the one designed primarily for the heat capacity measurements. The relevant part of the apparatus is shown in fig. 1. A narrow (2 mm diameter) thin-walled, German silver tube B connects the annular copper vessel A to a copper tube passing through the high pressure pot S, of a Simon-type helium liquefier, and then both to a source of helium gas and to an apparatus for making continuous measurements of volume changes.

Fig. 1

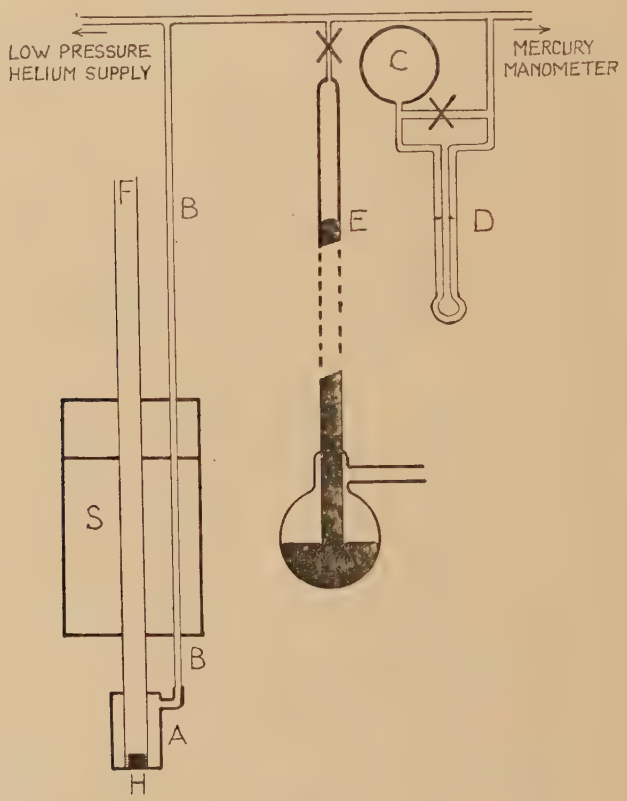

Apparatus.

The pressure in the system is measured on a mercury manometer, and by trapping this pressure in a litre flask C, the differential oil manometer D can be used as a sensitive detector of pressure change. The flask C is immersed in water to keep its temperature constant during the course of a single experiment (about 30 minutes). E consists of a tube of accurately constant cross-section, and is actually one of three 'Veridia' tubes of different diameters, used to allow various volume ranges to be measured. By changing the level of the mercury in E, the volume of the system can be changed while keeping the pressure accurately constant.

2.2. *Method*

Helium is liquefied in S, and then helium gas let into tube B to allow it to be condensed into A. The level of the mercury in E is pushed by compressed air up to the highest possible level.

On account of stray heat influx a steady flow of vapour leaves A and is measured by lowering the level E at such a rate that the pressure in the system is constant ; the height being read on a glass mirror scale. The height of mercury is read off every minute for 6 to 10 minutes. The points are plotted as soon as they are taken so that we can judge the degree of linearity of the background at any time.

Heat is then supplied to A by means of an electric heater H, for a measured time. On switching off the current the background is again reached after a few minutes. The vertical ' height ' between initial and final backgrounds then gives the volume corresponding to the heat supplied by the heater.

Wexler (1951) has carried out a similar determination at 4·228° K. In his experiment he found the volume evolved to depend upon the rate of heating as well as on the quantity of heat supplied. The large volume of escaping cold vapour reduced the temperature gradient in the equivalent of tube B and thus reduced the appreciable background caused by heat conducted down this tube. In our apparatus the background is almost entirely due to radiation down the wide central tube F, provided as a means of dropping specimens into the helium region, and not to conduction along tube B. To verify this, we measured the background evaporation of helium when the excess in pressure on S over that on A was increased from the usual 1 cm of mercury to 15 cm. The background changed from 0·2 cm^3 of gas per minute to 0·4 cm^3, showing that under our normal conditions only about 1/15 of the total background is due to conduction down tubes B and F. Any loss in background due to a reduced temperature gradient in tube B should then, for the times and rates of heating we used (generally $\sim$30 cm^3 gas evolved in $\sim$2 minutes), produce an error in the latent heat of less than 1/10%. We did indeed find that the values of latent heat were independent of the rate of heating.

Determinations of latent heat at pressures lower than normal atmospheric pressure are carried out by pumping the helium in S, and allowing the pressure in the main system to follow. As the pressure in S must be slightly in excess of that in A, to enable evaporating vapour to escape, once the pressure in A has reached the required value the rate of pumping is decreased and adjusted to stabilize the pressure in S at the required value. When higher pressures are required, the gas evaporating from S is made to pass through one of a series of fine capillaries chosen to give the required pressure heads. In this way constant pressure heads up to about 20 cm of mercury were applied. The pressure in the system is allowed to build up to the required value, and then the experiment is carried out in the same manner as at lower pressures.

§3. Results and Discussion

3.1. *Experimental Results*

The ' apparent ' latent heat of helium was measured between 2·9° and 4·5° K. The values found are tabulated in units of calories per mole of gas collected (table 1). At 4·23° we find agreement with the value determined by Wexler.

We calculated the true latent heat at 4·23° K from our values of the apparent latent heat by using the values of the liquid density measured by Kamerlingh Onnes and Boks (1924) and of the saturated vapour density

Table 1. Experimental Values of Latent Heat

Temperature ° K	Apparent latent heat $L_a \pm 0{\cdot}1$ cal/mole	$(1-\rho_V/\rho_L)$	True latent heat $L_a(1-\rho_V/\rho_L)$ cal/mole
2·867	22·9[5]	0·976	22·4
3·172	23·4	0·958	22·4
3·180	23·3	0·958	22·3[5]
3·714	23·5	0·922	21·6[5]
3·987	23·2[5]	0·893	20·7[5]
3·999	23·3	0·892	20·8
4·198	22·80* ±0·05	0·865	19·72
4·280	22·6	—	—
4·280	22·6[5]	—	—
4·434	22·2	—	—
4·440	22·1	—	—
4·510	21·6	—	—
4·512	21·7[5]	—	—
Extrapolated values at normal boiling point 4·211	22·7[7]	0·864	19·6[8]

* Mean of six values.

All calculations are made using $J=4{\cdot}18$ joules/calorie.

measured by Mathias, Crommelin, Kamerlingh Onnes and Swallow (1925) both taken from Keesom (1942). As was found by Wexler, this calculated latent heat does not agree with the direct determination by Dana and Kamerlingh Onnes and is about 1% too high. However, at the lowest temperatures at which we have made measurements the factor $(1-\rho_V/\rho_L)$ is near unity and can be calculated with more certainty from the virial coefficients. At these temperatures, by calculating the vapour density from the first three virial coefficients, using the table of ' adopted ' values given by Keesom (1942), we find good agreement between our corrected latent heat and the values of Dana and Kamerlingh Onnes.

This suggests that the discrepancy at higher temperatures is due to an error in the calculated correction factor, and therefore probably in the measured vapour density.

In order to obtain other values of the saturated vapour density we have plotted the isotherms, pressure versus density, of helium vapour obtained by Keesom and Walstra (1940). These extend to about 90% of the saturation pressure and we have extrapolated these up to the saturation pressure and read off the density. It was found that the experimentally

Fig. 2

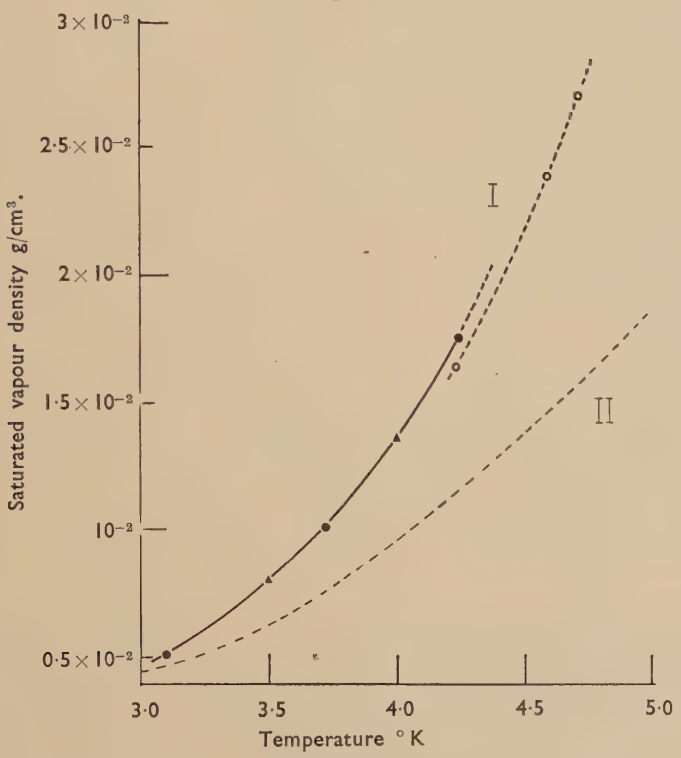

I. Saturated vapour density of helium
- ▲ Calculated from virial coefficients.
- ● From extrapolation of isotherms.
- ○ Experimental (Mathias *et al.*).

II. Vapour density which helium would have if it were ideal at saturation pressure.

determined saturated vapour density at 4·23° K is incompatible with the extrapolated isotherms. We have calculated some additional values of the saturated vapour density below 4° K by means of the virial coefficients given by Keesom and Walstra. Figure 2 shows the vapour density derived by these two methods, and also the direct measurements of Mathias *et al.*

Using values of vapour density taken from the curve of fig. 2 we have calculated the true latent heat from our experiments, as shown in table 1. We obtain good agreement with the measurements of Dana and Kamerlingh Onnes as can be seen in fig. 3. Our results go to higher temperatures than do those of Dana and Kamerlingh Onnes, but the uncertainty in ρ_V prevents us from converting our measured values into true latent heats. In this region any error in ρ_V would cause a serious error in the calculation.

Fig. 3

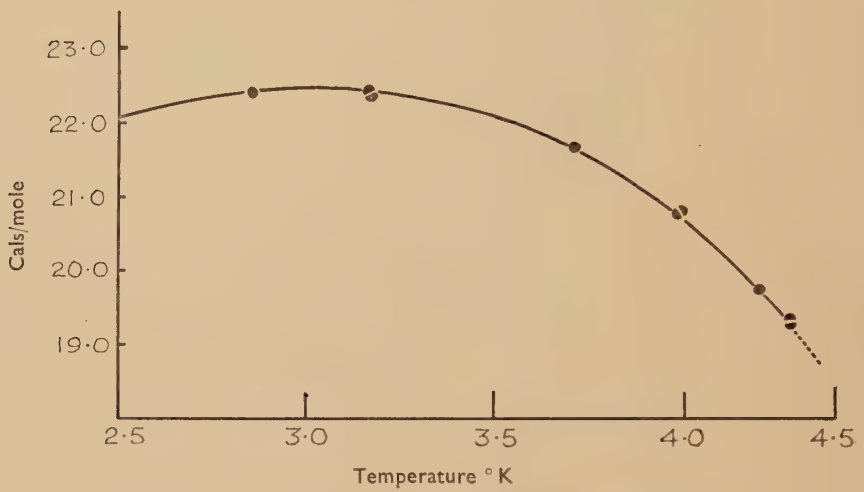

Latent heat of helium { — Dana and Kamerlingh Onnes. ● Present experiments.

3.2. *Comparison with Calculated Latent Heat*

Further evidence that the saturated vapour density is in error is provided by the discrepancy between the measured latent heat and the value calculated by Kistemaker (1946) from the Clausius–Clapeyron equation, $dP/dT = L/T(1/\rho_V - 1/\rho_L)$. In this calculation any error in the vapour density has a greater effect on the value of the latent heat derived than it has on the value derived from our measurements, and this is indeed found.

We have calculated the latent heat for various temperatures from the Clausius–Clapeyron equation using the values of vapour density from fig. 2. Table 2 shows the data used and the results of these calculations ; it is seen that there is agreement with the experimental values within the accuracy obtainable from the data used. The table includes values for one temperature as given by Kistemaker. It will be noted that some discrepancies occur due to the different vapour pressure–temperature scales used. We have taken values from the Royal Society Mond

Laboratory's tables (1949), whereas Kistemaker uses the '1937' scale to which he has applied corrections calculated from his own vapour pressure experiments.

Below 4·2° K Kistemaker has calculated the latent heat by equating the Gibbs free energies, G, of the liquid and of the saturated vapour for a particular temperature. At 3·5° K and below, these calculated values agree with the experimental values, but at 4° and 4·2° K the discrepancy

Table 2. Calculation of Latent Heat from Clausius-Clapeyron Equation

Temperature K	$dP/dT \times 10^6$ cg units ±2	ρ_V $\times 10^2$ g/cm³ ±0·01	ρ_L g/cm³	$T\frac{dP}{dT}\left(\frac{1}{\rho_V}-\frac{1}{\rho_L}\right)$ cal/mole	L exp. cal/mole
3·10	395	0·51	0·1404	22·2 ±0·5	22·4[5]
3·72	676	1·02	0·1336	21·9 ±0·3	21·7
4·23	979	1·73	0·1250	19·8 ±0·2	19·6
Kistemaker's calculation :—					
4·23	996	1·64	0·1250	21·27	19·6*

* See footnote.

is of the order of 4 to 5%,† whereas the stated uncertainty of the calculations is only 1½%. However, the virial coefficients which he uses at 4° K give a vapour density approximately in agreement with fig. 2. Thus the discrepancy must be elsewhere in Kistemaker's calculation by this method.

§ 4. Summary

We have determined the latent heat of helium between 2·9° and 4·5° K by measuring the volume of vapour produced by known amounts of heat. Using values of the saturated vapour density found by extrapolating isotherms we obtain good agreement with the experimental values of Dana and Kamerlingh Onnes between 2·9 and 4·2° K. This suggests that the discrepancies found by Kistemaker between the experimentally determined and the calculated values for latent heat at 4° and 4·2° K are not due to an error in the experimental values, as Kistemaker thought probable.

We have not converted our measurements above the normal boiling point into true latent heat as we do not think that the experimentally determined saturated vapour densities are sufficiently reliable.

† It appears that the 'smoothed' value of the experimental latent heat at 4·25° K given by Keesom (4.58 cal/g) is a misprint and should actually be 4·85 cal/g, and also that the value at 4·2° K given by Kistemaker is in error due to this misprint.

Values of the latent heat calculated from the Clausius–Clapeyron equation agree with the experimental values, but again the accuracy is limited by the lack of knowledge of vapour densities.

In view of the revealed uncertainty in vapour density values it is obviously desirable that more accurate determinations should be made.

Acknowledgment

One of us (J.P.) would like to thank the Ministry of Education for a maintenance grant.

References

Dana, L. I., and Kamerlingh Onnes, H., 1926, *Leiden Comm.* No. 179 c.
Dewar, J., 1905, *Proc. Roy. Soc.* A, **76,** 325.
Kamerlingh Onnes, H., and Boks, J. D. A., 1924, *Leiden Comm.* No. 170 b.
Keesom, W. H., 1942, *Helium* (Amsterdam : Elsevier).
Keesom, W. H., and Walstra, W. K., 1940, *Physica*, **7,** 985.
Kistemaker, J., 1946, *Physica*, **12,** 281.
Mathias, E., Crommelin, C. A., Kamerlingh Onnes, H., and Swallow, J. C., 1925, *Leiden Comm.* No. 172 b.
Wexler, A., 1951, *J. Appl. Phys.*, **22,** 1463.

CV. *The Mechanism of Rolling Friction*

By D. Tabor
Research Laboratory on the Physics and Chemistry of Surfaces,
Department of Physical Chemistry, Cambridge*

[Received July 19, 1952]

Summary

An investigation has been made of the friction and surface damage produced when a hard steel ball rolls between flat parallel surfaces of a softer metal. The behaviour may be divided into two parts. When rolling first commences, even at small loads, there is marked plastic flow and the resistance to rolling is due primarily to the plastic displacement of metal ahead of the ball. With successive traversals of the same track there is an increase in track width and a diminution in rolling resistance. An equilibrium state is ultimately reached where no further increase in track width occurs so that the deformations are essentially elastic. The rolling resistance is now constant and is unaffected by boundary lubricants. From a detailed study of the rolling of spheres and cylinders on rubber it is shown that there is no interfacial slip, the whole of the rolling resistance being due to elastic hysteresis losses. It is suggested that in the rolling experiments on metals within the elastic range the resistance to rolling is also due primarily to elastic hysteresis losses. Thus in rolling, there is no ' friction ' in the conventional sense of the word.

We have recently carried out an investigation of the friction and surface deformation produced when a hard steel sphere rolls between flat parallel surfaces of a softer metal. The greater part of the earlier work was carried out by Mr. K. R. Eldredge on apparatus which he has already briefly described (Eldredge 1950). The behaviour may be divided into two parts. When rolling first commences, even at small loads, there is marked plastic flow and the resistance to rolling is due primarily to the plastic displacement of the metal ahead of the ball. Indeed, there is a fairly close quantitative agreement between the observed resistance and the product of the cross-sectional area of the grooved track and the yield pressure of the metal. In the first roll, the ball is supported on the front half of the circle of contact. On rolling back along this track, there is no such support for the ball, unless it sinks further into the metal. This leads to an increase in the width of the groove and further plastic displacement of metal. With successive rolls there is a slow increase in groove-width and a gradual decrease in rolling resistance. For a metal which does not work-harden appreciably (so that the area supporting the load is substantially constant for each roll) a simple theory may be

---

* Communicated by the Author.

developed relating groove-width and friction as a function of the number of traverses. The results for tin are given in fig. 1 and it is seen that the agreement is reasonably good. Since this phase of the rolling process involves bulk deformation of the metal, the rolling resistance, as we might expect, depends little on the lubrication. With a metal like indium, however, the adhesion which is very marked for clean surfaces contributes some part of the rolling friction and this is naturally affected by the presence of lubricants.

As rolling proceeds, there is an increase in track-width as described above, a slight change in track curvature and, accompanying these

Fig. 1

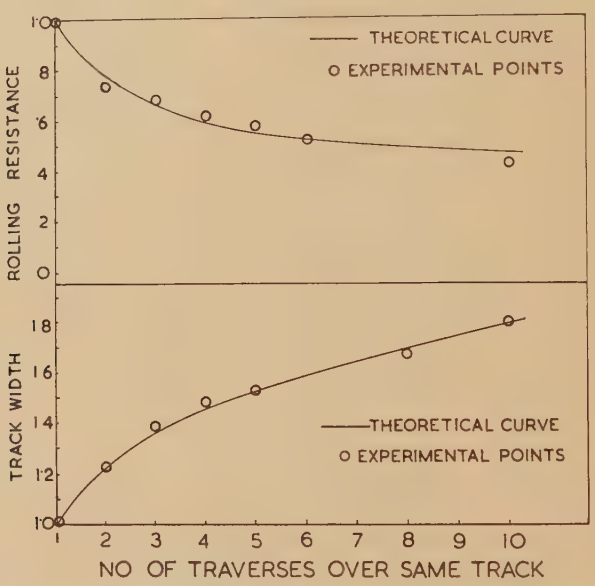

Variation of track width and rolling resistance for repeated traversals of same track. Steel ball on tin surface. Vertical ordinates are arbitrary.

changes, work-hardening of material around the track. As a result of these three factors a stage is gradually reached (after about 100 traverses) at which the whole of the load is borne by the ellipse of contact formed by *elastic* deformation within the width of the existing track. No further appreciable increase in track-width occurs and the rolling friction remains substantially constant for repeated traversals of the track. Here again, lubricants have practically no effect on the friction.

In order to study rolling friction in the elastic range a more detailed investigation was made of the rolling of hard spheres and cylinders on rubber. More than 70 years ago, Osborne Reynolds (1875) pointed out that when a hard metal cylinder rolls on rubber it traverses a distance less than its periphery in a single revolution. This is because it measures out its periphery on the stretched portion of the rubber within the region

of contact, and Reynolds regarded this as equivalent to a small amount of slip between the roller and the rubber. He also provided an ingenious explanation of the independence of the rolling friction on lubrication. Recently, Dr. Ailsa Lowen, working in this laboratory, has found that although there is, as Reynolds observed, a difference between the circumference and the distance travelled forward in one revolution, there is *no* slip between the rubber and the roller. The rubber is stretched before it enters and after it leaves the region of contact, and no interfacial slip occurs. Similar effects are observed when hard spherical surfaces roll on rubber. Tangential forces are developed during rolling at the interface, but these are always appreciably less than the force required to produce interfacial slip even in the presence of lubricant. This absence of slip between the rolling surfaces explains the fundamental observation that lubrication has no effect on rolling friction in the elastic range. (There is evidence that some adhesion may occur at the interface, so that some work may be expended in separating the ball from the surface as rolling proceeds. This will be reduced by lubricants but its contribution to the overall rolling resistance appears, in general, to be negligible.)

We must therefore seek a mechanism of rolling friction that does not involve surface slip or plastic flow. It is suggested here that the friction in the elastic range is primarily due to elastic hysteresis losses. If a steel ball, radius r_1 rolls in a groove of radius r_2 under a load W, it forms an ellipse of contact of semi-major axis a_0 and semi-minor axis b_0 where the ratio a_0/b_0 depends only on the ratio r_2/r_1. Using Hertz's classical equations for elastic deformation (see Allan 1945) we have shown that the elastic work done in rolling forward a distance of one centimetre is

$$\Phi = \frac{9}{16}\left(\frac{W}{a_0}\right)^2 f(E)\frac{1}{\pi}\,\mathscr{K}\,a_0/b_0, \quad . \quad . \quad . \quad . \quad . \quad . \quad (1)$$

where $f(E)=(1-\sigma_1^2)/E_1+(1-\sigma_2^2)/E_2$, σ_1, σ_2 being Poisson's ratio; E_1, E_2 Young's modulus for the ball and groove material respectively, and $\mathscr{K}$ is an elliptic integral depending only on the ratio a_0/b_0 itself, that is, on the ratio r_2/r_1. For a ball rolling on a flat surface, the region of contact is a circle, so that $a_0=b_0$ and $\mathscr{K}=\pi/2$.

If the hysteresis loss is constant, as it is for rubber at fairly constant rates of strain, the rolling friction F should be a constant fraction of Φ. Since a_0 is proportional to $W^{1\cdot3}$ it follows that $F \propto W^{4\cdot3}$. Typical results plotted on a log–log scale for a steel ball rolling on flat rubber specimens of the same Young's modulus but of widely differing hysteresis losses are shown in fig. 2. It is seen that $F \propto W^{1\cdot3}$, which is in good agreement with the theoretical slope. Further, direct determination of the hysteresis losses under normal loading, gave values of 11% for one rubber and 1·4% for the other. The observed frictional values agree with the calculated elastic energy values if hysteresis loss factors of 12% and 1·3% respectively are assumed. The agreement is very satisfactory.

These ideas have been extended to metals when the track has reached its equilibrium state. For metals such as copper and nickel the rolling friction is relatively high and falls off with load more rapidly than $W^{4/3}$; indeed F is more nearly proportional to W^2. Hysteresis losses can well explain these results if it is assumed (*a*) that for metals such as copper and nickel hysteresis losses of the order of 10% or more may occur, (*b*) that the hysteresis loss factor is not constant—as with rubber—but diminishes with decreasing strain. Both these assumptions are borne out by direct hysteresis experiments, on a standard Chevenard equipment, for metals deformed just beyond their elastic limit and then subjected to cyclic strains. Large hysteresis loops are observed which remain fairly constant in size for hundreds or thousands of cycles but fall off

Fig. 2

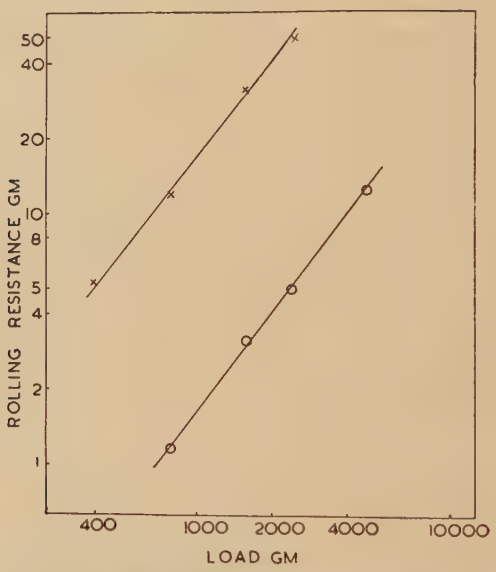

Rolling resistance of 5/8 in. steel ball rolling on rubber. × High hysteresis loss rubber. ○ Low hysteresis loss rubber. Note that the points are plotted on a log–log scale.

rapidly when the strain is reduced (Chevenard 1943). In this test the strains are torsional but the magnitude of the effect is confirmed. For typical ball-race steel the frictional resistance corresponds to a hysteresis loss of about 1%. This again is supported by direct hysteresis measurements on similar steels (Brophy 1936). If this value is used to calculate the frictional resistance of real ball or roller bearings it yields values of the right order of magnitude ($\mu \approx 10^{-3}$).

Although the behaviour of real ball and roller bearings is complicated by many other factors, the elastic hysteresis loss described in this communication must play a fundamental part. It is well known that ball

and roller bearings fail by sub-surface fatigue (Jones 1946) rather than by surface abrasion but the source of the rolling resistance itself has long been a matter of speculation. The work described here shows that in rolling there is no 'friction' in the conventional sense of the word. The resistance to rolling is primarily due to hysteresis losses. A fuller account of this work and a more detailed discussion of its practical implications are being published elsewhere.

I wish to thank the Ministry of Supply (Air) for a research grant, Vauxhall Motors Limited for a grant for equipment, Dr. Schallamach of the British Rubber Producers' Research Association for providing samples of rubber, and Dr. F. P. Bowden for his continuous interest.

References

Allan, R. K., 1945, *Roller Bearings*, Pitman.
Brophy, G. R., 1936, *Trans. Amer. Soc. Metals*, **24,** 154.
Chevenard, P., 1943, *Rev. Mét.*, **40,** 289.
Eldredge, K. R., 1950, *Rev. Sci. Instr.*, **21,** 199.
Jones, A. B., 1946, *A.S.T.M.*, **46,** 'Metallographic Observations of Ball-bearing fatigue phenomena'.
Reynolds, O., 1875, *Phil. Trans.*, **166,** 1.

CVI. *The Inelastic Scattering of Fast Neutrons*

By M. J. Poole
Atomic Energy Research Establishment, Harwell, Berks.*

[Received July 8, 1952]

Abstract

An anthracene scintillation counter has been used as a spectrometer to measure the energy distribution of initially monokinetic neutrons scattered from iron and aluminium. In each case discrete groups of neutrons with reduced energy were found, showing that the scattering nucleus was being raised to its excited states. The differential cross section for scattering through 97° has been measured for the various processes.

§1. Introduction

The inelastic scattering of neutrons has been reported by many observers (Allen and Hurst 1940, Barschall and Ladenburg 1942, Barschall, Manley and Weisskopf 1947, Dunlap and Little 1941, Grahame and Seaborg 1938, Mandeville and Swann 1951, Stelson and Preston 1952, Whitmore and Dennis 1951 and others) but only in comparatively few cases has the method been capable of measuring the spectrum of the scattered neutrons (Dunlap 1941, Mandeville 1951, Stelson 1952 and Whitmore 1951) and in only one case has the resolution been so good that individual groups were reported (Stelson 1952).

§2. The Neutron Spectrometer

The chief difficulty in all inelastic scattering measurements is to find a satisfactory neutron spectrometer. During the following work an anthracene scintillation counter has been used in the manner already described by the author (Poole 1952). A cylindrical piece of anthracene 1 cm diameter by 0·5 cm high was cemented to the window of an E.M.I. type VX 5045 photomultiplier, and the pulse height spectrum arising from recoil protons in the anthracene was recorded with a 30-channel pulse analyser. To convert this into the energy spectrum of the recoil protons the theoretical expression derived by Birks (1951) for the relation between pulse height and energy in anthracene was used. The result of a run allowing the 2·5 Mev neutrons from the D–D reaction

* Communicated by the Author.

to fall directly on to the counter is shown in fig. 1. Figure 1 (*a*) shows the pulse height spectrum and fig. 1 (*b*) the energy spectrum of recoil protons. The neutron spectrum is given in terms of the proton spectrum by the relation

$$N(E) \propto \frac{E}{\sigma(E)} \frac{d}{dx} P(E),$$

where $N(E)$ is the neutron spectrum, $P(E)$ the proton spectrum and $\sigma(E)$ the n–p scattering cross section. The resolution at 2·5 MeV was found to be about ± 150 kev.

Fig. 1

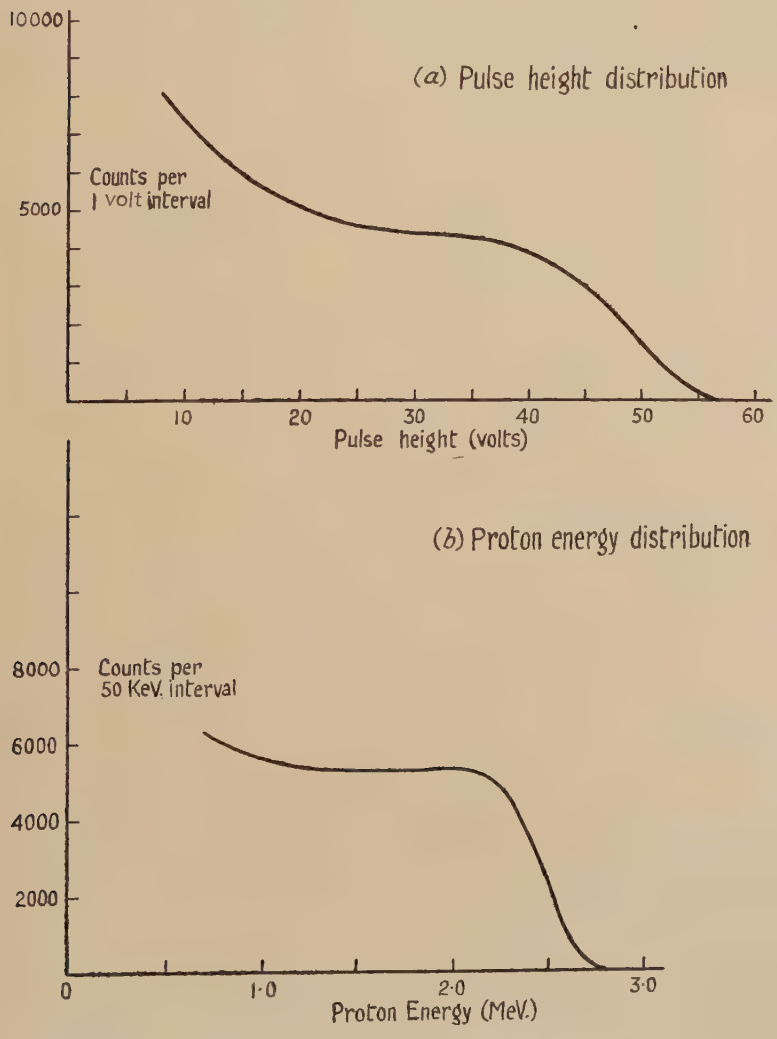

Response curves of an anthracene counter to D–D neutrons.

§3. Scattering Geometry

Before a scintillation counter of the type described can be used for scattering measurements, some method must be found to overcome its high sensitivity to γ-rays. Each neutron inelastically scattered leaves the target nucleus in an excited state which will usually decay to the ground state by γ-emission. Thus the number of γ-quanta from the scatterer itself will be of the same order of magnitude as the number of

Fig. 2

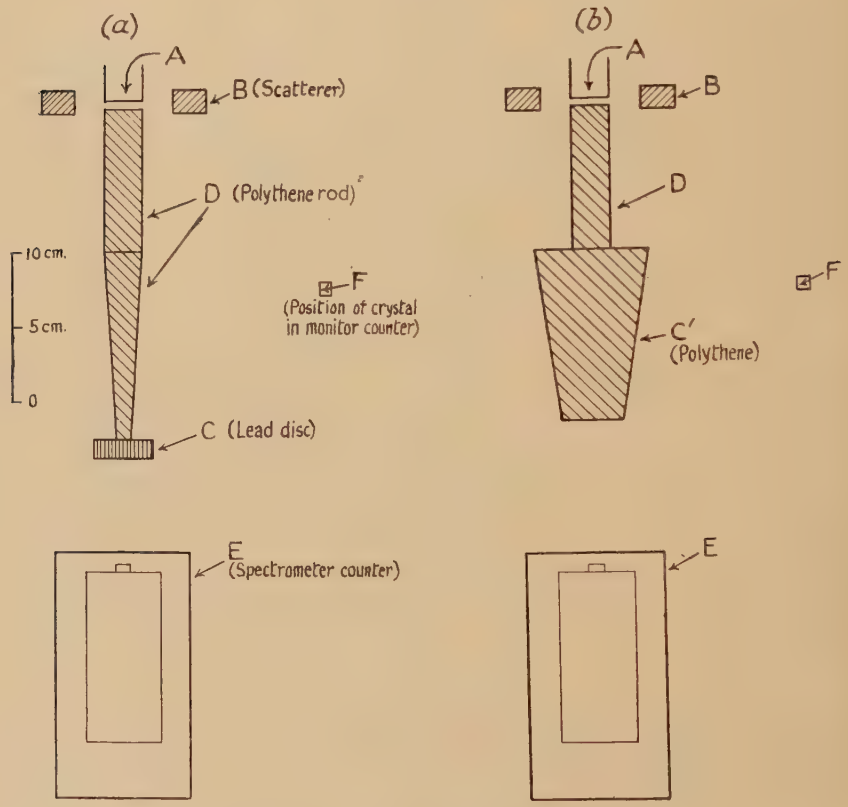

Diagram of the scattering apparatus.

scattered neutrons, and the counter sensitivity to, for example, a 1 MeV γ-ray is approximately equal to its sensitivity to a 2·5 MeV neutron. In addition there will be a background of capture and scattering γ-rays from all parts of the target room.

The way the γ-ray effect is eliminated is best seen from fig. 2. The target of the high-voltage machine is at A, and the D–D reaction was used to provide a monokinetic neutron source. As the target was thick, the scatterer (B) had to be placed in such a position that only the monokinetic neutrons emitted at 90° to the direction of the incident

deuteron beam were utilized, and it was therefore in the form of a ring placed round the target tube. Scattered neutrons were detected by the counter placed at E, directly below the neutron source, a polythene cylinder (D) preventing neutrons from reaching the counter directly from A. In addition either a 1-cm lead absorber (C, fig. 2 (*a*)) or an 11 cm polythene absorber (C′, fig. 2 (*b*)) could be placed in the path of the neutrons scattered from B into E. A second scintillation counter was placed at F to give a count proportional to the neutron emission from A during any run.

To obtain the distribution of recoil protons caused by scattered neutrons from B two runs were taken, one with the lead (C) in place and one with the polythene (C′). The difference between these is due only to neutrons from B if three conditions are satisfied. Firstly, the transparency of C and C′ to γ-rays must be equal at all γ-ray energies; secondly, the general background of pulses caused by γ-rays and neutrons

Fig. 3

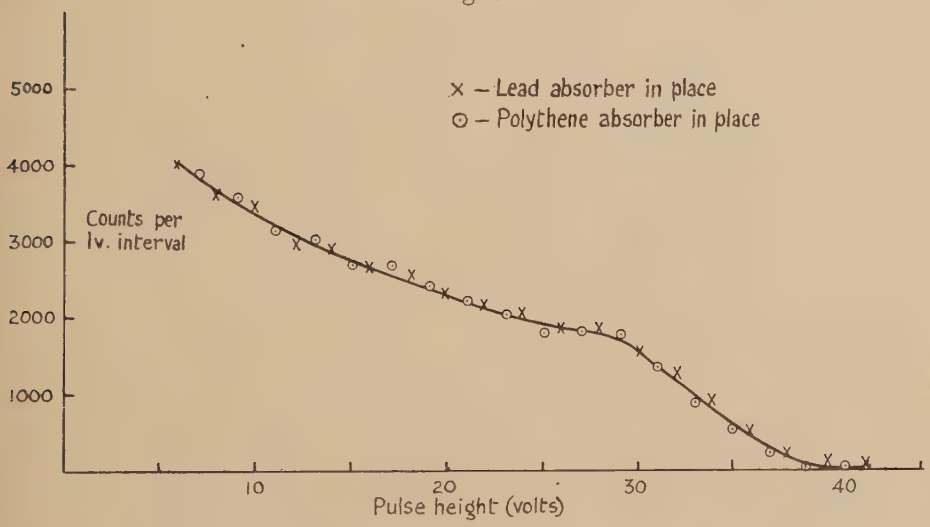

Response curve of the counter to γ-rays from ^{60}Co.

from the target room shall be unaltered when the lead and polythene are interchanged, and thirdly, the total neutron cross section for lead must be sensibly constant over the range of neutron energy concerned.

The first condition cannot be satisfied exactly for all γ-ray energies below 2·5 MeV, largely because of the effect of photoelectric absorption in the lead. In order to assess the error from this cause, the 'effective' sensitivity of the counter to γ-rays when used in the way described has been calculated as a fraction of its direct sensitivity. The γ-ray absorption coefficients were taken from the work of Cowan (1948), and the lengths of the absorbers were chosen so as to make their transparencies exactly equal at 1·2 MeV. The result of this calculation showed the residual γ-sensitivity to be 3% or less of the direct sensitivity in the range

0·8 MeV to 3·0 MeV, rising to 5% at 0·6 MeV. To check that interchanging the lead and paraffin absorbers did not alter the shape of the pulse-height distribution from γ-rays a trial run was made with a ring of ^{60}Co sources

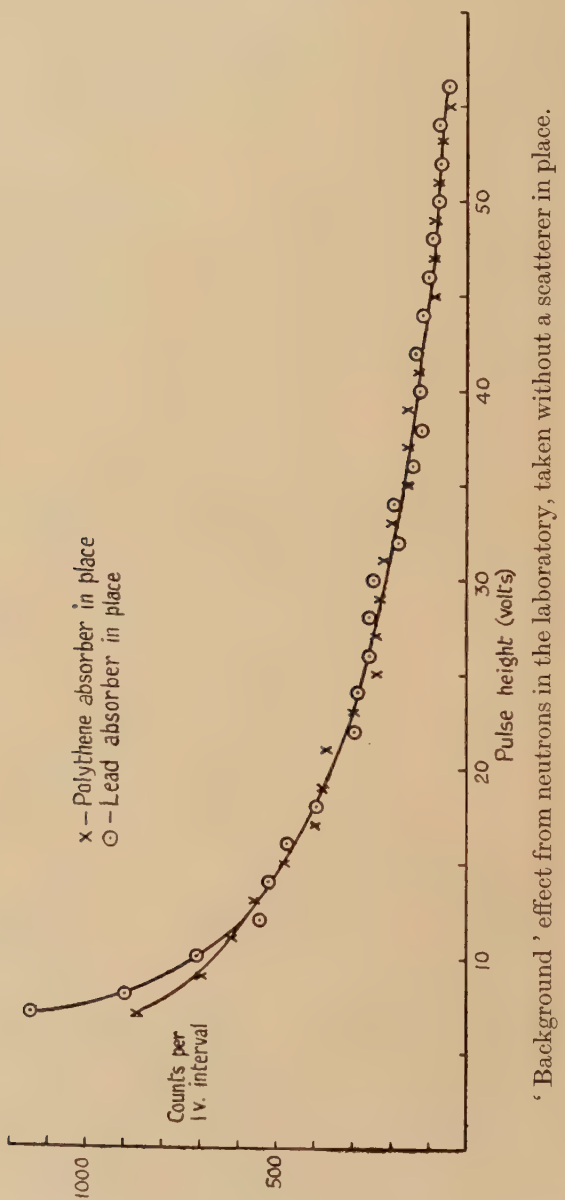

Fig. 4

'Background' effect from neutrons in the laboratory, taken without a scatterer in place.

substituted for the scatterer B. This same run was used to adjust the length of the polythene absorber to give equal transparencies, and the result, after this adjustment had been made is shown in fig. 3.

The validity of the second assumption was checked by making runs without ring B in place, the results of which are plotted in fig. 4. The agreement of the two sets of points is satisfactory provided that no use is made of any points below 10 v bias (0·8 MeV energy). Finally, the third assumption was checked by making use of the figures published for the total cross section of lead (Adair 1950). This cross section varies smoothly from 5·4 barns at 0·8 MeV neutron energy to 5·2 barns at 2·5 MeV, giving a variation of neutron attenuation from 17·8% to 17·2% in the lead disc.

§4. Experimental Procedure

For each run the following operations were carried out :—

1. Counter E was placed at a known distance from the target, in a direction at 90° to the beam, and a pulse-analyser run made during the arrival of 5.10^3 monitor counts. This run served as an energy calibration for counter E and also related the sensitivity of the monitor (F) to that of E, which was needed to calculate the scattering cross section from the results.

2. Counter, scatterer, polythene rod and lead absorber were set up as in fig. 2 (*a*) and a pulse analyser run taken during the arrival of 5.10^4 monitor counts.

3. The polythene absorber was substituted for lead, as in fig. 2 (*b*) and the run repeated.

4. The channel widths of the pulse analyser were measured with a precision pulse generator.

The last three operations were repeated about six times to reach the statistical accuracy required, and then the spectrum of recoil protons in the counter crystal, due to scattered neutrons from B (fig. 2) was obtained from the difference between 2 and 3 by correcting for the non-linear response of anthracene to protons. To derive the neutron spectrum two methods were used. In the case of runs made with an iron scatterer (fig. 5) a smooth curve was drawn through the recoil proton energy distribution, this curve differentiated and the neutron spectrum calculated from the differential coefficient. In the case of the aluminium runs (fig. 6) where the shape of the proton recoil curve was not so clear, it was felt that this procedure might lead to too much personal error, and an arithmetical method was used. Groups of five points were taken ($\sim$200 kev energy interval) and the gradient of the best straight line through these points determined by a least squares method. These values were then used to determine the neutron spectrum plotted in fig. 6 (*b*). This procedure corresponds to taking the mean gradient of protons over an interval of $\pm$100 kev, each side of the point required, which has some justification as the resolution of the counter is known to be not better than $\pm$150 kev, and any fluctuations in gradient within this range are therefore legitimately ascribed to statistical deviations, and may be smoothed out.

§ 5. Results

1. *Iron Scatterer*

Figure 5 shows the proton recoil spectrum and the spectrum of scattered neutrons derived from this. Two groups of neutrons are clearly resolved, one at 2·35 Mev and the second at 1·55 Mev. The higher group

Fig. 5

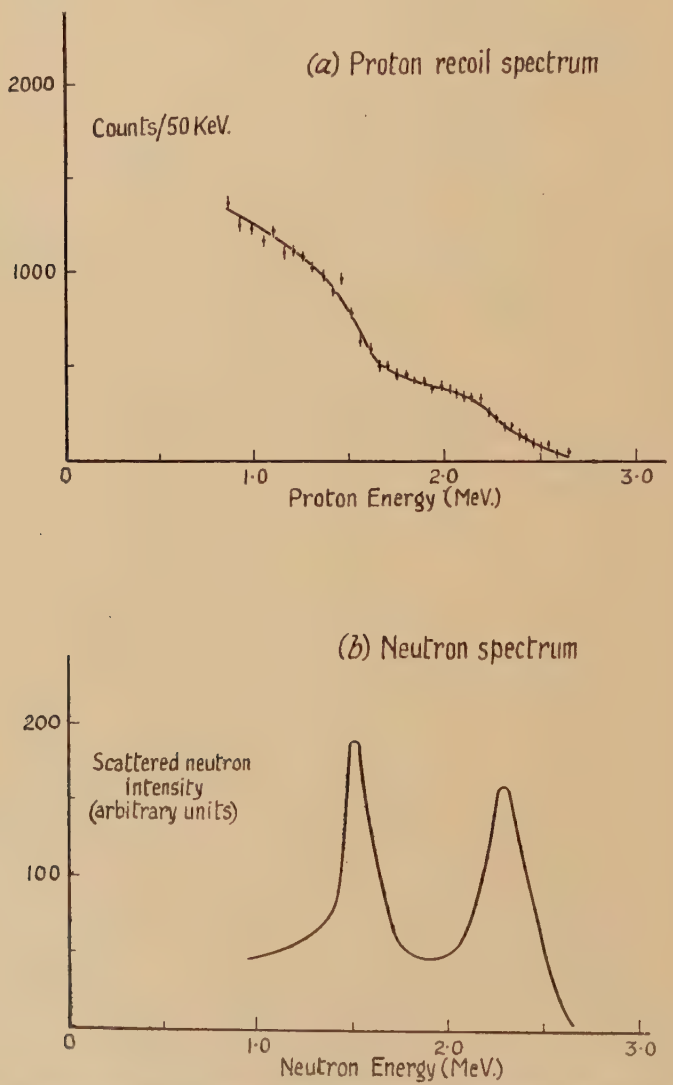

Results of scattering D–D neutrons from iron. Incident energy ~2·4 Mev.

corresponds to elastic scattering of the incident neutrons (mean energy 2·4 Mev), while that at 1·55 Mev may be attributed to inelastic scattering, leaving the iron nucleus excited to a level at $0{\cdot}8 \pm 0{\cdot}1$ Mev. This is in

agreement with the work of Stelson and Preston (1952) who report a level at $0{\cdot}85 \pm 0{\cdot}05$ MEV, and with the measurements of Elliott and Deutsch (1943) who find a level at 0·845 MEV in ^{56}Fe, by observations on the radioactivity of ^{56}Mn, and at 0·82 MEV by observations on ^{56}Co.

Fig. 6

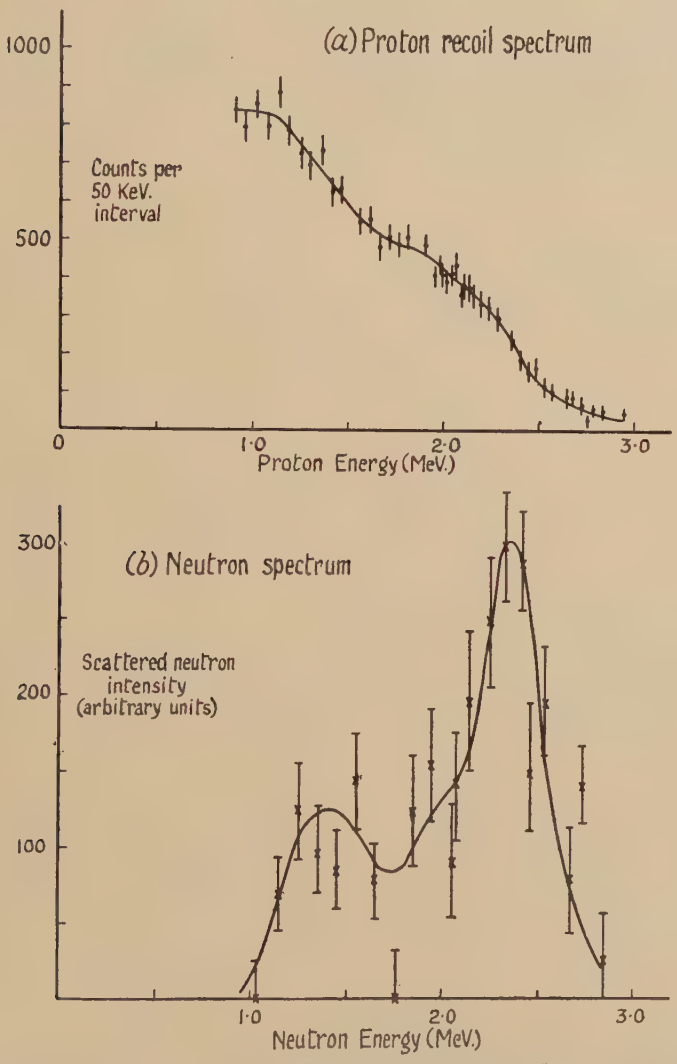

Results of scattering D–D neutrons from aluminium. Incident energy ~2·4 MEV.

2. *Aluminium Scatterer*

Figure 6 shows the proton and neutron spectra for scattering from aluminium. There is a neutron group at 1·5 MEV, and a second group, ascribed to elastic scattering, at 2·3 MEV. Between these two is possibly a third group at 1·95 MEV.

The group at 1·5 MeV corresponds to an excitation of the residual nucleus of 0·9 MeV. This must be compared with the results of Reilley *et al.* (1952) on inelastic scattering of protons, giving levels at 0·81 and 0·99 MeV excitation, and also with the γ-spectra of Hedgran, Hole and Benes (1948) and of Itoh (1941), who place the levels of ^{27}Al at 0·84 MeVs and 1·85 MeV. The level found here at 0·9 MeV is not in disagreement with this, particularly when it is remembered that two levels at 0·81 and 0·99 MeV would certainly not be resolved. The neutron group at 1·95 MeV, if present, would correspond to a level at 0·35 MeV excitation, which has not appeared yet in either the proton scattering or the γ-spectrum work, but it is not sufficiently clearly resolved here to be certain that it is present.

3. *Cross Section Values*

The differential cross section for scattering 2·5 MeV neutrons through 97° has been calculated for the various processes. These are tabulated below.

Element	Elastic	Inelastic	Comments
Iron	0·10±1·01 barns/ steradian	0·08±0·02 barns/ steradian	With 0·8 MeV energy loss
Aluminium	0·13±0·03 barns/ steradian	0·05±0·02 barns/ steradian	With 0·9 MeV energy loss.

As the total cross section for iron at 2·5 MeV is 2·8 barns, and that for aluminium 2·5 barns, these figures seem high when it is remembered that a large proportion of scattering is commonly said to be potential scattering into the forward angles, but in the absence of any information concerning angular distributions, no definite conclusions can be drawn.

Acknowledgments

The author wishes to thank the Director, A.E.R.E., Harwell, for permission to publish this paper, Dr. E. Bretscher for his continued interest in the work, and Mr. W. Howe who carried out much tedious counting with the pulse analyser.

References

Adair, R. K., 1950, *Rev. Mod. Phys.*, **22**, 3.
Allen, W. D., and Hurst, C., 1940, *Proc. Phys. Soc.*, **52**, 501.
Barschall, H. H., and Ladenburg, R., 1942, *Phys. Rev.*, **61**, 3.
Barschall, H. H., Manley, J. H., and Weisskopf, V. F., 1947, *Phys. Rev.*, **72**, 10.
Birks, J. B., 1951, *Proc. Phys. Soc.* A, **64**, 10.
Cowan, C. L., 1948, *Phys. Rev.*, **74**, 12.
Dunlap, H., and Little, R. N., 1941, *Phys. Rev.*, **60**, 10.

Elliott, L. G., and Deutsch, M., 1943, *Phys. Rev.*, **64,** 321.
Grahame, D. C., and Seaborg, G. T., 1938, *Phys. Rev.*, **53,** 695.
Hedgran, A. G., Hole, N., and Benes, , 1947, *Arkiv. f. Mat. Astr. o. Fys.*, **34B**, 19.
Itoh, Z., 1941, *Proc. Phys. Math. Soc. Japan,* **23,** 405.
Mandeville, C. E., and Swann, C. P., 1951, *Phys. Rev.*, **84,** 214.
Poole, M. J., 1952, *Proc. Phys. Soc.* A, **65,** 453.
Reilley, E. M., Allen, A. J., Arthur, J. S., Bonder, R. S., Ely, R. L., and Hausmann, H. J., 1952, *Phys. Rev.*, **85,** 4.
Stelson, P. H., and Preston, W. M., 1952, *Phys. Rev.*, **86,** 132.
Whitmore, B. G., and Dennis, G. E., 1951, *Phys. Rev.*, **84,** 296.

CVII. *The Natural Radioactivity of Rubidium*

By G. M. Lewis
Department of Natural Philosophy, The University, Glasgow*

[Received July 28, 1952]

Abstract

The radioactive decay of ^{87}Rb has been studied using the scintillations from a crystal of rubidium iodide activated with thallium, some fluorescent properties of which are described. This method free from source absorption and scattering troubles, indicates a β-spectrum with an end point of 275 kev. The Fermi plot gave a forbidden shape, for the most part close to that given by recent proportional counter work using 2π geometry, but having slightly more counts at the high energy end, and fewer at the low energy end; the half-life has been determined at $(5{\cdot}90\pm0{\cdot}3)\times10^{10}$ years. The theoretical interpretations are indicated.

§1. Introduction

The exact nature of the decay process of ^{87}Rb has been in dispute. Conversion peaks were reported by Ollano (1941) and β-e coincidences by Haxel, Houtermans, and Kemmerich (1948). Curran, Dixon and Wilson (1951) using a proportional counter to determine β-ray shape found no evidence of conversion lines, and McGregor and Wiedenbeck (1952) have recently shown electron–electron coincidences unlikely. The end point which was thought by Libby and Lee (1939) to be 130 kev has been more recently specified at 270–275 kev (cf. Bell, Cassidy and Davis 1950, and Curran, Dixon and Wilson 1951). Several estimates of lifetime have been made, generally dependent on correction factors; and recent values lie in the neighbourhood of 6×10^{10} years.

In view of the various results, and considering the methods to date, it was felt that an investigation using an activated crystal of rubidium iodide would help in several ways, providing suitable scintillations could be obtained. The absence of self-absorption and back-scattering errors would make this 4π-method especially suitable for estimating lower energy particles without distortion, and also for yielding an estimate of lifetime. Further the higher energy particles would be counted fairly completely in a crystal; and the radiation background could be made negligible.

§2. General Method, Properties of the Crystals and Calibration

A few grams of rubidium iodide activated with 0·5% thallium iodide were placed in a quartz container which was evacuated near the melting point of the mixture and sealed. The whole was made to traverse a

* Communicated by Professor P. I. Dee, F.R.S.

temperature gradient which permitted melting and slow cooling to room temperature. Transparent, glassy crystals were obtained, relatively free from hygroscopic tendencies.

Such a crystal was mounted in paraffin on an E.M.I. multiplier type VX 5032 and covered by an aluminium reflector. The system was enclosed by a two-inch thickness of lead. The amplified pulses led into a single channel 'kicksorter', activated by a gating unit normally triggered by the pulse itself. The pulses observed under γ-ray bombardment were of height $\frac{1}{6}$ those of thallium activated sodium iodide, and had a rise time better than about 1 μ sec. It was early observed however that a phosphorescence decay was also produced lasting the order of a millisecond. Crystals prepared with considerably less than 0·5%, and with 2% of thallium iodide also showed this phosphorescence. To investigate and avoid this radiation, a paralysis circuit, fed by a discriminator, could be used to operate the gating unit of the kicksorter. It was found that the phosphorescence had no ill effect except in studying the very low energies, where it gave, in the absence of paralysis, spurious counts. At the lowest energies paralysis of order 1–3 milliseconds enabled the investigation to be carried out to regions where the tube noise became a final barrier.

The main pulse was shown to vary linearly with energy for electrons moving in the crystal, over a range 17 kev–630 kev, using various x- and γ-rays and higher energy electrons. Calibration was effected using the fluorescent Kαx-rays of molybdenum, the fluorescent Kx-rays of silver, ^{114}In (Kx and conversion electrons), RaD (46·7 kev γ-ray), ^{203}Hg (Kx and γ-ray), ^{137}Cs (conversion electrons). Calibration with x- and γ-rays generally involves production of a photoelectron and subsequent capture of the associated x-ray. This would imply linearity of calibration here some kev below the figure of 17 mentioned above.

§3. Results

The pulse height distribution using a crystal 4 mm × 4 mm × $2\frac{1}{2}$ mm is shown in fig. 1. The curve is composed of three sets of points. The amplifier gain was greater for the two sets at lower energy. The points indicated by triangles were obtained using paralysis—other points (omitted for clarity of drawing) at higher energies using paralysis fell on the curve drawn. Reliable calibration was not readily possible below ~17 kev, but one point has been included in fig. 1, below this (viz., at ~13 kev) assuming the linear energy relation to continue.

The curve of fig. 1 reaches background just after 300 kev, but the character of the curve appears to alter at about 250 kev, indicating an end point near 275 kev. The straggle here is due to the resolving power of the crystal—the ^{203}Hg γ-ray peak at 280 kev had half width at half height ~15%. The value of 275 kev is confirmed from the Fermi plot below. The curve is smooth in form and further intermediate points have been taken which support this view. This confirms the

absence of conversion peaks and γ-rays in the range investigated. With 4π geometry, these would appear as part of an integrated spectrum (cf. Bannerman, Lewis and Curran 1951). Preliminary work with another

Fig. 1

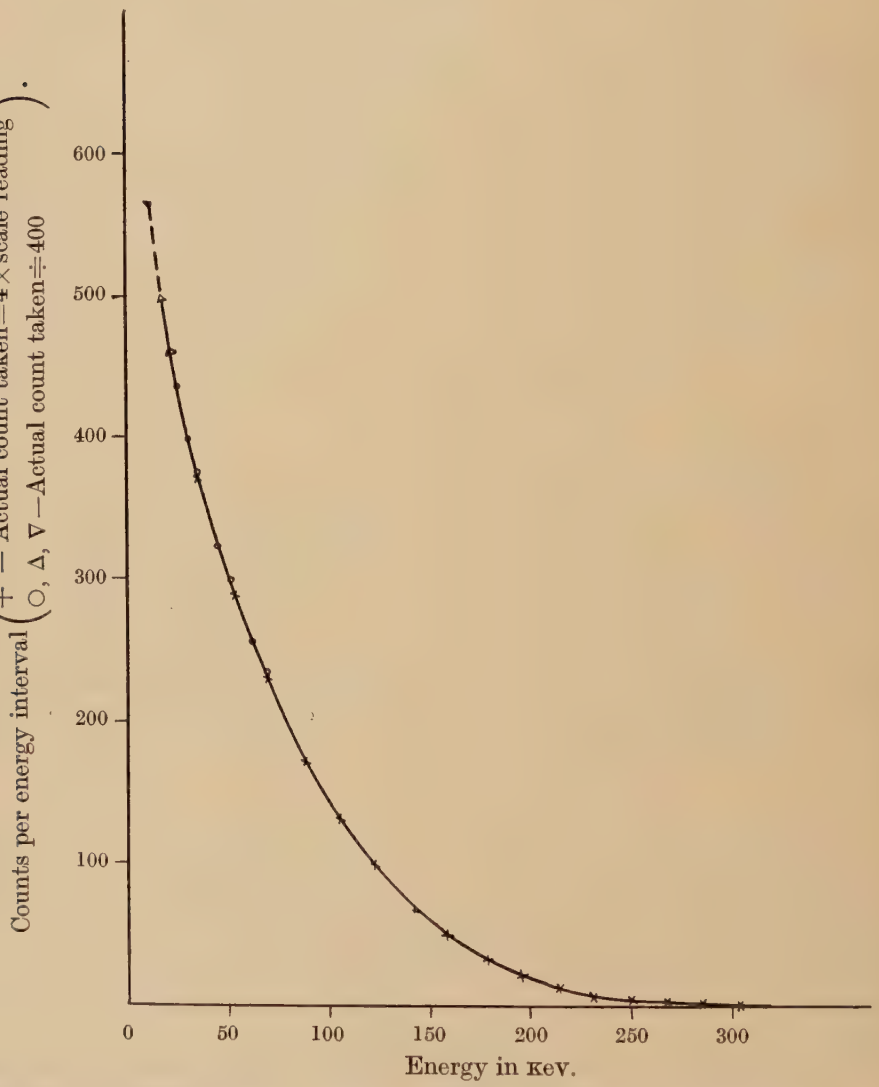

Spectrum of ^{87}Rb obtained using an activated rubidium iodide crystal. × Amplifier at low gain ; ○, Δ, ∇ amplifier at higher gain (points Δ, ∇ were taken in runs with paralysis ; point ∇ involves slight extrapolation of linear calibration).

crystal gave similar results. It should be pointed out here that Curran, Dixon and Wilson (1951) could find no evidence of K and L x-rays in their investigation.

The energy distribution $N(W)\,dW$ can be written :—

$$N(W)\,dW = CF(W, Z)(Wo - W)^2(W^2-1)^{1/2}W\,dW - (1),$$

where Wo is the maximum energy and $F(W, Z)$ is the Coulomb correction factor ; C is constant for allowed transitions, but is more generally, energy dependent. The Fermi plot given by

$$\{N(W)/F(W, Z)(W^2-1)^{1/2}W\}^{1/2}$$

is shown in fig. 2, where the Bethe–Bacher approximation has been used for $F(W, Z)$. Points in the straggle area have been omitted. The Fermi plot indicates an end point of 275 kev. The curve shows good agreement over most of the energy range with the proportional counter curve shown

Fig. 2

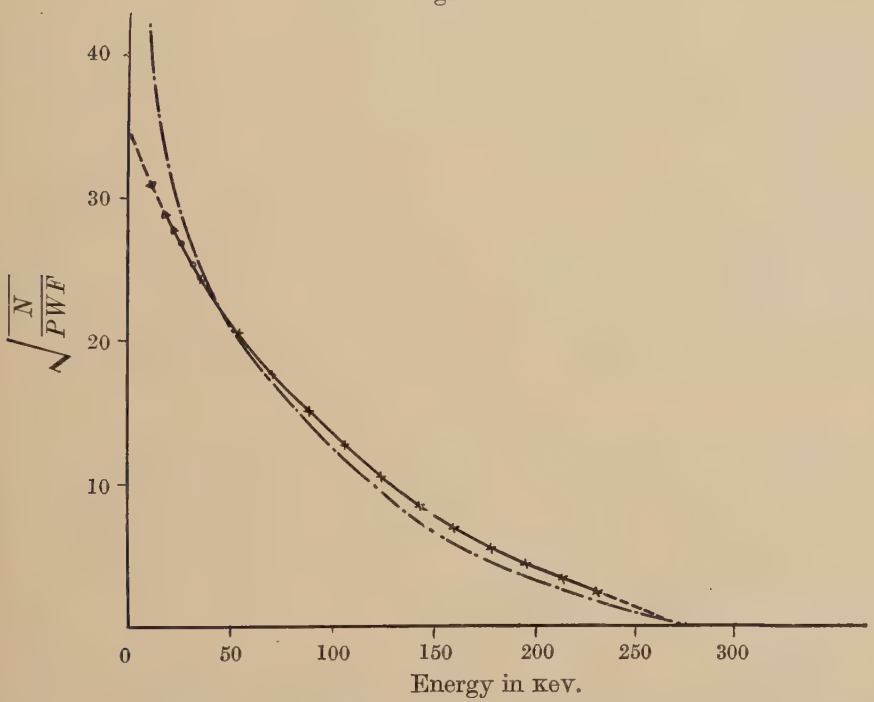

Solid curve —Fermi plot of ^{87}Rb β-spectrum obtained with activated rubidium iodide crystal. .—.—. Fermi Plot obtained by Curran, Dixon and Wilson (1951) with the proportional counter.

for comparison in fig. 2. There are slightly more counts at the higher energy. This is to be expected as these particles are absorbed fairly completely in the crystal and not so well in the gas counter. There are less counts at the lower energy. This is due to the absence of back scattering, and also to the lower resolution of the crystal method at these energies.

The total count above 17·4 kev has been determined using various paralysis times in the neighbourhood of 0–3 milliseconds. Allowing for

loss of proper counts through coincident arrival within the paralysis time, the crystals of weight 0·1487 gm gave a total count above this energy of 1975/min. To estimate the overall counts, extrapolation of the Fermi plot along the dotted line to zero energy is necessary, involving an additional 600 counts/min. A half life figure of $(5{\cdot}90 \pm 0{\cdot}3)10^{10}$ years is obtained when the ^{87}Rb abundance figure is taken as 27·2%.

§4. Discussion

With an end point energy of 275 kev and half life of $5{\cdot}90 \times 10^{10}$ years, log ft.=17·5, and the transition $^{87}\mathrm{Rb} \rightarrow {}^{87}\mathrm{Sr}$ is third forbidden. The nuclear spin change between the ground states, $3/2 \rightarrow 9/2$, accords with this. According to the nuclear shell model, the transition, $\mathrm{p}3/2 \rightarrow \mathrm{g}9/2$, involves a parity change. Theoretical correction factors (involving C of eqn. (1)) to the Fermi plot shape have been formulated by Greuling (1942). Pseudoscalar interaction ($3P$) is eliminated on parity considerations. Calculation shows that scalar interaction ($3S$) does not explain the ^{87}Rb plot either. Generally the correction factors involve knowledge of certain nuclear matrix elements ; Tomozawa, Umezawa and Nakamura (1952) have recently shown that this type of plot for ^{87}Rb could be given by and only by polar vector ($3V$) or tensor ($3T$) interaction. Their theoretical data, involving one chosen parameter, has been derived for the region 50–280 kev, and gives good fits with both the experimental curves of fig. 2 ; thus division of the ordinates of points on these curves by the root of their correction factor ($\sqrt{C}$) gives approximately linear plots.

Acknowledgments

The author wishes to thank Dr. S. C. Curran for his suggestions commending the method and for discussions, also Mr. J. T. Lloyd for his help in connection with the growing of the crystals, and Prof. P. I. Dee for his interest in the work.

References*

Bannerman, R. C., Lewis, G. M., and Curran, S. C., 1951, *Phil. Mag.*, **42**, 1097.
Bell, P. R., Cassidy, J. M., and Davis, R. C., 1950, *Nuclear Data*, Supp. 1. N.B.S. Circular, **499**, 20.
Bethe, H. A., and Bacher, R. F., 1936, *Rev. Mod. Phys.*, **8**, 194.
Curran, S. C., Dixon, D., and Wilson, H. W., 1951, *Phys. Rev.*, **84**, 151.
Greuling, E., 1942, *Phys. Rev.*, **61**, 568.
Haxel, D., Houtermans, F. G., and Kemmerich, M., 1948, *Phys. Rev.*, **74**, 1886.
Libby, W. F., and Lee, D. D., 1939, *Phys. Rev.*, **55**, 245.
McGregor, M. H., and Wiedenbeck, M. L., 1952, *Phys. Rev.*, **86**, 420.
Ollano, Z., 1941, *Il Nuovo Cimento*, **18**, 11.
Towozawa, Y., Umezawa, M., and Nakamura, S., 1952, *Phys. Rev.*, **86**, 791.

* Some results of this investigation have been mentioned by Dr. S. C. Curran at the Physical Society Conference at Glasgow, July, 1952.

CVIII. *The Deformation of Silver at High Temperature*

By A. P. Greenough*
Royal Aircraft Establishment, Farnborough, Hants.†

[Received June 19, 1952]

Summary

The deformation of silver wires at high temperatures and low applied stresses has been investigated experimentally. Considerable evidence has been obtained that the crystal grains in the wires deform by the self-diffusion mechanism postulated by Nabarro and considered in detail by Herring (1950). A new explanation of the development of kinking is advanced to account for the experimental observations. It is shown that surface energy effects can give rise to offsetting in a direction which causes the wires to shorten.

§1. Introduction

In a recent theoretical paper on the deformation of polycrystalline solids at high temperatures under small stresses, Herring (1950) considered in detail the case of wires in which the crystal grains occupied the entire cross-section. He suggested that in this case the grains themselves would deform by the self-diffusion mechanism proposed by Nabarro (1948), the migration of vacant sites through the crystal lattice effectively transporting material in the opposite direction. Assuming that the external surfaces and grain boundaries could act as sources or sinks of vacant lattice sites, he derived an expression for the magnitude of this effect which compared favourably with existing experimental observations.

In addition, he predicted that offsetting and kinking of the wires would take place under certain conditions. Offsetting is produced when slip occurs in the plane of a grain boundary whose normal is inclined to the wire axis. Herring considered that this effect would be observed only when the applied stress was somewhat larger than that necessary to prevent the shortening of a long grain under its own surface energy. Kinking, or the development of an angle between the axes of adjacent grains in the wires, could be produced in two ways. A relative rotation of two grains about an axis normal to the wire axis would give rise to kinking, but Herring considered that this process would be slow. Secondly, the anisotropy of grain boundary energy could cause the relative rotation of two grains about a normal to a plane grain boundary inclined to the wire axis. This would produce a kink, and also an axial twisting of the wire, but since no transport of matter would be required, the rate at which the kink developed might be faster than that of the first process.

* Communicated by the Author.
† Now at Metallurgy Department, University College, Swansea.

The deformation of copper wires at high temperatures has been studied by Udin, Shaler and Wulff (1949). Alexander, Dawson and Kling (1951), working with gold, reported a lack of reproducibility of strain measurements on their wires, which they attributed to kinking, to offsetting, and to the necking which developed in some of their wires. Recently, the surface ' tension ' of the solid metals has been estimated from observations on wires by Funk, Udin and Wulff (1951) for silver, and by Buttner, Udin and Wulff (1951) for gold. Buttner, Funk and Udin (1952) investigated the mechanism of deformation of gold wires, and showed that the diffusion mechanism would account for the creep observed at stresses less than about $5{\cdot}5\times10^5$ dynes/cm^2, but that above this stress an additional slip mechanism occurs. They reported the development of kinks and offsets in their wires, but failed to observe the bulging and necking reported by Alexander, Dawson and Kling, and observed no axial rotation of the wires at the grain boundaries.

§2. Experiments on Polycrystalline Specimens

In these experiments, the specimens resembled the copper specimens of Udin, Shaler and Wulff. They were prepared from cold-drawn silver wire of 42 s.w.g. (0·01016 cm diam.) supplied by Johnson Matthey and Co. Ltd., who estimated the purity to be greater than 99·999%. A knot was tied in the wire at one end, and the wire cut at a measured distance from this knot. A second knot was tied about 10 cm below the first, and the remainder of the wire coiled to form a weight. The knots were arranged to be as nearly as possible in the same plane, so that any appreciable twisting of the wire about its axis could be observed.

After being straightened as far as possible by hand the specimens were hung on silver supports and lowered into a vertical silica tube furnace in which an atmosphere of oxygen-free nitrogen, purified as already described (Greenough and King 1951), was then established. The specimens were first annealed for $1\frac{1}{2}$ hours at the temperature of test. When cool, the wires were raised out of the furnace and examined, the gauge length being measured by a travelling microscope, and the relative planes of the knots noted. These observations were repeated at the end of each successive annealing treatment.

(a) *Kinking*

At the end of the preliminary annealing treatment the wires were quite straight. Subsequently kinks developed, and became apparent in all specimens when the strain exceeded about $\pm0{\cdot}1\%$, but no appreciable axial twisting of the specimens was observed during this process.

It was found that the grain boundaries in the wire could be seen because of the thermal etching which took place in the furnace. If the wire was mounted on a glass slide and examined microscopically with a 4 mm objective and the illumination coming from behind, enough light was reflected by the surface of the objective to enable the grain structure

of the wire to be seen. Simultaneously the outline of the wire was seen against bright ground (figs. 2, 3, 4 and 7, Plates LXIX and LXX).

Although the grains generally occupied the whole cross-section of the wire, a small number occupied only a part of the cross-section, producing a forked grain boundary as shown in figs. 2 and 3. In these cases, there are two grain boundaries on one side of the specimen, but only one on the other. Thus one side of the specimen will tend to deform at twice the rate of the other if the grain boundaries are acting as sources or sinks of the diffusion currents, and a kink will tend to develop. In wires which are shortening under surface energy effects, the small grain will be on the concave side of the kink (fig. 2), but on the convex side if the wire is increasing in length (fig. 3). The stresses set up in the wire below the kink could cause kinking in the opposite direction to take place at plane grain boundaries as shown at B in fig. 1. In all cases, the angle of kink is limited.

Fig. 1

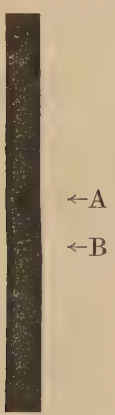

×50

After 85 hours at 920° c.
Wire shortening.

Fig. 6

×50

After 61 hours at 920° c.
Wire extending.

When the wire is contracting, the equilibrium angle of kink is reached when the reduction in energy due to the destruction of the wire surface on the inside of the kink is balanced by the increase in energy due to the raising of the centre of gravity of the wire below. When the wire is extending under the applied load, energy is required to create the extra surface on the outside of the kink and this must come from the lowering of the centre of gravity of the wire below, which occurs only when the angle of kink is small. It appears that the kinks in gold wires illustrated by Alexander, Dawson and Kling can be explained on the basis of this theory. As no axial twisting of the wires was noticed during the development of the kinks, it seems unlikely that either of the rotation mechanisms postulated by Herring leads to the development of kinks to any appreciable extent.

(b) *Offsetting*

The offset shown in fig. 4 cannot have developed by the mechanism postulated by Herring since the direction of offsetting is such as to raise the weight of material under the plane of slip. However, slip must have taken place since the centre-line of the wire is offset. Consider a grain boundary inclined to the axis of the wire, shown in section in fig. 5 (*a*). At equilibrium in the absence of an applied stress, the plane of the grain boundary bisects the angle between the two external surfaces (Chalmers, King and Shuttleworth 1948, Greenough and King 1951). Thus equilibrium could be attained either by the development of bulges (fig. 5 (*b*)), or by slip taking place in the plane of the boundary, as indicated in fig. 5 (*c*). Of these two processes, the latter results in a final state of lower energy than the former, since the resultant increase in external surface area is less and the grain boundary area has decreased. This is the situation in fig. 4 where the load on the wire was very small compared with the surface energy effects.

Fig. 5

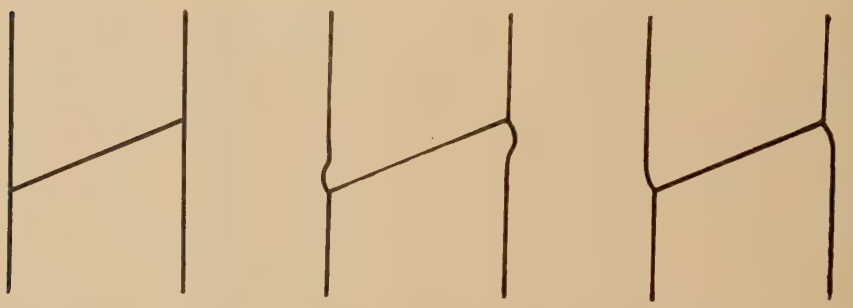

(*a*) No equilibrium. (*b*) Equilibrium. No offsetting. (*c*) Equilibrium. Offsetting.

As the tensile stress in the wire increases, there will be an increasing tendency for slip on the plane of the boundary to increase the length of the wire (figs. 6 and 7), until, as Herring points out, the tensile stress is sufficient to provide the energy necessary for the grain boundary to become two external surfaces. At a stress of this magnitude, or greater, no equilibrium is possible and the two grains could slide apart at the grain boundary.

(c) *Necking*

Wires which broke under the applied stress usually showed a series of necks near the fracture. Each neck occurred at a grain boundary, as would be expected if the grain boundaries were serving as sources for the vacant lattice sites. A crystallographic slip mechanism (Cottrell and Jaswon 1949) would be expected to lead to necking at the centre of the grains. No bulging was observed in any of the specimens.

(d) *Rate of Strain*

For a wire of radius r, and plane grain boundaries normal to the axis of the wire spaced a distance L apart, Herring derived an expression (his eqn. 16) from which the rate of strain under a given stress may be calculated. Using the data of Hoffman and Turnbull (1951) for the self-diffusion coefficient of silver, this reduces to :

$$\text{Strain rate} = 2{\cdot}05 \times 10^{-18}\, S/Lr, \text{ per sec}, \quad . \quad . \quad . \quad . \quad (1)$$

for silver wire at 920° c, when $L \geqslant 2r$, and S is the applied stress, corrected for surface energy effects (Udin 1951), in dynes/cm^2.

Much quantitative data was obtained on the strains shown by wires, but the reproducibility of the results was poor. Specimens heated simultaneously, and the same specimen on two successive heats, would show very different strain rates. The values of the surface energy of silver given by successive experiments with the same specimens steadily increased so that the final value would be two or three times the original. These effects may have been due to temperature variations, since an increase in temperature of 10° c increases the strain rate by about 17%. There was evidence to suggest that specimens heated simultaneously were not all at the same temperature, and it was known that the temperature of the furnace was not constant over long periods. However, it seems unlikely that this was the main cause, for with very good temperature control, the results obtained for gold by Buttner, Funk and Udin also show poor reproducibility, as can be seen from their figs. 2 and 3.

It is nevertheless interesting to note that the average strain rates observed in the silver wires agreed with those predicted by Herring. Table 1 gives the strain measurements on nine similar specimens. Other experiments indicated that the surface energy of silver at 920° c was 1 500 ergs/cm^2 $\pm$ 50%, a value in agreement with that obtained by Funk, Udin and Wulff. Thus, in eqn. (1), S is $-22{\cdot}0 \times 10^4$ dynes/cm^2, and the calculated strain rate is $-3{\cdot}00 \times 10^{-9}$ per sec, compared with the observed rate of $-7{\cdot}61 \times 10^{-9}$ per sec. In a second experiment the calculated strain rate was $-5{\cdot}02 \times 10^{-9}$ per sec, and the observed strain rate $-10{\cdot}6 \times 10^{-9}$ per sec.

The agreement between the experimentally observed and the theoretically predicted strain rates is satisfactory, when the accuracy of the experimental data and the nature of the theoretical calculations are considered. The expression used to calculate strain rate takes no account of kinking, offsetting, and the departure of some of the grain boundary shapes from the ideal transverse planes, all factors which would increase the calculated strain rate.

The strain rate observed in copper wires by Udin, Shaler and Wulff was greater than the calculated strain rate by a factor of four to ten. In gold wires, the observed strain rate was about 30% less than the calculated strain rate (Buttner, Funk and Udin 1952).

Table 1. Strain Measurements

Total length of wire below top knot was 10·0 cm in all specimens

Specimen	Initial gauge length cm	Change in gauge length after each annealing treatment cm						Total change after 741 hr. cm	Strain after 741 hr.	Average grain length cm
		37 hr.	112½ hr.	114½ hr.	89½ hr.	300 hr.	87½ hr.			
1	8·899	−0·013	−0·052	−0·024	−0·017	−0·056	−0·021	−0·183	−0·0207	0·0295
2	8·842	−0·016	−0·023	−0·019	−0·011	−0·060	−0·028	−0·157	−0·0178	0·0303
3	8·919	−0·023	−0·038	−0·029	−0·010	−0·067	−0·031	−0·198	−0·0222	0·0335
4	8·743	−0·025	−0·055	−0·033	−0·022	−0·077	−0·020	−0·232	−0·0265	0·0306
5	8·991	−0·011	−0·035	−0·031	−0·010	−0·063	−0·029	−0·179	−0·0199	0·0270
6	8·707	−0·010	−0·037	−0·025	−0·017	−0·073	−0·017	−0·179	−0·0205	0·0257
7	8·594	−0·010	−0·037	−0·019	−0·009	−0·069	−0·020	−0·164	−0·0191	0·0286
8	8·410	−0·019	−0·015	−0·022	−0·006	−0·044	−0·015	−0·121	−0·0144	0·0316
9	8·365	−0·029	−0·039	−0·033	−0·008	−0·071	−0·025	−0·205	−0·0219	0·0305
Average	8·719								−0·0203	0·0297

Temperature of tests was 920° c.

The maximum possible error in the change in gauge length is ±0·004 cm in every case.

§3. Experiment on Single Crystals

An experiment was carried out with two single crystal wires of assay silver, 0·1 cm diameter, grown from the melt in graphite moulds by the travelling furnace method. For comparison, a specimen which recrystallized to give several grains in the cross-section was made from hard-drawn assay silver wire of the same diameter. Silver weights hung from hooks formed at the lower ends of the specimens were used to provide loads. The gauge length was taken as the distance between two loops of fine wire sintered on to the specimens, this method being adopted to avoid recrystallization in the gauge length of the single crystal specimens.

Table 2 compares the behaviour of the two single crystal wires with the polycrystalline specimen. The three specimens were annealed simultaneously for 282·5 hours at 910° c.

Table 2

	Applied stress at middle of gauge length dynes/cm^2	Initial gauge length cm	Increase of gauge length cm
Single crystal 1	131 000	4·044	+0·005
Single crystal 2	114 000	4·339	+0·001
Polycrystalline wire	126 000	4·492	+0·058

The maximum possible error in the measurement of the change in gauge length was $\pm 0{\cdot}012$ cm. The applied stress will be reduced by approximately 30 000 dynes/cm^2 in each case by surface energy effects. The effect of the grain-boundary energy in the case of the polycrystalline wire will be small. Herring has pointed out (private communication) that the observed creep rate in the polycrystalline wire would agree with the theoretical rate (Herring 1950, eqn. 11) if the average grain diameter were of the order of a fifth of the diameter of the wire. This was experimentally confirmed.

The stress applied to the single crystals was considerably less than that which would be expected to produce appreciable micro-creep (Chalmers 1936, 1937). A stress of about 10^7 dynes/cm^2 gave a strain rate of about 5×10^{-9} per sec in tin single crystals.

§4. Conclusions

An experimental study of the high temperature deformation of silver wires under low stresses indicated that the principal mechanisms which operate are as follows :

(1) The crystals themselves deform, probably by the self-diffusion mechanism first suggested by Nabarro. The diffusion currents flow between the external surfaces and the grain boundaries. This was shown

experimentally by the behaviour of single crystals, the mode of development of kinks and necks, and the agreement between the experimentally observed strain rate and the strain rate calculated by Herring. It seems unlikely that dislocations in the crystal play any appreciable part in the diffusion process under the conditions of the experiment.

(2) Deformation by offsetting takes place at grain boundaries inclined to the wire axis in such a way that the overall length of the wire either decreases or increases, depending on the relation between the applied load and the surface energy.

(3) It is unlikely that kinking is produced by the mechanisms suggested by Herring. Kinking was observed, however, and an explanation of this is proposed.

Acknowledgments

The author wishes to express his thanks to his colleagues for helpful discussions.

Acknowledgment is made to the Chief Scientist, Ministry of Supply, and to the Controller, H.M. Stationery Office, for permission to publish this paper.

References

Alexander, B. H., Dawson, M. H., and Kling, H. P., 1951, *J. Appl. Phys.*, **22,** 439.

Buttner, H. H., Funk, E. R., and Udin, H., 1952, *J. Metals*, **4,** 401.

Buttner, H. H., Udin, H., and Wulff, J., 1951, *J. Metals*, **3,** 1209.

Chalmers, B., 1936, *Proc. Roy. Soc.* A, **156,** 427 ; 1937, *J. Inst. Metals*, **61,** 103.

Chalmers, B., King, R., and Shuttleworth, R., 1948, *Proc. Roy. Soc.* A, **193,** 465.

Cottrell, A. H., and Jaswon, M. A., 1949, *Proc. Roy. Soc.* A, **199,** 104.

Funk, E. R., Udin, H., and Wulff, J., *J. Metals*, **3,** 1206.

Greenough, A. P., and King, R., 1951, *J. Inst. Metals*, **79,** 415.

Herring, C., 1950, *J. Appl. Phys.*, **21,** 459.

Hoffman, R. E., and Turnbull, D., 1951, *J. Appl. Phys.*, **22,** 634, 984.

Nabarro, F. R. N., 1948, *Report of a Conference on the Strength of Solids* (London : Physical Society), p. 75.

Udin, H., 1951, *J. Metals*, **191,** 63.

Udin, H., Shaler, A. J., and Wulff, J., 1949, *Trans. A.I.M.E.*, **185,** 186.

CIX. *The Zero Point Energy and Θ Values of Crystals*

By C. Domb and L. Salter
Clarendon Laboratory, Oxford*

[Received July 29, 1952]

Summary

The calculations of Montroll of the moments of the frequency spectrum of a number of crystal lattices enable an accurate estimate to be made of the zero point energy of these lattices. It has been customary to use the value $\frac{9}{8}k\Theta$, based on the Debye approximation, to estimate the zero point energy, and it is shown that this formula is only accurate if Θ_∞, the limiting value of Θ for high temperatures is used. It is shown that Θ_∞ can be simply expressed in terms of the force constants between atoms of the crystal.

§1. The Zero Point Energy

There are a number of substances in which zero point energy plays an important part in the behaviour of the solid state at low temperatures, and recent experiments by Dugdale and Simon (1952) have shown that for solid helium under pressure zero point energy plays a dominant part even at relatively high temperatures. In calculating the value of the zero point energy it has been customary to use the Debye approximation for the distribution of normal modes in the solid (Simon 1934, London 1936). A normal mode of frequency ν contributes $\frac{1}{2}h\nu$ to the zero point energy, so that the total zero point energy per atom of a crystal is

$$E_0=\frac{9}{2\nu_D{}^3}\int_0^{\nu_D} h\nu^3\,d\nu=\frac{9}{8}h\nu_D=\frac{9}{8}k\Theta. \quad . \quad . \quad . \quad . \quad . \quad (1)$$

The Debye approximation takes correct account of two important features of the true spectrum, the distribution for sufficiently low frequencies, and the total number of normal frequencies of the crystal. However, as a detailed representation of the spectrum over the whole frequency range it is not very adequate (Blackman 1941), and, since low frequencies make almost no contribution to the zero point energy, it would be rather surprising if the formula (1) were at all accurate.

In fact there is little difficulty in obtaining a much closer estimate of the value of the zero point energy if we make use of some results of Montroll (1942, 1943, 1944) on the nature of the true spectrum $g(\nu)\,d\nu$. Montroll employed a simple analytic method first introduced by Thirring (1913, 1914) for deriving the even moments of the spectrum,

$$\mu_k=\frac{1}{3N}\int_0^\infty \nu^k g(\nu)\,d\nu \quad (k \text{ even}), \quad . \quad . \quad . \quad . \quad . \quad (2)$$

* Communicated by the Authors.

and he applied this to the determination of the first seven moments for several different lattices. We shall use throughout the closely related moments,

$$I(k)=\int_0^1 x^k f(x)\,dx=\frac{\mu_k}{\nu_m{}^k}\left(x=\frac{\nu}{\nu_m},\ f(x)=\nu_m g(\nu_m x)\right). \quad . \quad . \quad . \quad (3)$$

(Note that the parameter ν_m appearing in these expressions is not the Debye ν_D, which is artificially defined in such a manner that integration of the Debye ν^2 distribution over all ν gives $3N$; on the more exact lattice theory ν_m is the true maximum frequency, defined in terms of the force constants.) Essentially the zero point energy is given by the first odd moment, i.e. $E_0=\frac{3}{2}h\nu_m I(1)$, and the problem reduces to estimating $I(1)$ from the known values of $I(k)$. We have made use of two independent methods for this estimation.

(*a*) The origin is transferred to ν_m, and the modified moments, $J(k)$, are calculated from

$$J(k)=\int_0^1 x'^k f(x)\,dx, \quad (x'^2=1-x^2). \quad . \quad . \quad . \quad . \quad . \quad . \quad (4)$$

Then x can be expanded as a power series in x'^2,

$$x=(1-x'^2)^{1/2}=1-\tfrac{1}{2}x'^2-\tfrac{1}{8}x'^4-\ldots. \quad . \quad . \quad . \quad . \quad (5)$$

The $J(k)$ are all positive and decrease rapidly because of the behaviour of $g(\nu)$ near $\nu=0$; we can thus substitute the known values of $J(k)$ and obtain the first few terms of a rapidly converging series for $I(1)$. The terms after the first are consistent in sign, and it is possible to estimate fairly accurately the contribution of the higher terms. This method is somewhat tedious, since the calculations must be performed afresh for each lattice, but it is susceptible of high accuracy.

(*b*) (Suggested by Professor M. H. L. Pryce.) The value of $I(1)$ is determined by a Lagrange interpolation from the known values of $I(k)$. From the known behaviour of $g(\nu)$ near $\nu=0$ it is clear that $I(k)$ will have an infinity at $k=-3$; for the purpose of interpolation it is therefore better to use $(k+3)\ I(k)$. The calculation involved in this method is considerably simpler than in the previous method, and once the Lagrangian coefficients have been determined, they can be used for all lattices.

Both methods were employed for the calculation of the zero point energy of the face centred cubic lattice, taking only nearest neighbour interactions into account. The results differed by less than 1 part in 1000 (as will be seen from the next section), and it therefore seems that one can apply method (*b*) to other lattices with considerable confidence.

§2. Detailed Calculations for Various Lattices

Montroll (1943, 1944) has derived moments for the simple cubic and body centred cubic lattices taking into account first and second neighbour interactions. If in a simple cubic lattice first neighbour interactions are zero, the lattice breaks up into a pair of independent face centred cubic lattices. We can thus from Montroll's calculations deduce the

moments for the face centred cubic lattice with nearest neighbour interactions only, and they are as follows :

$$\left.\begin{aligned}&\mu_0=1,\quad \mu_2=4\beta,\quad \mu_4=20\beta^2,\quad \mu_6=114\beta^3,\quad \mu_8=703\beta^4,\\&\mu_{10}=4549\beta^5,\quad \mu_{12}=30353\beta^6,\quad \mu_{14}=206757\tfrac{3}{4}\beta^7,\\&\qquad\qquad\qquad\qquad(\beta=\alpha/4\pi^2m).\end{aligned}\right\}\quad . \quad . \quad . \quad (6)$$

Here α is the force constant between nearest neighbours, m is the particle mass, $\nu_m=1/\pi\sqrt{(2\alpha/m)}$.

Applying method (a) we derive the following series for the zero point energy:

$$E_0=\tfrac{3}{2}h\nu_m[1-0{\cdot}25-0{\cdot}039063-0{\cdot}013428$$
$$-0{\cdot}006094-0{\cdot}003220-0{\cdot}001880-0{\cdot}001180\ldots] \quad . \quad . \quad . \quad (7)$$

The terms are decreasing steadily, and can be fitted asymptotically to an expression of the form A/n^r. Extrapolating in this manner, we estimate the sum of the series to be

$$E_0=1{\cdot}0225h\nu_m. \quad . \quad . \quad . \quad . \quad . \quad . \quad . \quad (8)$$

The terms involved in the extrapolation amount only to 0·0050, so that the correction is quite a small one.

Method (b) gives $I(1)$ as a linear combination of the known $I(k)$ in the form

$$I(1)=0{\cdot}209473+1{\cdot}466309I(2)-1{\cdot}466309I(4)$$
$$+1{\cdot}466309I(6)-1{\cdot}047363I(8)+0{\cdot}488770I(10)$$
$$-0{\cdot}133301I(12)+0{\cdot}016113I(14). \quad . \quad . \quad . \quad . \quad . \quad . \quad . \quad (9)$$

This formula is applicable to all the three dimensional lattices for which the moments have been determined, and in the particular case under consideration gives

$$E_0=1{\cdot}0220h\nu_m. \quad . \quad . \quad . \quad . \quad . \quad . \quad . \quad (10)$$

It is interesting to check the interpolation method for the simple cubic lattice with nearest neighbour interactions only. The spectrum is in this case equivalent to that of a one dimensional lattice, so that the zero point energy can be calculated exactly. We should use $(k+1)I(k)$ in the interpolation formula, and we derive the estimate

$$E_0=0{\cdot}95437h\nu_m, \quad . \quad . \quad . \quad . \quad . \quad . \quad . \quad (11)$$

whereas the correct value should be

$$E_0=\frac{3}{\pi}h\nu_m=0{\cdot}95493h\nu_m. \quad . \quad . \quad . \quad . \quad . \quad . \quad (12)$$

§3. The Use of Θ_∞

The detailed behaviour of Θ as a function of temperature for a face centred cubic lattice has been calculated by Leighton (1948). He finds that after an initial variation of about 15% in the range $T<\Theta/10$, Θ settles down to a steady value ; we shall denote by Θ_∞ the theoretical limiting value of Θ as $T\to\infty$, and for the face centred cubic lattice

Θ rapidly approaches Θ_∞ when $T>\Theta/5$. The calculations of Blackman (1937) for the simple cubic lattice, and of Smith (1948) for the diamond lattice seems to indicate that this behaviour is fairly general.

There are a number of properties of Θ_∞ which are of considerable practical benefit. Θ_∞ can be defined even for systems whose spectrum at low frequencies does not conform to the Debye law (e.g. a simple cubic lattice with nearest neighbour interactions). It will be shown shortly that Θ_∞ can be very simply calculated for any lattice from given force constants, and that the formula (1) for the zero point energy provides a good approximation if Θ_∞ is used.

At high temperatures the specific heat can be expanded as a series (Thirring 1913):

$$\frac{C_v}{3Nk}=1-\frac{\mu_2}{12}\left(\frac{h}{kT}\right)^2+\frac{\mu_4}{240}\left(\frac{h}{kT}\right)^4-\frac{\mu_6}{6048}\left(\frac{h}{kT}\right)^6 \quad . \quad . \quad (13)$$

where the general terms is given by $(-1)^n\frac{B_{2n}}{2n!}\mu_{2n}\left(\frac{h}{kT}\right)^{2n}$, the B_n being the Bernoulli numbers $B_2=\frac{1}{6}$, $B_4=\frac{1}{30}$, $B_6=\frac{1}{42}$, giving in terms of the $I(k)$

$$\frac{C_v}{3Nk}=1-\frac{I(2)}{12}\left(\frac{h\nu_m}{kT}\right)^2+\frac{I(4)}{240}\left(\frac{h\nu_m}{kT}\right)^4-\frac{I(6)}{6048}\left(\frac{h\nu_m}{kT}\right)^6. \quad . \quad (13')$$

For the Debye spectrum the moments are given by

$$\mu_k=\frac{3{\nu_D}^k}{k+3}, \quad I_D(k)=3/k+3. \quad . \quad . \quad . \quad . \quad . \quad (14)$$

Equations (13) and (14) can be used to derive an expansion of Θ in inverse powers of the temperature, and in particular, retaining only the first term in the limit as $T\to\infty$, we find that

$$\Theta_\infty=\frac{h}{k}\sqrt{\frac{5\mu_2}{3}}=\frac{h\nu_m}{k}\sqrt{\frac{5I(2)}{3}}. \quad . \quad . \quad . \quad . \quad . \quad (15)$$

Formula (15) furnishes a simple means of calculating Θ_∞ for any lattice with given force constants. μ_2 can easily be deduced from the original equations of motion of the lattice. If these are written in the matrix form

$$Ax=4\pi^2m\nu^2x, \quad . \quad . \quad . \quad . \quad . \quad . \quad . \quad . \quad (16)$$

μ_2 is essentially the diagonal sum or trace of A. It should be observed that the matrix A entering here is of order $3N$, and is not the same as the matrices used by Thirring, Blackman and Montroll which are of order 3 (or 3s when there are s atoms in unit cell). This matrix can be used to derive the first few moments without appeal to the cyclic boundary condition; the complication increases very rapidly, however, for the higher moments. The parameter ν_m, corresponding to the maximum frequency, is irrelevant to the discussion, and has only been introduced to facilitate computation and numerical comparison.

For the face centred cubic lattice considered in § 2, $I(2)=\frac{1}{2}$, and we find that

$$\Theta_\infty = \sqrt{\frac{5}{6}}\frac{h\nu_m}{k} = 0{\cdot}9129\frac{h\nu_m}{k}, \quad \ldots\ldots (17)$$

and this is in close agreement with the result obtained by Leighton (1948). This can be written, substituting for ν_m, or using μ_2 directly :

$$\Theta_\infty = \frac{0{\cdot}9129}{\pi}\frac{h}{k}\left(\frac{2\alpha}{m}\right)^{1/2}. \quad \ldots\ldots (18)$$

The numerical factor 0·9129, or $\sqrt{\frac{5}{6}}$, occurring in eqn. (17), would seem to apply more generally since $I(2)$ is found to be equal to $\frac{1}{2}$ for each of the three cubic lattice structures, irrespective of ratio of first to second neighbour interaction. This means that ν_m is related to the trace of the matrix for the lattice in each case by the same numerical factor; the reason for this simple relationship would appear to merit further investigation.

We could equally well take account of distant neighbour interactions and write more generally

$$\Theta_\infty = 0{\cdot}4109\frac{h}{k}\left(\frac{\Sigma\alpha_i}{m}\right)^{1/2}, \quad \ldots\ldots (19)$$

where α_i is the 'force constant' of the ith neighbour interaction which can be readily determined from the equations of motion. The lattice sums involved in the α_i have been evaluated for a number of lattices by Lennard-Jones and Ingham (1924) for potentials involving power laws. For an attractive law falling off as the inverse sixth power of the distance, the α_i fall off as the eighth power, and the effect of distant neighbours on Θ_∞ in the face centred lattice is small ($\sim$3%).

The above method of calculating Θ_∞ (and thus the zero point energy), is substantially simpler, and probably more accurate, than previous methods which made use of an average over elastic constants (Herzfeld and Goeppert-Mayer 1934, de Boer and Blaisse 1948).

The method would also seem to be applicable to mixed crystals containing different atoms, using the matrix of eqn. (16). When these atoms form a well ordered mixture, the methods of lattice dynamics can be used, although the spectrum becomes more complicated (Smith 1948). But when the mixtures are random, the symmetry of the system disappears, and it is difficult to see how to use classical theory without a large increase in labour. The second moment can still be determined very simply from the trace of the above matrix, and hence Θ_∞ can be calculated. If, for example, we assume that the force constants between all atoms are the same, but only their masses differ, we should have instead of (19),

$$\Theta_\infty = 0{\cdot}4109\frac{h}{k}(\Sigma\alpha_i)^{1/2}\left(\frac{p_1}{m_1}+\frac{p_2}{m_2}\right)^{1/2}, \quad \ldots\ldots (20)$$

p_1 and p_2 being the fractions of the two constituents. It is hoped to apply this method to the effect of vibration terms in the theory of regular solutions, a problem which has been discussed recently by other writers (Prigogine and Garikian 1950, Rushbrooke and Ziman 1952).

§4. The $\frac{9}{8}k\Theta$ Formula

If we use the values of Θ_∞ given by (17), and estimate the zero point energy from the Debye formula (1) we obtain the value $E_0=1{\cdot}0270h\nu_m$. It will be seen that this is close to the value (8) given by refined calculations. If, instead, we had used the value of Θ at $T=0$ given by Leighton's calculations, we should have obtained a result in error by 15%. It is fairly clear that the variation in Θ in the neighbourhood of $T=0$ is caused by the long wave region of the spectrum, and we should not expect this to contribute much to the zero point energy.

Table 1

Lattice	Ratio 2nd : 1st Neighbour	Zero Point/$h\nu_m$ Energy (Interpolation)	$\frac{9}{8}k\Theta_\infty/h\nu_m$	% Difference
S.C.	$\frac{1}{2}$	1·0344	1·0270	0·7
S.C.	1	1·0329	1·0270	0·6
S.C.	2	1·0297	1·0270	0·3
B.C.C.	0	0·9956	1·0270	3·1
B.C.C.	$\frac{1}{2}$	1·0242	1·0270	0·3
B.C.C.	1	1·0276	1·0270	0·1
B.C.C.	2	1·0226	1·0270	0·4
F.C.C.	0	1·0220	1·0270	0·5
S.C. (Linear Chain)	0	0·9549	1·0270	7·0
[3] Einstein Oscillator	0	1·5000	1·4524	3·2

An alternative argument favouring the use of Θ_∞ for estimating zero point energy is as follows : by our determination of Θ_∞ we have ensured that the moments $I(0)$ and $I(2)$ for the correct distribution and equivalent Debye distribution are the same, and we should not therefore expect $I(1)$ to differ very much. As a test of the formula we have compared the results with those derived from the interpolation formula (9) for a number of particular cases in which the moments had already been derived (Montroll 1943, 1944). The results are collected in table 1. The final two entries correspond to spectra which do not follow the Debye law, but even here it will be seen that the error is surprisingly small. In the other cubic lattice cases the only error greater than 1% corresponds to the body centred lattice with no second neighbour interaction. For this lattice, however, the second neighbours are not much further distant than the nearest neighbours, and their interactions should be taken into account in practice.

§5. High Temperature Variation of Θ

The small variation in Θ at high temperatures was referred to at the beginning of § 3. Formula (13) can be used to derive an expansion of Θ in inverse powers of the temperature, and the first two terms are

$$\frac{\Theta}{\Theta_\infty}=1-\frac{1}{40}\sqrt{\frac{5}{3I(2)}}\left[I(4)-\frac{25}{21}I(2)^2\right]\left(\frac{h\nu_m}{kT}\right)^2 \quad . \quad . \quad . \quad . \quad (21)$$

The expression for the higher terms rapidly becomes very complicated, but in the particular case of the face centred cubic lattice we have evaluated the first seven terms, as follows:

$$\begin{aligned}\Theta_\infty=0{\cdot}9129\chi[1&-7{\cdot}441\times10^{-4}(\chi/T)^2+1{\cdot}447\times10^{-5}(\chi/T)^4\\&-1{\cdot}549\times10^{-7}(\chi/T)^6+1{\cdot}735\times10^{-9}(\chi/T)^8\\&-1{\cdot}463\times10^{-11}(\chi/T)^{10}+4{\cdot}928\times10^{-13}(\chi/T)^{12}\ldots].\quad(\chi=h\nu_m/k)\end{aligned}$$

$$. \quad . \quad . \quad (22)$$

It will be noted that the coefficients of the inverse powers of T are extremely small. The formula can be used to evaluate Θ from $T=\infty$ to $T\approx\Theta/6$ and it is found that in the whole of this range the variation is less than 2%. These results are in agreement with the calculations of Leighton.

Acknowledgments

The authors are indebted to Professor M. H. L. Pryce and Professor F. E. Simon for helpful discussion. One of them (C. D.) would like to express his gratitude to the University of Oxford for the award of an I.C.I. Fellowship, and the other (L. S.) to the Rhodes Trust for financial assistance.

References

Blackman, M., 1937, *Proc. Roy. Soc.* A, **159,** 416; 1941, *Rep. Progr. Phys.*, **8,** 11.
de Boer, J., and Blaisse, B. S., 1948, *Physica*, **14,** 149.
Dugdale, J. S., and Simon, F. E., 1952 (to be published).
Herzfeld, K. F., and Goeppert Mayer, M., 1934, *Phys. Rev.*, **46,** 995.
Leighton, R. B., 1948, *Rev. Mod. Phys.*, **20,** 165.
Lennard Jones, J. E., and Ingham, A. E., 1925, *Proc. Roy. Soc.* A, **107,** 636.
London, F., 1936, *Proc. Roy. Soc.* A, **153,** 576.
Montroll, E. W., 1942, *J. Chem. Phys.*, **10,** 218; 1943, *Ibid.*, **11,** 481; 1944, *Ibid.*, **12,** 98.
Prigogine, I., and Garikian, G., 1950, *Physica*, **16,** 239.
Rushbrooke, G. S., and Ziman, J. M., see Rushbrooke, *Proc. International Conference on Phase Transitions*, Paris, 1952.
Simon, F. E., 1934, *Nature, Lond.*, **133,** 529.
Smith, H. M. J., 1948, *Phil. Trans. Roy. Soc.* A, **241,** 105.
Thirring, H., 1913, *Phys. Z.*, **14,** 867; 1914, *Ibid.*, **15,** 127, 180.

CX. *The Spatial Correlation of Electrons in Atoms and Molecules: II—Two-Electron Systems in Excited States*

By A. Brickstock and J. A. Pople
Department of Theoretical Chemistry, University of Cambridge*

[Received July 12, 1952]

Summary

This paper extends the treatment of the ground state of helium and similar two-electron systems, given in Part I, to excited states which are not spherically symmetric. The wave function is expanded in a series of surface harmonics, the coefficients being functions of the radial distances. Symmetry considerations and the angular momentum operators are used to simplify the problem and a set of coupled equations for the radial functions are then given. This general theory is exact. In the final section it is used to discuss the effect of the exclusion principle on angular correlation in atomic P-states and is applied to excited states of beryllium.

§ 1. Introduction

This series of papers is concerned with attempts to take into account the electrostatic repulsion between electrons in atoms and molecules and to find the effect this has on the relative distribution or *correlation* of electrons in the six-dimensional, two-electron configurational space. The simplest systems to discuss are two-electron systems moving in a spherical field. In Part I (Lennard-Jones and Pople 1952), the ground states of two-electron systems such as the helium atom have been examined in some detail. This problem could be solved exactly were it not for the interelectronic potential energy term $(1/r_{12})$ in the Hamiltonian. This term can be expanded in terms of a series of Legendre functions of the cosine of the angle subtended at the centre. It was shown in Part I that many approximate trial wave functions are approximations whereby $(1/r_{12})$ is replaced by some simpler potential consisting of only the first few terms in the expansion. The Hartree-Fock wave function, for example, consisting as it does of a product of two similar functions, actually takes into account only the first term in the expansion of $(1/r_{12})$ and since this is independent of the angular positions of the electrons the wave function does not give angular correlation.

In Part I a general method for systematically including the effect of all terms in the expansion of $(1/r_{12})$ was described. This method was based on an expansion of the wave function similar to that used for the electrostatic term in the Hamiltonian. This is possible for states with

* Communicated by Sir John Lennard-Jones, F.R.S.

spherical symmetry, for the wave function then only depends on the relative angular position of the electrons. The wave functions for excited states with non-zero orbital angular momentum cannot be handled in this way. Such states are no longer spherically symmetric and cannot be completely described in terms of the three coordinates used for the ground state. In this paper a more general method is described which can be applied to all states of two electrons in a spherically symmetric field. The spatial part of the wave function can be expanded in a series of surface harmonics, referred to some fixed axes, the coefficients in such an expansion being functions of the radii of the two electrons. The orbital angular momentum vectors can then be used to obtain relations between the radial functions, thereby reducing the problem considerably. Further simplifications follow when the symmetry of the spin wave function and the behaviour under inversion are taken into account. No approximations are made in this theory. It is therefore a more rigorous treatment of the angular moments of atomic states, usually handled by an orbital approximation.

In the latter part of the paper, P-states are discussed in greater detail. These differ from the S-states considered in Part I in that the first term of the general expansion allows for some degree of angular correlation. It is shown that the antisymmetry principle plays a very significant part in this angular correlation. For triplet states, the spatial part of the wave function has to be antisymmetric, so that the probability of the two electrons being close together is small. In singlet states, on the other hand, the effect of the anti-symmetry principle is to bring the electrons closer together. This is the main reason for the well-known splitting of singlet and triplet states. Higher terms in the general expansion of the wave function will allow for the way in which the complete $(1/r_{12})$ expression will influence the spatial distribution of electrons. The general discussion is illustrated in the last section by some calculations on excited P-states of beryllium.

§ 2. The General State of Two Electrons in a Spherically Symmetric Field

If the potential field in which the two electrons move is $V(r)$ we have to investigate general solutions of the Schrödinger equation using the Hamiltonian

$$\mathscr{H}=H_1+H_2+1/r_{12}, \quad . \quad . \quad . \quad . \quad . \quad . \quad . \quad (2.1)$$

where H is a one-electron Hamiltonian

$$H_1=-\tfrac{1}{2}\nabla_1^2+V(r_1), \quad . \quad . \quad . \quad . \quad . \quad . \quad (2.2)$$
$$H_2=-\tfrac{1}{2}\nabla_2^2+V(r_2).$$

In these formulae r_1 and r_2 are the distances of the two electrons from the centre of the field and r_{12} is the inter-electronic distance.

If the electrostatic term $(1/r_{12})$ were not present in (2.1), the wave equation would be separable and the problem would reduce to that of

two particles moving independently in the field $V(r)$. To investigate the effect of the electrostatic term on the electron distribution, it is convenient to expand it in the form

$$1/r_{12}=\sum_{l=0}^{\infty}(r_<^l/r_>^{l+1})P_l(\cos\theta_{12}), \quad . \quad . \quad . \quad . \quad . \quad (3.2)$$

where $r_<$ and $r_>$ are the smaller and greater of r_1 and r_2 and θ_{12} is the angle subtended at the centre by the two electrons. $P_l(\mu)$ are Legendre polynomials defined so that $P_l(1)=1$.

For the ground state, or for any other spherically symmetric state, the spatial part of the wave function $\psi(1, 2)$ will also depend only on the three variables r_1, r_2 and θ_{12} and can be expanded in a form similar to (2.3). This was the method followed in Part I. For states which are not spherically symmetric, however, an expansion in terms of relative co-ordinates is no longer possible. Instead we have to expand in terms of the angular symmetrics with respect to the two electrons separately. The electrostatic term $(1/r_{12})$ can then be written

$$1/r_{12}=\sum_{l=0}^{\infty}U_l(r_1, r_2)\sum_{m=-l}^{+l}S_{lm}(\theta_1, \phi_1)S_{lm}(\theta_2, \phi_2), \quad . \quad . \quad . \quad (2.4)$$

where $U_l(r_1, r_2)$ has been written for $(r_<^l/r_>^{l+1})$ and $S_{lm}(\theta, \phi)$ is a surface harmonic defined by

$$S_{lm}(\theta, \phi)=\left[\frac{(l-|m|)!}{(l+|m|)!}\right]^{1/2}P_l^{|m|}(\cos\theta)\exp(im\phi), \quad (|m|\leqslant l), \quad (2.5)$$

$P_l^m(\mu)$ being associated Legrendre polynomials defined by

$$P_l^m(\mu)=(-1)^m(1-\mu^2)^{m/2}\frac{d^mP_l(\mu)}{d\mu^m}. \quad . \quad . \quad . \quad . \quad (2.6)$$

The spatial part of the wave-function in the general state can be expanded in the form

$$\psi(1, 2)=\sum_{lml'm'}\psi_{lm:l'm'}(r_1, r_2)S_{lm}(\theta_1, \phi_1)S_{l'm'}(\theta_2, \phi_2). \quad . \quad . \quad (2.7)$$

In this general form the expansion is considerably more complicated than the expansion in terms of relative coordinates for spherically symmetric states. Fortunately, however, it is possible to find many relations connecting the $\psi_{lm:l'm'}$ by using three supplementary conditions.

(*a*) In addition to being an eigenfunction of the Hamiltonian, the wave-function (2.7) must also be an eigenfunction of the total orbital angular momentum operators $\mathscr{L}^2$ and $\mathscr{L}_z$, so that there are integers L and M $(-L\leqslant M\leqslant L)$ such that

$$\mathscr{L}^2\psi(1, 2)=L(L+1)\psi(1, 2), \quad . \quad . \quad . \quad . \quad . \quad . \quad (2.8)$$

$$\mathscr{L}_z\psi(1, 2)=M\psi(1, 2). \quad . \quad . \quad . \quad . \quad . \quad . \quad . \quad . \quad (2.9)$$

(*b*) For states with odd total angular quantum number L, further simplification follows if we specify whether the wave-function is even or odd under inversion with respect to the centre of force.

(*c*) Thirdly, the number of independent radial functions is reduced by imposing the antisymmetry condition on the total wave-function. If the spin part is antisymmetric, the spatial wave-function $\psi(1, 2)$ is symmetric for interchange of electron coordinates and the state is a singlet. For triplet states, on the other hand, $\psi(1, 2)$ is antisymmetric.

Since all states with the same value of L are degenerate (in the absence of a magnetic field), there is no loss of generality in supposing $M=0$. This eliminates all $\psi_{lm:l'm'}$ except those for which

$$m+m'=0. \quad . \quad . \quad . \quad . \quad . \quad . \quad . \quad . \quad (2.10)$$

The operator $\mathscr{L}^2$ can be written

$$\mathscr{L}^2=\mathscr{L}_1{}^2+\mathscr{L}_2{}^2+(\mathscr{L}_{1x}+i\mathscr{L}_{1y})(\mathscr{L}_{2x}-i\mathscr{L}_{2y})+(\mathscr{L}_{1x}-i\mathscr{L}_{1y})(\mathscr{L}_{2x}+i\mathscr{L}_{2y}) +2\mathscr{L}_{1z}\mathscr{L}_{2z}, \quad . \quad . \quad . \quad . \quad . \quad (2.11)$$

where $\mathscr{L}_1$ and $\mathscr{L}_2$ are one-electron angular momentum operators and $\mathscr{L}_{1x}$ etc. are the corresponding components. Using the formulae

$$\left.\begin{aligned}(\mathscr{L}_{1x}+i\mathscr{L}_{1y})S_{lm}(\theta_1, \phi_1)&=(-1)^{m+1}\{l(l+1)-m(m+1)\}^{1/2}S_{l,m+1}(\theta_1, \phi_1),\\ (\mathscr{L}_{1x}-i\mathscr{L}_{1y})S_{lm}(\theta_1, \phi_1)&=(-1)^{m}\{l(l+1)-m(m-1)\}^{1/2}S_{l,m-1}(\theta_1, \phi_1),\\ \mathscr{L}_{1z}S_{lm}(\theta_1, \phi_1)&=mS_{lm}(\theta_1, \phi_1),\end{aligned}\right\} \quad . \quad . \quad . \quad (2.12)$$

eqn. (2.8) becomes

$$\sum_{l,l'}\{l(l+1)+l'(l'+1)-L(L+1)\}\sum_m\psi_{lm:l',-m}S_{lm}S_{l',-m} = \sum_{l,l',m}\{A_{ll'}^{(m)}S_{l,m+1}S_{l',-m-1}+A_{ll'}^{(m-1)}S_{l,m-1}S_{l',-m+1} +2m^2S_{lm}S_{l',-m}\}\psi_{lm:l',-m}, \quad . \quad . \quad . \quad (2.13)$$

where

$$A_{ll'}^{(m)}=\{[l(l+1)-m(m+1)][l'(l'+1)-m(m+1)]\}^{1/2}. \quad . \quad (2.14)$$

Serial notation has been used in equation (2.3) and later in the paper. Thus $S_{lm}S_{l'm'}$ is short for $S_{lm}(\theta_1, \phi_1)S_{l'm'}(\theta_2, \phi_2)$ and $\psi_{lm:l'm'}$ for $\psi_{lm:l'm'}(r_1, r_2)$. The summations over m are from $-\min(l, l')$ to $+\min(l, l')$.

By equating coefficients of the various surface harmonics on both sides of (2.13), certain relations between the radial functions $\psi_{lm:l'm'}$ are obtained. Condition (*b*) then specifies the parity of $l+l'$ (even or odd) and finally condition (*c*) can be used to obtain relations between $\psi_{lm:l'm'}$ and $\psi_{l'm':lm}$.

For S-states ($L=0$) it is found that this procedure eliminates all $\psi_{lm:l'm'}$ except those for which $l=l'$ and also shows that $\psi_{lm:l',-m}$ is independent of m. But since

$$P_l(\cos\theta_{12})=\sum_{m=-l}^{+l}S_{lm}(\theta_1, \phi_1)S_{l,-m}(\theta_2, \phi_2), \quad . \quad . \quad . \quad (2.15)$$

this shows that the wave-function depends only on the relative coordinates.

We shall not attempt to obtain the relations between the $\psi_{lm:l'm'}$ in a general form, but in the next section various P-states ($L=1$) will be dealt with as examples.

§ 3. Examples of Non-spherical States

To discuss examples, it is convenient to write the expanded form of the wave-function

$$\psi(1,2)=\sum_{l\leqslant l'}\zeta_{ll'}(1,2), \quad . \quad . \quad . \quad . \quad . \quad . \quad (3.1)$$

where

$$\zeta_{ll'}(1,2)=\sum_{m=-\min(l,l')}^{+\min(l,l')}\{\psi_{lm:l'-m}S_{lm}S_{l'-m}+\psi_{l'm:l-m}S_{l'm}S_{l-m}\}. \quad . \quad (3.2)$$

$\zeta_{ll'}(1,2)$ is then that part of the total wave-function whose angular symmetry corresponds to l nodes in the angular coordinates of one electron and l' in those of the other. It may be described as the contribution to $\psi(1,2)$ of the particular configuration (l,l'). If $l=1$ and $l'=2$, for example, we are dealing with the contribution of the configuration (pd). It should be noted that no approximations have been made in this development, so that the expansion (3.1) does give a precise significance to configuration interaction in these atomic systems.

To exemplify the procedures described in the last section, we will deal with P-states for which $L=1$. These divide into even and odd states according to their behaviour under inversion.

Odd P-states

For odd states, only terms with $l+l'$ odd contribute so that

$$\psi(1,2)=\zeta_{01}(1,2)+\zeta_{12}(1,2)+\zeta_{03}(1,2)+\ldots . \quad . \quad . \quad . \quad (3.3)$$

These terms correspond to configurations (sp), (pd), (sf) . . . There are no conditions implied by (2.13) for the configuration (sp). For (pd) we find

$$\left.\begin{aligned}\psi_{11:2-1}=\psi_{1-1:21}&=\frac{\sqrt{3}}{2}\psi_{10:20},\\ \psi_{21:1-1}=\psi_{2-1:11}&=\frac{\sqrt{3}}{2}\psi_{20:10}.\end{aligned}\right\} \quad . \quad . \quad . \quad . \quad (3.4)$$

$\zeta_{03}(1,2)$ is found to vanish identically. Higher terms in the expansion can be dealt with in a similar way.

The wave-function $\psi(1,2)$ can therefore be written

$$\begin{aligned}\psi(1,2)=&S_{00}S_{10}\psi_{00:10}+S_{10}S_{00}\psi_{10:00}\\ &+\left\{S_{10}S_{20}+\frac{\sqrt{3}}{2}S_{1-1}S_{21}+\frac{\sqrt{3}}{2}S_{11}S_{2-1}\right\}\psi_{10:20}\\ &+\left\{S_{20}S_{10}+\frac{\sqrt{3}}{2}S_{2-1}S_{11}+\frac{\sqrt{3}}{2}S_{21}S_{1-1}\right\}\psi_{20:10}+\ldots . \quad (3.5)\end{aligned}$$

The two independent radial functions for each configuration can be related if we specify the symmetry under interchange of coordinates. We then have

$$\left.\begin{aligned}\psi_{00:10}(r_1,r_2)&=\pm\psi_{10:00}(r_2,r_1)\\ \psi_{10:20}(r_1,r_2)&=\pm\psi_{20:10}(r_2,r_1)\end{aligned}\right\}, \quad . \quad . \quad . \quad (3.6)$$

the positive sign being taken for a singlet and the negative for a triplet.

Even P-states

The lower configurations which contribute to even P-states are (p^2) and (d^2). The conditions implied by (2.13) for the configuration (p^2) lead to

$$\left.\begin{aligned}\psi_{10:10}&=0,\\ \psi_{11:1-1}+\psi_{1-1:11}&=0,\end{aligned}\right\} \quad . \quad . \quad . \quad . \quad . \quad . \quad (3.7)$$

so that $$\zeta_{11}(1,2)=\{S_{11}S_{1-1}-S_{1-1}S_{11}\}\psi_{11:1-1}. \quad . \quad . \quad . \quad . \quad (3.8)$$

The radial function $\psi_{11:1-1}(r_1, r_2)$ must be symmetric for a ^{3}P state and antisymmetric for a ^{1}P-state. This makes it clear why two equivalent p-electrons in the usual vector coupling theory cannot give rise to a ^{1}P state. Such theories express $\psi_{11:1-1}$ as a simple product of two one-electron function and this cannot be antisymmetric.

§ 4. Equations for the Radial Functions

Using (2.4) and the wave-function expansion (2.7), the complete Schrödinger equation can be expressed in atomic units in the form

$$\begin{aligned}\sum_{lml'm'}&\left\{-\frac{1}{2}\left[\frac{1}{r_1^2}\frac{\partial}{\partial r_1}\left(r_1^2\frac{\partial}{\partial r_1}\right)+\frac{1}{r_2^2}\frac{\partial}{\partial r_2}\left(r_2^2\frac{\partial}{\partial r_2}\right)\right]+\frac{l(l+1)}{2r_1^2}+\frac{l'(l'+1)}{2r_2^2}\right.\\ &\left.+V(r_1)+V(r_2)\right\}\psi_{lm:l'm'}S_{lm}S_{l'm'}\\ &+\sum_{lml'm'}\sum_{p=0}^{\infty}{\sum_{q=-p}^{p}}'\psi_{lm:l'm'}U_p(r_1,r_2)S_{pq}(1)S_{lm}(1)S_{p,-q}(2)S_{l'm'}(2)\\ &=E\sum_{lml'm'}\psi_{lm:l'm'}S_{lm}S_{l'm'}. \quad . \quad . \quad . \quad (4.1)\end{aligned}$$

A product of surface harmonics can be expanded in terms of surface harmonics in the form

$$S_{ij}(\theta_1,\phi_1)S_{kl}(\theta_1,\phi_1)=\sum_{\alpha\beta}a_{ijkl}^{(\alpha\beta)}S_{\alpha\beta}(\theta_1,\phi_1), \quad . \quad . \quad . \quad (4.2)$$

where $a_{ijkl}^{(\alpha\beta)}$ are numerical coefficients. Equating coefficients of the various harmonic products in (4.1) we get a set of coupled equations for the radial functions $\psi_{lm:l'm'}$.

$$\begin{aligned}&\left\{-\frac{1}{2}\left[\frac{1}{r_1^2}\frac{\partial}{\partial r_1}\left(r_1^2\frac{\partial}{\partial r_1}\right)+\frac{1}{r_2^2}\frac{\partial}{\partial r_2}\left(r_2^2\frac{\partial}{\partial r_2}\right)\right]+\frac{l(l+1)}{2r_1^2}+\frac{l'(l'+1)}{2r_2^2}\right.\\ &\left.+V(r_1)+V(r_2)-E\right\}\psi_{lm:l'm'}\\ &=-\sum_{abcd}\sum_{p=0}^{\infty}{\sum_{q=-p}^{+p}}'a_{pq,ab}^{(lm)}a_{p-q,cd}^{(l'm')}U_p(r_1,r_2)\psi_{ab:cd}. \quad . \quad . \quad . \quad (4.3)\end{aligned}$$

§ 5. Correlation in Two-electron ^{1}P and ^{3}P States

In Part I the wave-function for the ground state of a two-electron system was expanded in a way similar to that described in this paper and the physical significance of the various terms was examined in some detail. In particular, it was found that the first term of the expansion,

corresponding to the configuration (s^2), did not allow in any way for angular correlation, that is dependence on the relative angular positions of the electrons.

The situation is different, however, for a P-state. For odd P-states the simplest approximation is to consider only the term $\zeta_{01}(1, 2)$ corresponding to the (sp) configuration. Form (3.5) and (3.6), these first terms can be written

$$\left.\begin{aligned} {}^1\zeta_{01}(1, 2) &= {}^1\psi_{00:10}(1, 2)\cos\theta_2 + {}^1\psi_{00:10}(2, 1)\cos\theta_1, \\ {}^3\zeta_{01}(1, 2) &= {}^3\psi_{00:10}(1, 2)\cos\theta_2 - {}^3\psi_{00:10}(2, 1)\cos\theta_1. \end{aligned}\right\} \quad . \quad (5$$

The two radial functions ${}^1\psi_{00:10}$ and ${}^3\psi_{00:10}$ are not necessarily identic but the major difference between the triplet and singlet states is t change of sign in (5.1). This has an important effect on the angul correlation. If all the radial functions in (5.1) have the same sign, th most probable configuration in the singlet state is given by $\theta_1=\theta_2=0$ This corresponds to both electrons on the polar axis and both on the same side of the nucleus. For the triplet state, however, $|{}^3\zeta_{01}|$ has a maximum when $\theta_1=0$ and $\theta_2=\pi$, when the electrons are on the polar axis but on opposite sides of the nucleus. This correlative property of P-states was pointed out in connection with the orbital theory in a previous paper (Lennard-Jones and Pople 1950). From the present analysis, it is clear that these are general properties of the ζ_{01} component of the exact wave-function. We may illustrate the overall effects of this correlation by calculating the mean values of $\cos\theta_{12}$, given the values of r_1 and r_2, θ_{12} being the angle subtended at the centre. In the absence of correlation $\overline{\cos\theta_{12}}$ would be zero. Using the functions (5.1) we get

$$\left.\begin{aligned} \overline{(\cos\theta_{12})}_{\text{singlet}} &= +\frac{2}{3}\frac{{}^1\psi_{00:10}(1, 2)\,{}^1\psi_{00:10}(2, 1)}{[{}^1\psi_{00:10}(1, 2)]^2+[{}^1\psi_{00:10}(2, 1)]^2}, \\ \overline{(\cos\theta_{12})}_{\text{triplet}} &= -\frac{2}{3}\frac{{}^3\psi_{00:10}(1, 2)\,{}^3\psi_{00:10}(2, 1)}{[{}^3\psi_{00:10}(1, 2)]^2+[{}^3\psi_{00:10}(2, 1)]^2}. \end{aligned}\right\} \quad . \quad (5.2)$$

These functions are numerically greatest for $r_1=r_2$, when

$$\overline{(\cos\theta_{12})}_{\text{singlet}}=+\tfrac{1}{3}, \qquad \overline{(\cos\theta_{12})}_{\text{triplet}}=-\tfrac{1}{3}. \quad . \quad . \quad . \quad (5.3)$$

These correspond to values of 70·5° and 109·5° for θ_{12}.

The conclusion to be drawn, therefore, is that, according to the first term of expansion, angular correlation is most important when $r_1=r_2$ and then it tends to bring electrons together in the ^{1}P state and to keep them apart in the ^{3}P state. This angular correlation arises *because of the exclusion principle* and is much larger than the corresponding correlation due to the electrostatic effect. (It was shown in Part I that the greatest angular correlation in the ground state of helium is $\overline{\cos\theta_{12}}=-0{\cdot}1073$.) The observed splitting between ^{1}P° and ^{3}P° states can be largely attributed to this type of correlation.

It should be noted that in the above discussion no explicit forms have been assumed for the radial functions. The main details of radial

correlation will be included in the radial function $\psi_{00:10}$, while functions corresponding to higher configurations, such as (pd) will refine the details of the angular correlation. To illustrate the effect of higher configurations on the angular correlation, we shall describe some calculations on excited states of beryllium in the next section.

§ 6. Illustrative Numerical Results for Excited States of the Beryllium Atom

The type of correlation discussed above is likely to be important in P° and $^1P^\circ$ states of atoms which have two electrons outside a closed shell. The simplest examples are the states of beryllium usually represented by configurations $(1s)^2(2s)(2p)^3P^\circ$ and $(1s)^2(2s)(2p)^1P^\circ$. The effect of the inner shell can be represented to a good degree of accuracy by a smoothed potential field $V(r)$.

If the inner shell electrons are described by 1s orbitals ψ_{1s}, then

$$V(r_1)=-\frac{4}{r_1}+2\int \overline{\psi}_{1s}(r_2)\frac{1}{r_{12}}\psi_{1s}(r_2)\,d\tau_2. \quad . \quad . \quad . \quad . \quad (6.1)$$

Analytical approximations to $\psi_{00:10}(1, 2)$, $\psi_{10:20}(1, 2)$ and ψ_{1s} were taken as follows:

$$\left.\begin{aligned}\psi_{00:10}(1, 2)&=N_{00:10}\{r_1\exp(-\mu r_1)-3A/\mu\exp(-\mu b r_1)\}r_2\exp(-\mu c r_2),\\ \psi_{10:20}(1, 2)&=N_{10:20}r_1\exp(-\mu' r_1)r_2{}^2\exp(-\mu'' r_2),\\ \psi_{1s}(r)&=(\mu^3a^3/\pi)^{1/2}\exp(-\mu a r),\end{aligned}\right\} \quad . \quad . \quad . \quad (6.2)$$

where μ, a, b, c, μ' and μ'' are constants to be determined by the variation method and A is chosen so that $\{r_1\exp(-\mu r_1)-3A/\mu\exp(-\mu b r_1)\}$ is orthogonal to $\psi_{1s}(r_1)$. $N_{00:10}$ and $N_{00:20}$ are constants whose values are also determined by the variation method.

The simplest approximation to the wave-function for the two outer electrons is to use only $\zeta_{01}(1, 2)$ in the expansion (3.1). This corresponds to using the (sp) configuration alone. Details of the angular correlation are modified if $\zeta_{12}(1, 2)$ is also included, corresponding to the (pd) configuration. In these calculations the values of μ, a, b, c were taken from the work of Morse, Young and Haurwitz (1935), these values subsequently being kept constant while μ' and μ'' were varied when $\zeta_{12}(1, 2)$ was included. Optimum values of μ' and μ'' were found to be 1·0 and 0·9 respectively. The energies calculated for the singlet and triplet states of the two outer electrons are given in table 1. The observed splitting between the lowest ^1P and ^3P-states of beryllium is 0·0940.

The most striking feature about the results summarized in table 1 is the fact that the (pd) configuration lowers the singlet energy very much more than the triplet. The reason for this becomes clearer if we evaluate the angular correlation as measured by the value of $\cos\theta_{12}$ averaged over the entire configuration space of both electrons. These values are shown together with the corresponding angles θ_{12} in table 2.

These results show how the angular distribution of the electrons has been modified by the inclusion of the (pd) configuration. In the triplet state the effect of the antisymmetry principle in the first approximation is to keep the electrons on opposite sides of the nucleus. The effect of the electrostatic repulsion between the electrons is then small and corresponds to a slight accentuation of this separation. For the singlet state, however, the two effects are opposed to one another and the

Table 1. Energies of Outer Electrons in Excited P-states of Beryllium (units of e^2/a_0)

Configurations	Energy of triplet state	Energy of singlet state	Singlet–triplet splitting
(sp) only	−1·1248	−0·9771	0·1477
(sp) and (pd)	−1·1276	−1·0014	0·1262
Improvement	0·0028	0·0243	0·0215

Table 2. Angular Correlation in Excited P-states of Beryllium

Configurations	Triplet	Singlet
(sp) only	$\overline{\cos\theta_{12}}=-0{\cdot}3195$, $\theta_{12}=108{\cdot}5°$	$\overline{\cos\theta_{12}}=0{\cdot}3164$, $\theta_{12}=71{\cdot}5°$
(sp) and (pd)	$\overline{\cos\theta_{12}}=-0{\cdot}3584$, $\theta_{12}=111{\cdot}0°$	$\overline{\cos\theta_{12}}=0{\cdot}1713$, $\theta_{12}=80{\cdot}0°$

tendency of the antisymmetry principle to bring the electrons together is strongly resisted by the electrostatic repulsion. This is the reason why higher configurations have a larger effect on the singlet states than on the triplet. It should be noted that on account of this, the calculated singlet-triplet splitting is reduced by inclusion of the (pd) configuration and brought nearer to the observed value.

The authors are indebted to Professor Sir John Lennard-Jones for suggesting this work and for valuable advice.

References

Lennard-Jones, Sir J., and Pople, J. A., 1950, *Proc. Roy. Soc.* A, **202**, 166 ; 1952, *Phil. Mag.*, **43**, 581.

Morse, P. M., Young, L. A., and Haurwitz, E. S., 1935, *Phys. Rev.*, **48**, 948.

CXI. *Two Dimensional Diffusion Phenomena in Crystal Growth from Solution*

By F. S. A. Sultan
Royal Holloway College, University of London*

[Received August 19, 1951]

Abstract

Multiple-beam white light fringes of equal chromatic order are used for the study of the growth from solution of sodium chlorate. They are sharper and much more informative than monochromatic Fizeau fringes, and have proved to be very sensitive for the measurement of variation of concentration.

The experimental results are found to be in agreement with the assumption of the existence of the quasi-stationary state theory introduced by Rieck and further developed recently by Frank.

According to this theory, the radial gradient of concentration is analogous to a static potential field multiplied by a Gaussian cut off factor. The law relating the concentration to the radius is found to be of logarithmic form near the crystal and exponential at larger distances.

§1. Introduction

For a crystal growing in a supersaturated solution, there is a diminution of concentration near the crystal boundary due to material deposited on its surfaces. A gradient of concentration is established which causes diffusion of solute to take place.

The growth of sodium chlorate crystals from solution, effectively in two dimensions, has been studied by Berg (1937) and Humphreys-Owen (1948).

They used multiple beam monochromatic-light fringes of equal optical path characteristic of the wedge. In the region where the crystal grows, a distortion in the straight line fringes characteristic of a wedge takes place. Each fringe follows a line of equal μh, where μ is the refractive index at a point, and h the height of the wedge at this point.

Berg (1937) measured the variation of refractive index $(\mu-\mu_\infty)$ at a point, in terms of a fraction of an order separation Δn. The value of h was measured by focusing on the top and the lower surface of the crystal and μ was determined by using the relationship $[(\mu-\mu_\infty)=\Delta n\lambda/h]$, where μ_∞ is the refractive index of the mother liquid.

* Communicated by Professor S. Tolansky.

Humphreys-Owen (1948) inferred the value of h from certain measurements involving a determination of the distance of a given point to the ' pole ' of the wedge on the stage of the microscope. The method neglects the optical separation at the edge of the wedge which can be considerable in an interferometer containing aqueous solution. The elaborate method used for measuring and drawing the contours of equal concentration around the crystal, required a large number of points in the field. In order to obtain a reasonable number of fringes near the crystal, the wedge angle, and consequently h, had to be large. This introduced the possibility of convection currents occurring at right angles to the direction of growth because of the large gradient of concentration at the face of the growing new phase. Under these conditions, convective transport is likely to be large compared with diffusive flux in the plane of the crystal (Frank 1949).

On reducing the wedge angle of the cell, the Fizeau fringes become more dispersed, and the information which can be obtained from the system decreases.

These difficulties are overcome by using white light fringes of equal chromatic order (Tolansky 1948). They are further preferable in that they also permit a high precision in measuring small variations of refractive index.

§2. Experimental Technique

A crystal of sodium chlorate is allowed to grow spontaneously from solution between two aluminized optical flats.

The Fizeau fringes produced do not easily permit the detection of small changes of μ which occur at large distances from the crystal, whereas with the white light fringes of equal chromatic order, one can accurately observe small variations of μ and consequently test the theoretical predictions over a wider range. In these experiments the Fizeau fringes (λ 5461Å) can be projected on to the slit of a spectrograph or a grating, or alternatively white light can be employed to form fringes of equal chromatic order.

To simplify the method of calculation, the stage on which the interferometer is lying is turned round to make the edge of the wedge parallel to the slit. The straight part of the Fizeau fringe pattern distant from the crystal will then be parallel to the slit. The mercury arc is replaced by a point-o-lite lamp, and the slit is adjusted to give sharp fringes. The system of fringes in the spectral plane is focussed on the photographic plate of the spectrograph.

The region then under investigation is a straight narrow region selected by the spectrograph slit, and due to the concentration gradient around the growing crystal, the concentration and therefore the refractive index will vary along this (region) line. Since each member of the system of fringes is a line of equal $\mu h/\lambda$, the fringes appear to bulge towards the shorter wave length end of the spectrum. The fringes resemble

gaussian curves and can be considered as representing the concentration distribution along the line selected by the slit. The separation of the fringes depends only on the value of the interferometer gap h and the dispersion of the spectrograph. Several photographs of this system were taken at successive intervals of time during the growth, and repeated for different distances from the crystal edges, as shown in Plate LXXI.

§3. Theoretical Treatment

In order to interpret the experimental results in terms of diffusion theory, it is necessary to solve the differential equation under the appropriate boundary conditions. These determine whether a stationary or a quasi-stationary state will occur.

The diffusion equation :

$$D\nabla^2\phi=-\frac{\partial\phi}{\partial t}, \quad . \quad . \quad . \quad . \quad . \quad . \quad . \quad . \quad (1)$$

reduces to $D\nabla^2\phi=0$ in a stationary state, where D is the diffusivity, and ϕ is the concentration at time t.

Considering the flow to be radial, the amount of solute crossing a circumference of radius r is constant and equal to $2\pi r D(d\phi/dr)$. Imposing as boundary conditions that the concentration $\phi\rightarrow\phi_\infty$ as r reaches a certain value r_∞, the diffusion potential at a point in the diffusion field is found to be a logarithmic function of the distance r measured from the centre of the crystal. It will be seen below that this is valid for small values of r.

The assumption that a stationary state exists during crystal growth is not quite true, since the faces of the crystal are advancing with time, the source of solute is not infinite and the boundary defined by r_∞ is liable to move under the effect of diffusion. Also we have to consider that sodium chlorate is a very soluble substance and it is growing from a considerably supersaturated solution.

In a quasi-stationary state it is considered that the growth of a new phase has cylindrical symmetry and that it is controlled by radial diffusion of solute (Rieck 1924; Frank 1950). The particular solution of the diffusion equation assumes that the diffusion potential ϕ round the growing phase at distance r and time t is a function of a dimensionless parameter defined by $r/\sqrt{(Dt)}$, where D is the diffusivity measured in $cm^2\ sec^{-1}$.

$$\phi(r,\,t)=\phi[r/\sqrt{(Dt)}]. \quad . \quad . \quad . \quad . \quad . \quad . \quad . \quad (2)$$

This follows from the fact that migration of particles follow a Boltzmann law (1894) according to which $r/\sqrt{t}$ is a constant for a given concentration.

Under these assumptions, introducing $s=r\,D^{-\frac{1}{2}}t^{-\frac{1}{2}}$ a dimensionless reduced radius, and substituting in eqn. (1), it is found that :

$$s\frac{d\phi}{ds}=-A\exp\left(-\frac{s^2}{4}\right). \quad . \quad . \quad . \quad . \quad . \quad . \quad . \quad (3)$$

A is the integrating constant defined by the $\lim_{s\to 0} s\,(d\phi/ds)$ and represents the strength of the sink. Its value could be found from the rate of growth of the crystal and the amount of flux arriving at its faces.

Integrating (3) between $s^2/4$ and ∞,

$$\phi-\phi_\infty=-\tfrac{1}{2}AEi(-s^2/4). \quad . \quad . \quad . \quad . \quad . \quad . \quad (4)$$

A square crystal of side $2a$ growing uniformly is taken to be equivalent to a cylindrical crystal of radius $R=ka$ and reduced radius $S=R/\sqrt{(Dt)}$.

The value of k will be discussed later.

A is determined by equating the amount of flux per unit time arriving at a cylinder of reduced radius S and thickness h to the rate of growth of the crystal.

Since the rate of growth in the region around the crystal is measured by the amount (q) of diffusing entity expelled per unit volume of solute deposited at the crystal faces, it follows that :

$$-2\pi ShD\frac{d\phi}{ds}_{s=S}=q\frac{d}{dt}\pi R^2h.$$

From (4)

$$2\pi hDA\exp(-S^2/4)=q\pi S^2Dh. \quad . \quad . \quad . \quad . \quad . \quad (5)$$

$$A=\tfrac{1}{2}qS^2\exp(S^2/4). \quad . \quad . \quad . \quad . \quad . \quad . \quad . \quad (6)$$

§4. Method of Calculation

The dispersion of the fringes on the spectral plane gives a measure of the optical path of the light in the wedge.

If we consider that μ_∞ is the refractive index corresponding to a concentration ϕ_∞ at a large distance from the crystal, the optical path in the solution is :

$$\mu_\infty h=\frac{1}{2\Delta\nu_1}$$

where $\Delta\nu_1$ is the wave number separation of two successive orders at wave lengths λ_1 and λ_2. A similar formula :

$$h=\frac{1}{2\Delta\nu_2},$$

holds for the air gap of equal h in the vicinity of the solution, and thus the value of μ_∞ can be determined.

An alternative method is to have the slit running along the crystal and the solution, in which case we have for the crystal :

$$\mu_c h=\frac{1}{2\Delta\nu_c}.$$

This method can provide accurate values of μ and h.

A typical white light fringe of order n is shown as $\mathrm{YX\overline{Y}}$ in fig. 1, occupying the region between λ_0 and $\bar{\lambda}$; $\mu h/\lambda$ is constant along that fringe. Since the edge of the interferometer is parallel to the spectrograph slit, i.e., the interferometer gap h is constant, the refractive index

at a point on the slit is proportional to its position on the wave length scale of the spectrograph.

Viz : $\mu_1/\lambda_1=\mu_2/\lambda_2=\ldots\mu_\infty/\lambda_\infty=$constant, where μ_∞ is the refractive index over the straight part of the fringe at λ_0.

The variation in refractive index $(\mu-\mu_\infty)$ is represented by the co-ordinates x_1, x_2, . . . which consequently are measures of concentration

Fig. 1

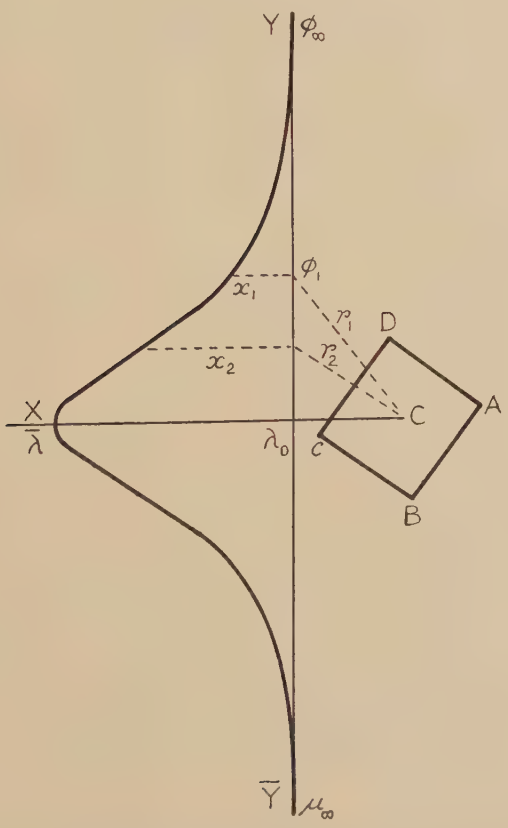

Illustration of the method of calculating the variations of concentration $(\phi-\phi_\infty)$ along the section selected by the slit and the position of this section with respect to the crystal.

differences $(\phi_1-\phi_\infty)$, $(\phi_2-\phi_\infty)$, . . ., along the line cutting the diffusion field around the crystal and selected by the slit.

In fig. 1 Y $\bar{Y}$ represents the line in the plane of the crystal selected by the slit. Let ϕ_1, ϕ_2, . . . be the concentration at points on the line Y $\bar{Y}$ defined by the radius vectors r_1, r_2, . . . drawn from the centre C at a given time.

In fig. 2 $\ln r \,.\, t^{-\frac{1}{2}}$ as determined experimentally is plotted against $(\phi-\phi_\infty)$. It shows the decrease of concentration as a function of radius

round the growing crystal; the radius of the crystal is proportional to the square root of time. This curve is found to fit with that obtained from eqn. (4) where $\ln s$ is plotted versus the exponential integral of $s^2/4$ derived from the tables of Jahnke and Emde (1943). The curve represents the growth-diffusion function of cylindrical symmetry for A equal to unity. The concentration of the solution is measured in terms of volume fraction of solvent (cm^3 water/cm^3 solution). The strength of the sink A is evaluated by comparing the slopes of the linear portions of the curves. Since $r \cdot t^{-\frac{1}{2}} = s \cdot D^{-\frac{1}{2}}$, the difference between the abscissa of equal ordinates of the two curves counts for the diffusivity D.

Fig. 2

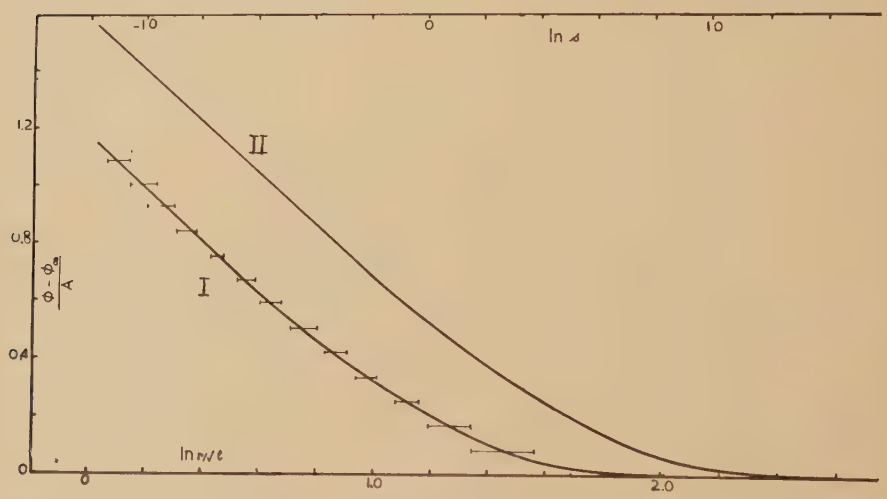

Curve (I) shows the concentration round the crystal as a function of the distance from the centre of the crystal as determined experimentally. Whilst Curve (II) illustrates the theoretical relationship between $\ln s$ and $Ei[-(s^2/4)]$ for A equal to unity.

§5. Results and Discussion

The crystal grows as a rectangle, the sides AB and DA advancing at equal rates, as do BC and CD. These rates are proportional to the value of a^2/t.

face	a^2/t cm^2 sec^{-1}
AB, DA	$0{\cdot}054 \times 10^{-5}$
BC, CD	$0{\cdot}045 \times 10^{-5}$

The rate of growth of the crystal as defined by $a_1 a_2/t$ is equal to $0{\cdot}0495\ 10^{-5}$ cm^2 sec^{-1}. The diffusivity $D = 0{\cdot}438 \times 10^{-5}$ cm^2 sec^{-1} and the integrating constant A as deduced from the experimental curve is 0·0457.

In order to apply the theoretical formulae (which implies cylindrical symmetry) to the growth of a polygonal crystal, it is necessary to define an equivalent radius. This can be done in several ways. The following methods were tried.

(*a*) The average radius of the square of side $2a$

$$\frac{4}{\pi}\int_0^{\pi/4} a \sec\theta \, d\theta$$

which gives an equivalent radius ($R=1{\cdot}122\ a$).

(*b*) The radius of the circle which has the same area as that of the rectangle. If $2a_1$, $2a_2$ are its sides $R=\sqrt{(4a_1\, a_2/\pi)}$

$$R=(1{\cdot}128\ a).$$

(*c*) A definition based on the fact that the concentration, measured in volume fraction of solvent, within the crystal is equal to zero. If $\bar{\phi}$ is the mean value of concentration within a circle corresponding to r, then

$$\phi_\infty-\bar{\phi}=\tfrac{1}{2}A\left[Ei\left(-\frac{r^2}{4Dt}\right)+\frac{4Dt}{r^2}\exp\left(-\frac{r^2}{4Dt}\right)\right].$$

The equivalent radius is the value of r at which $\bar{\phi}$ is equal to zero :

$$\frac{2\phi_\infty}{A}=Ei(-x)+x^{-1}\,e^{-x}.$$

Solving the equation for x using the experimental value A in $R^2=4Dt\,x$, gives $R=1{\cdot}04\ a$.

(*d*) If saturation is found at the crystal faces, this should be at the point of lowest concentration, which is the face centre.

The value of r for which ϕ is equal to (ϕ—saturation), is that of the circle which touches the crystal internally. So R could be defined as that value at which the concentration ϕ extrapolated has the saturation value. This gives $R=0{\cdot}78\ a$. This factor being less than unity could be explained by the fact that the lowest point of concentration is not that of saturation.

The definitions (*c*), (*d*) were proposed to the author in a private communication by Dr. F. C. Frank.

We have, therefore, reached the following values for the equivalent radius R.

(*a*) $R=1{\cdot}122\ a$.
(*b*) $R=1{\cdot}128\ a$.
(*c*) $R=1{\cdot}04\ a$.
(*d*) $R=0{\cdot}78\ a$.

The result from (*d*) is neglected at the moment, because a high degree of experimental accuracy must be present to give the result a physical meaning.

The determination of R in (*c*) involves as experimental data the concentration ϕ, the diffusivity D and the value of A. The lack of agreement between different reference tables may account for an error

of about 5% in R. This gives $R=1{\cdot}10\,a$ in (*c*) and so the values obtained from the three definitions could be in agreement within a few per cent.

The volume rate of growth expressed by $\pi S^2 hD$ can be calculated from R and a^2/t taken as the average rate of growth in the experiment. We then get from

(*a*) $1{\cdot}22\times10^{-8}$ cm^3 sec^{-1},
(*b*) $1{\cdot}24\times10^{-8}$ cm^3 sec^{-1},
(*c*) $1{\cdot}08\ 10^{-8}$ for $R=1{\cdot}04\,a$,

and from (*c*) using $R=1{\cdot}10$ we get $1{\cdot}19\times10^{-8}$ which is in agreement within the experimental error with the volume rate of growth as derived directly from the experiment

$$\frac{4a_1a_2}{t}=1{\cdot}25\times10^{-8}\ \text{cm}^3\ \text{sec}^{-1}.$$

The results are thus seen to verify Frank's theoretical treatment of the two dimensional diffusion problem in crystal growth from solution ; taking the diffusion field to have a cylindrical symmetry, and for a given concentration at a point in the diffusion field, the radius vector is proportional to the square root of the time (eqn. (2)). The radial gradient $d\phi/ds$ is similar to the static potential field multiplied by a factor $\exp -(r^2/4Dt)$, where $2D^{-1/2}t^{-1/2}$ is its characteristic radius (eqn. (3)).

Acknowledgments

I wish to express my gratitude to Professor S. Tolansky for his constant advice and encouragement. I am very grateful to Dr. F. C. Frank for his helpful suggestions and guidance. Thanks are also due to Dr. K. Singer and Mr. H. Rahbek for useful discussions.

References

Berg, W. F., 1938, *Proc. Roy. Soc.* A, **164,** 79.
Boltzmann, L., 1894, *Ann. Physik,* **53,** 959.
Frank, F. C., 1949, *Disc. Faraday Soc.* No. 5 (*Crystal Growth*), p. 189 ; 1950, *Proc. Roy. Soc.* A, **201,** 586.
Humphreys-Owen, S. P. F., 1949, *Proc. Roy. Soc.* A, **197,** 218.
Jahnke, E., and Emde, F., 1943, *Tables of Functions* (Dover reprint), p. 6.
Rieck, R., 1924, see Huber, 1939, *Z. angew. Math. Mech.*, **19,** 1.
Tolansky, S., 1948, *Multiple Beam Interferometry of Surfaces and Thin Films* (Oxford : University Press).

CXII. *Current-Noise in Semi-Conductors : A Re-examination of Bernamont's Data*

By D. A. Bell
Electrical Engineering Department, University of Birmingham*

[Received August 11, 1952]

Summary

In 1937 Bernamont published the results of his experiments showing that the current-noise in certain thin metal films varied approximately as the inverse of the frequency over the range 96 to 162 000 c/s. The text of his paper shows, however, that he omitted to allow for the presence of Johnson noise when the steady current was reduced to zero. After correcting for this, and making another adjustment necessary to make the results physically possible, the noise from his resistor ' B ' shows a close inverse-frequency law for all current densities, whereas Bernamont found an inverse power of the frequency varying between 0·883 and 0·983 for different values of current.

When a steady current flows through a semi-conductor, the fluctuation voltage at the terminals of the conductor rises substantially above the Johnson-noise level, and the additional noise is variously known as ' excess noise ' or ' current noise '. There has been some diversity in the recorded experimental results and in the hypotheses proposed to explain them, but the simple law which approximates to the experimental evidence may be written

$$\overline{e_\nu^2}=(xI^2/\nu)\Delta\nu, \quad . \quad . \quad . \quad . \quad . \quad . \quad . \quad . \quad (1)$$

where $\overline{e_\nu^2}$ is the mean square voltage at frequency ν, I the steady current causing the additional noise, $\Delta\nu$ the bandwidth ($\Delta\nu \ll \nu$) and x a constant of the particular resistor in question.

The classic paper on the subject is one by Bernamont (1937) which is notable both for the internal consistency of the sets of measurements and for the wide range of frequency covered, namely about $3\frac{1}{2}$ decades. (Bernamont's data relate to thin films of metal, but the reasons for regarding these as semi-conductors are given in the Appendix.) There are, however, some small anomalies in this paper, the adjustment of which makes Bernamont's results even more outstanding as a set of consistent data. In discussing his resistor ' B ' (a commercial product, consisting of a tungsten film on a glass rod and having a resistance of 190 000 ohms), he stated that at high frequencies the current-noise increased less rapidly

---

* Communicated by the Author.

than as the square of the steady current, and that the inverse power of the frequency involved was less than unity by different amounts for different values of mean current. Now the type of curve shown for e_ν^2 versus I^2 at high frequency is sketched in the inset to fig. 1, and the curve appeared not to extrapolate back to the origin. In the author's experiments such curves always have extrapolated back to the origin, so that the general form of Bernamont's curves suggested a false zero to the measurement. Re-examination of the text of the paper showed that the zero-point of the noise scale was established by " replacing the

Fig. 1

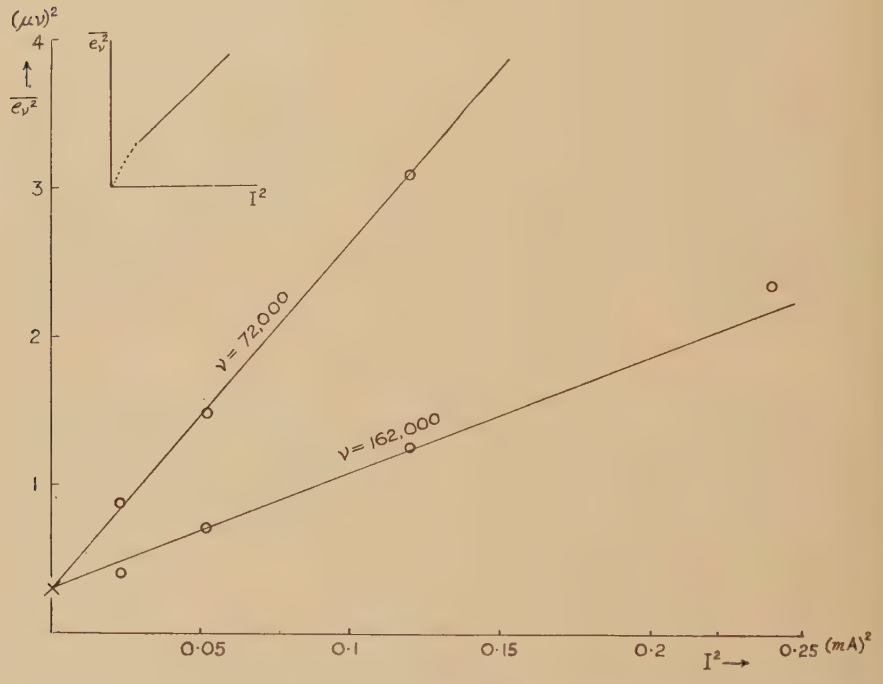

battery by a short-circuit ", the resistor under examination being thus left connected to the input of the amplifier. In this condition the input to the amplifier would not be zero, but would be the normal Johnson noise appropriate to the resistance in question, thus giving a false zero to Bernamont's noise scale. (This does not materially affect the results obtained on his resistor ' A ' in which the current-noise was throughout very much greater than Johnson noise.) One then finds that the high-frequency values of noise output from resistor ' B ' (Bernamont's Table III) are less than the Johnson noise ; and since the description of the method of measurement shows that the noise output was the sum of Johnson noise and current-noise, this is clearly impossible. (There are both theoretical and experimental grounds for believing that in the absence of a steady current a semi-conductor generates precisely the

normal Johnson noise.) But if it be assumed that a factor of 10 has been lost somewhere in the calculation of absolute values of squared microvolts per 100 c/s from galvanometer deflections, the two curves of $\overline{e_\nu^2}$ versus I^2 for the two highest frequencies are reasonably convergent on the calculated value of Johnson noise which is marked with a cross in fig. 1. Bernamont's data in his Table III have therefore been adjusted by multiplying by 10 and subtracting the calculated Johnson noise of 0·312 $(\mu V)^2$ for 190 000 Ω and a bandwidth of 100 c/s, as shown in the table. The fluctuation voltages for different currents can be made comparable by dividing each value of $\overline{e_\nu^2}$ by the value of I^2 and the values of $\overline{e_\nu^2}/I^2$ are plotted against ν in fig. 2. The full line through the points ' B ' has a slope of unity, while the dotted line has a slope of 0·95. It is evident that the slope is at least within 5% of unity for all values of steady current, and may well be exactly unity, whereas Bernamont found from his results in their original form slopes ranging from $0{\cdot}883 \pm 0{\cdot}020$ for the smallest current to $0{\cdot}983 \pm 0{\cdot}008$ for the largest.

Table. Adjustment of data given in Bernamont's Table III, referring to his resistor ' B '. Bernamont's original figures are shown for mean-square fluctuation voltage in 100 c/s bandwidth at various frequencies and values of d.c., together with the adjusted values in italics.

d.c., mA	0·151		0·228		0·347		0·490	
Frequency								
96	36·6	*366*	76·7	*767*	180·2	*1802*	354	*3540*
256	14·9	*149*	30·3	*303*	68·5	*685*	135·1	*1351*
1,024	3·86	*38·3*	8·15	*81·2*	18·4	*184*	35·1	*351*
4,096	1·105	*10·74*	2·26	*22·3*	4·92	*48·9*	9·52	*94·9*
18,000	0·252	*2·21*	0·514	*4·83*	1·10	*10·7*	2·09	*20·6*
72,000	0·087	*0·56*	0·148	*1·17*	0·307	*2·76*	0·550	*5·19*
162,000	0·040	*0·009*	0·070	*0·39*	0·124	*0·93*	0·232	*2·01*

For his resistor ' C ' (a cathode-sputtered and annealed platinum film) Bernamont reported a slope against frequency of 1·062 within limits of 12 parts in 1 000, and one would like to see this small difference from unity also eliminated. But in this case the adjustment for Johnson noise is very small and, moreover, is in the wrong sense. The plot of $\overline{e_\nu^2}/I^2$ versus ν is shown at ' C ' in fig. 2, where the full line has a slope of unity and the dotted line a slope of 1·06. It seems definite that in this case the bulk of the evidence is not consistent with a slope of unity. Yet the essential semi-conductor phenomenon may be inversely proportional to the exact first power of the frequency for the following reason. All experimenters on semi-conductor noise have reported that when the steady current is increased beyond a certain point there is a new phenomenon which is characterized by (*a*) noise increasing less rapidly than

the square of the steady current and (*b*) isolated peaks of low-frequency noise which appear as crackles or ' frying noises ' in an acoustic reproducer or as unsteadiness of reading on a galvanometer. But Bernamont did remark that his resistor ' C ' gave less steady galvanometer readings than ' B '. It is therefore possible that measurements on ' C ' included

Fig. 2

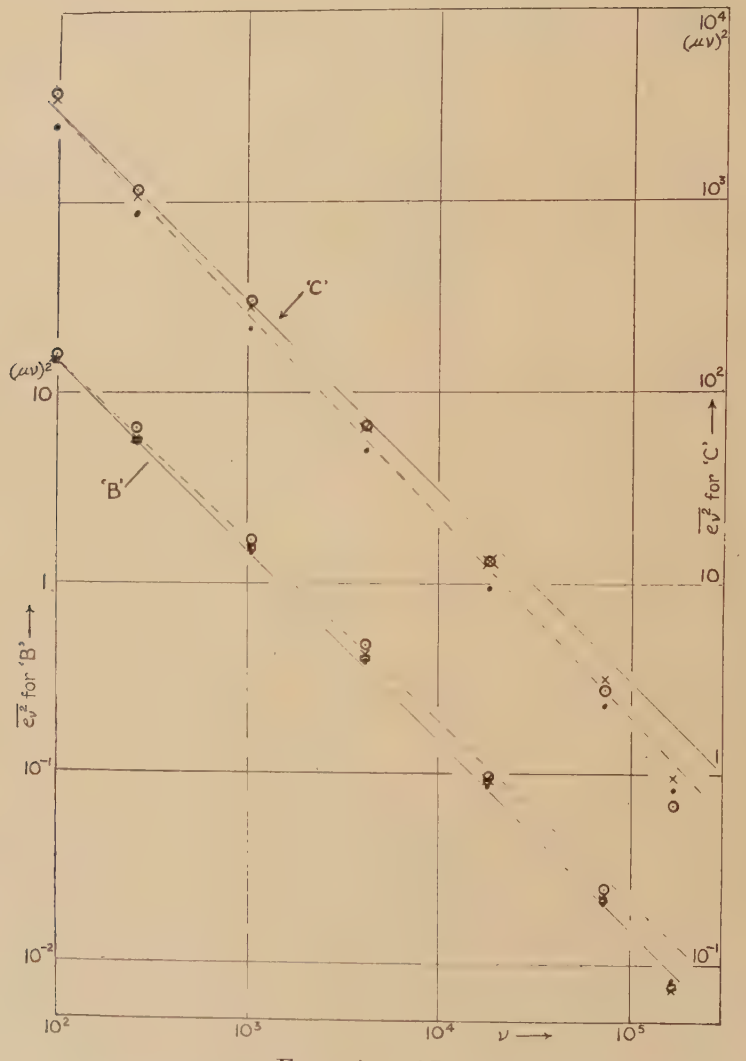

For resistor ' B '

○ I=0·151 mA ⊡ I=0·347 mA

× I=0·228 mA ● I=0·490 mA

For resistor ' C '

⊙ I=0·270 mA × I=0·409 mA

● I=0·647 mA

a small component of such noise (too small to be distinguishable on the loudspeaker) and that this has a frequency spectrum falling off more rapidly than $1/\nu$ thus slightly steepening the characteristic of the total noise.

The author has learned with regret that Bernamont died within a year or two of the publication of the paper in question. The possibility of Johnson noise being an appreciable correction would have been less obvious when the original paper was written, and the author hopes that this note will serve to maintain the status of Bernamont's paper as the classical work on current-noise.

Reference

Bernamont, J., 1937, *Annales de Physique*, **7**, 71.

APPENDIX

The Thin Film of Metal as a Semi-Conductor

It must first be remarked that one class of semi-conductors is ' ohmic ', i.e. there is a linear relationship between voltage and current. This class includes both thin films of metal and composite oxides such as those used in ' thermistors ' or the spinels used in ' Ferroxcube '. A semi-conductor may then be defined either as a material having a conductivity substantially less than that of a metal but substantially more than an insulator, or as a conductor in which the number of free charge-carriers is subject to statistical fluctuation. Bernamont specifically stated that the thin metal film which he prepared had a conductivity more than 100 times less than that deduced from its dimensions and the specific conductivity of the bulk metal, thus satisfying the first definition. The existence of current-noise is evidence that it satisfies the second definition. The reason for the semi-conducting behaviour of a very thin film of metal is not strictly relevant to the present note, but there are at least two suggestions. It is practically impossible to guarantee that a cathode-sputtered film is free from occluded gas, which might form barriers between the units of a ' mosaic '. Alternatively one might ask whether the normal ' conduction band ' of overlapping energy levels would be established in films of tungsten or platinum so thin as to be possibly two-dimensional arrays more nearly than three-dimensional.

CXIII. *Notices of New Books and Periodicals received*

Cosmology. By H. Bondi. [Pp. 179.] (Cambridge University Press.) Price 22*s.* 6*d.*

Although the author of this latest *Cambridge Monograph on Physics* takes the ' optimistic ' view that ' theoretical cosmology is on the way to becoming an interesting branch of physics ', he has taken considerable pains to present a reasonably fair account of the present state of the main conflicting theories and does not gloss over the profound differences of opinion which still abound. As part author of one of these theories he does not claim to be a dispassionate observer standing outside the fray, but clearly states both his own views and those of others. His book can therefore be recommended as a serious contribution to the literature of the subject as a whole by an active participant in the theoretical branch.

The book falls into three parts: (i) a discussion of the principles of cosmology, (ii) an account of the observational evidence, and (iii) descriptions of various theories. Of these the first suffers from being too compressed. The most satisfactory part is the last. The chapters devoted to Newtonian cosmology, relativistic cosmology, kinematic relativity, and the steady state theory are among the best in the book; that on the theories of Eddington, Dirac and Jordan is too scrappy to be of much value to anyone.

The second part is not very homogeneous. Both the chapter on ' Observations of Distant Nebulae ', with its useful appendix on the K-term in the red shift, and the following chapter on ' Astrophysical and Geophysical Data ' are apposite; but the other three chapters on ' The Background Light of the Sky ', ' The problem of Inertia ' and ' Microphysics and Cosmology ', particularly the first two, are on a much more abstract footing. The discussion of Olbers' classical paper (1826) on the cosmological significance of the darkness of the night sky is one of the liveliest in the book. Indeed, it is the most thorough account in English of this paper and of its implications which I have read. Despite Olbers' elementary empirical starting point the subject is, however, essentially *theoretical*, as is the problem of inertia discussed in the following chapter.

Notwithstanding these and other criticisms of detail, I consider that this is a book which every student of physical cosmology ought to read and that the author should be congratulated on presenting a difficult subject in so clear and stimulating a manner. G. J. W.

Theory of Superconductivity. By M. von Laue. Translated by Lothar Meyer and William Band. (New York: Academic Press Inc.) [Pp. 140.] Price $4.00.

This is a translation of the 1949 edition of the ' Theorie der Supraleitung '. It deals with von Laue's modifications and applications of the London phenomenological equations, and to some extent its title is misleading. In the interval since the completion of the translation three years ago, developments in the subject have been rapid. One wonders indeed why it was thought desirable to persist with the publication of a book which—to quote but two examples—does not mention the isotope effect and its implications, and dismisses the post-war work on the high frequency effect resistance of superconductors in a few lines. F. London's ' Superfluids ', Vol. 1, covers almost the same ground as the present book, but brings matters up-to-date and indicates the promising lines for future developments. E. M.

An Introduction to Modern Thermodynamical Principles. By A. R. Ubbelohde. (Oxford, 1952.) Second edition. [Pp. 185.] Price 21*s.*

This second edition of Ubbelohde's well known book has been modernized by including references to recent literature. Among the subjects which are new or treated in more detail than in the first edition are the thermodynamics of continuous phase transitions, statistical mechanics of the solid state, theories of melting, statistical mechanics of rubber elasticity, and a chapter on practical evaluation of thermodynamic functions. A. S.

The Initiation and Growth of Explosions in Liquids and Solids. By F. P. Bowden and A. D. Yoffe. Cambridge Monographs on Physics. [Pp.104+ 68 diagrams.] Price 22*s.* 6*d.* net.

During the last war, there was developed at the Tribophysics Division of the Australian Council for Scientific and Industrial Research, a new approach to the study of the initiation of explosion and detonation. This had, for a basis, investigations previously made by Dr. Bowden on the physical processes involved in the impact and friction of solids. This explosives research continued since at Cambridge is summarized in the present monograph.

One of the great merits of the researches is that they provide visual evidence of most of the phenomena, made possible by the elaboration of very interesting experimental techniques.

The work will prove invaluable to those who are engaged in investigations of explosives, not only through the new facts but also because the new techniques have applications over much of the explosives field. It has also a wider appeal, especially to those interested in chemical kinetics. W. E. G.

Detonation in Condensed Systems. By J. Taylor. [Pp. 186 with 10 plates.] (Oxford : Clarendon Press.) Price 25*s.* net.

Very considerable developments of the theory of detonation of solids with special reference to military explosives were made in this country and the U.S.A. during the war. In this book is given a concise and yet comprehensive account of the hydrodynamic theory of detonation including these recent developments. The author applies these theories to calculations of the velocities of detonation of industrial explosives and the results of these calculations are checked against experimental data supplied very largely by the author and his colleagues from the laboratories at Ardeer. The function of diluents in 'safety' explosives, the influence of density of loading, confinement and cartridge diameter are specially examined, from which it would appear that the design of explosives for industrial use has passed out of the empirical stage.

Although the practical aspects of such calculations are not ignored, the main intention of the book is academic and long range. Thus the nature of the processes occurring in the reaction zone are reviewed in the light of the theories of Eyring and of Kistiakowski, the Bowden theory of hot spots, and the theory of bulk initiation by shock waves. The phenomenon of two stable detonation velocities observed especially in liquid explosives is tentatively examined in the light of these theories.

Those interested in the design of explosives for industrial or military use cannot afford to be without this book. It has also considerable value for those interested in shock waves or in the kinetics of chemical reactions.

W. E. G.

The Theory of Relativity. By C. Møller. (Oxford : Clarendon Press.) [Pp. 386.] Price 35*s*.

This book contains a very thorough and detailed account of the well established part of the classical theory of relativity ; quantum theory is not mentioned, and cosmological problems are dealt with only briefly. The first chapter contains a useful historical account of the difficulties in classical physics that led to the formulation of the special theory of relativity ; the rest of the book is about equally divided between special relativity and general relativity. As well as the usual applications to dynamics and electromagnetic theory the book also discusses the effect of relativity on elastic theory, hydromechanics, and thermodynamics. The detailed treatment will add to the value of the book to many readers, since it contains material that is difficult to find elsewhere ; it makes it less suitable to the student who is only interested in general principles, since these are necessarily somewhat obscured. A. F. D.

[*The Editors do not hold themselves responsible for the views expressed by their correspondents.*]

Fig. 1

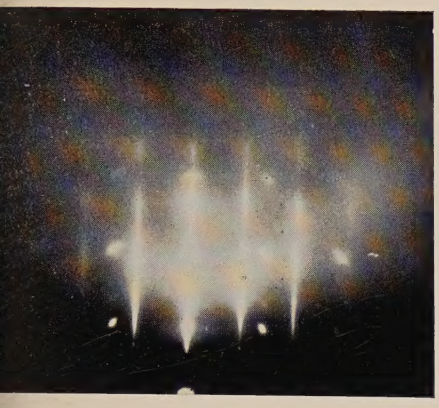

Fig. 2

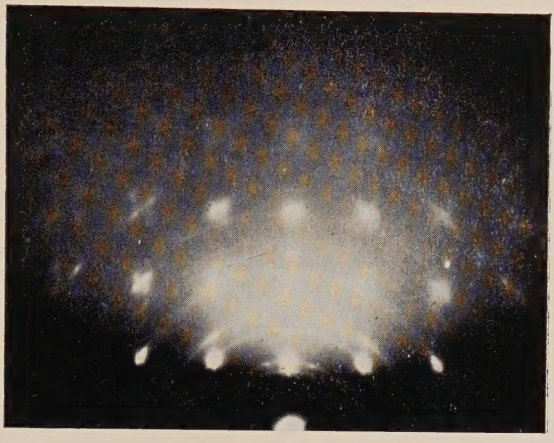

Fig. 3

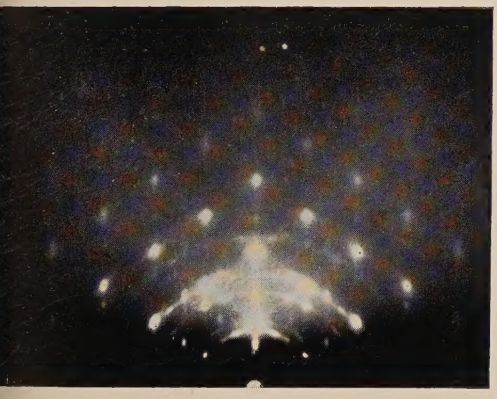

Fig. 6

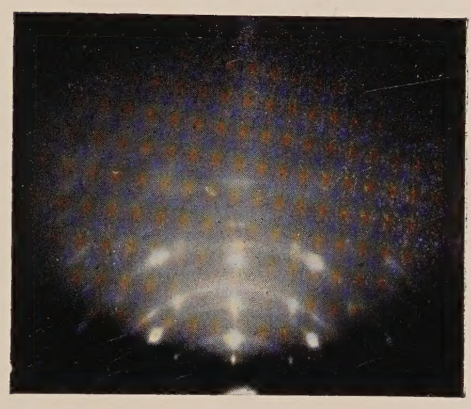

Fig. 7

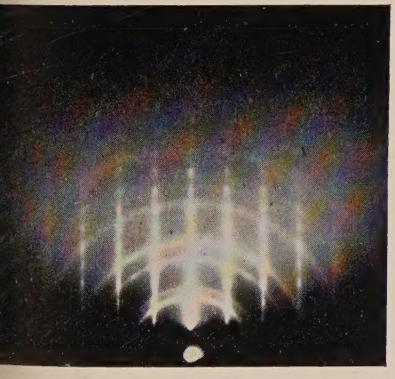

Fig. 8

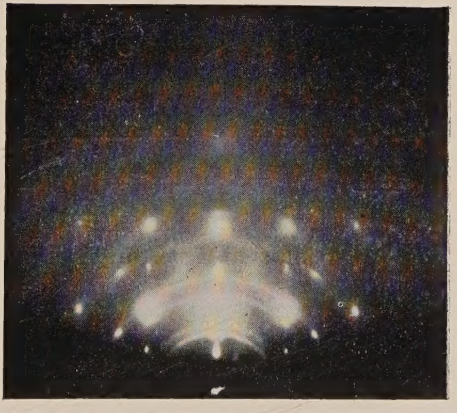

Fig. 2

← Wire diameter →

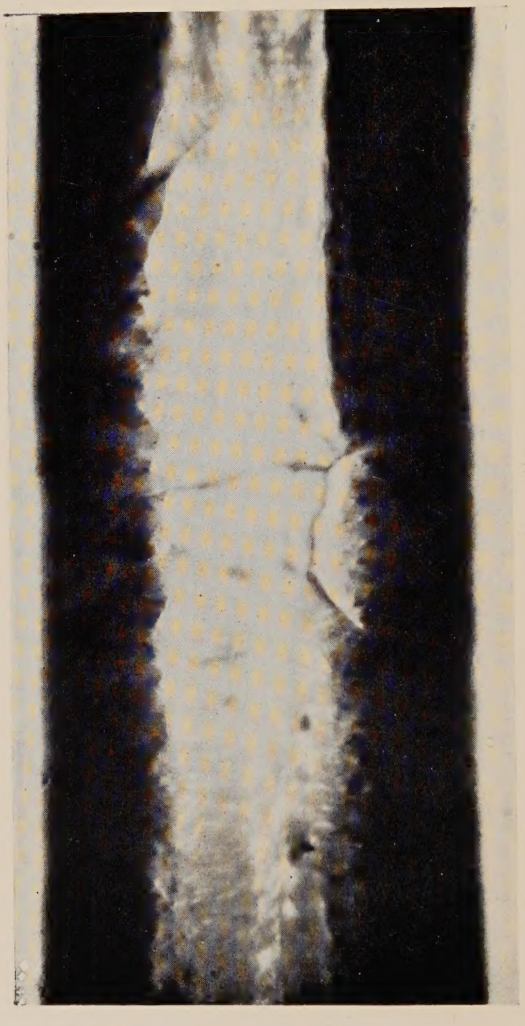

← Wire diameter →

×600

Kink shown at A in fig. 1.

Fig. 3

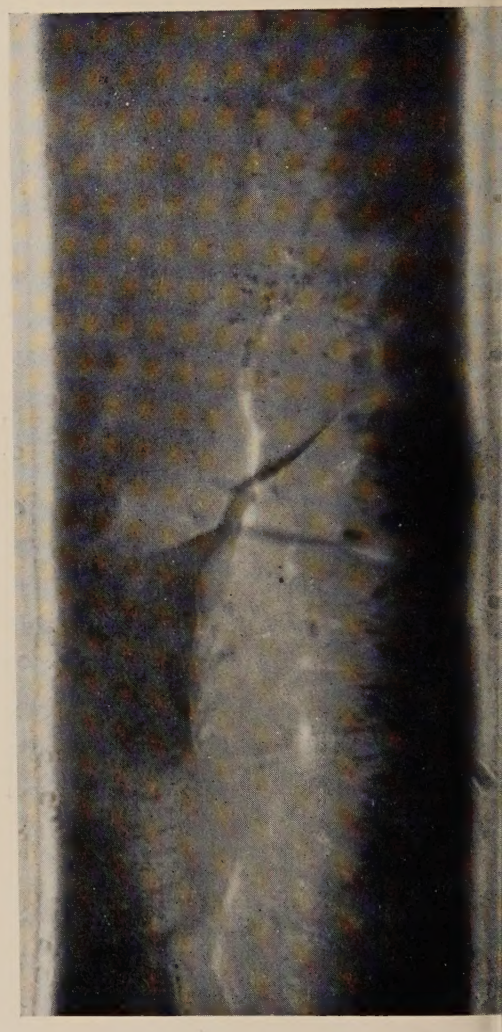

×550

After 336 hours at 920° c. Wire extendin

Fig. 4

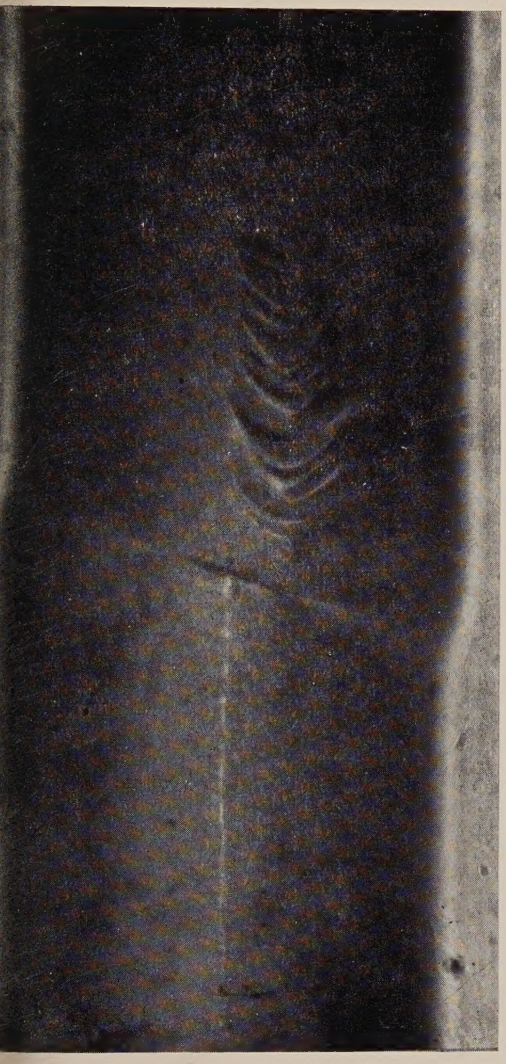

×600
fter 410 hours at 920° c. Wire shortening.

Fig. 7

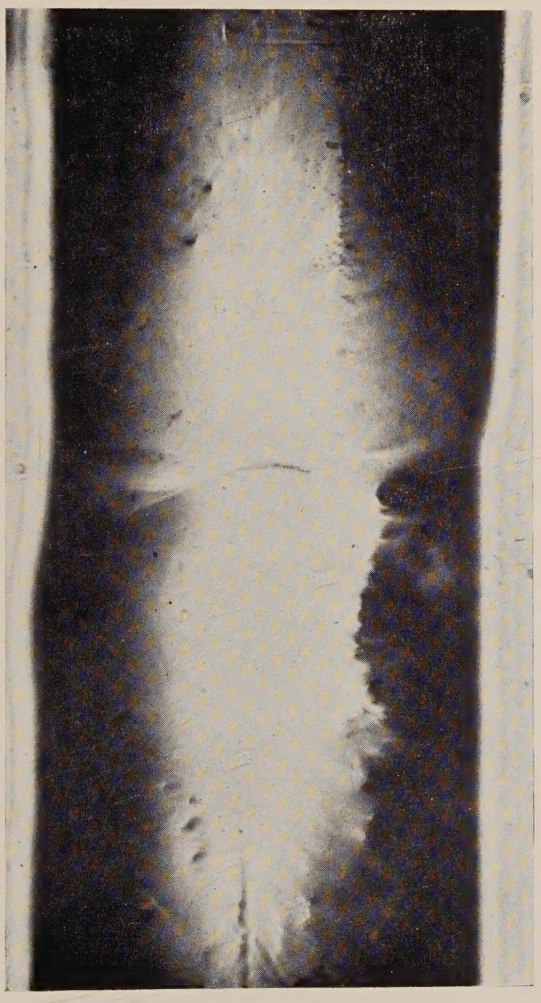

×600
Offset shown at A in fig. 6.

Fig. 3

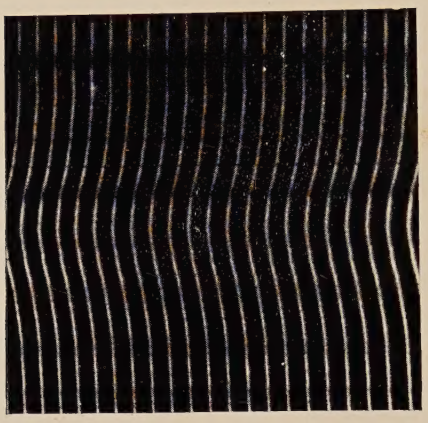

Fig. 4

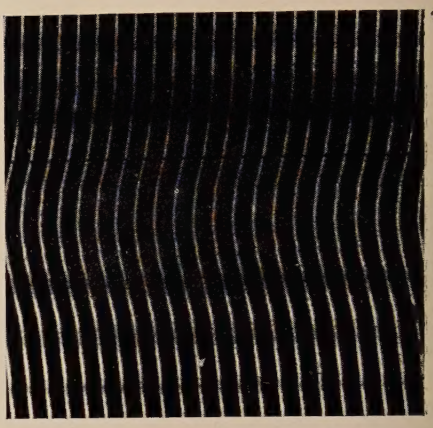

Fig. 5

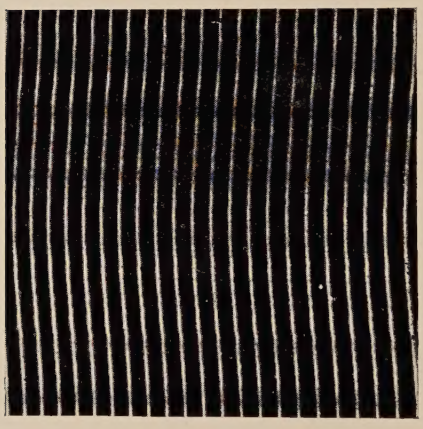

Fig. 6

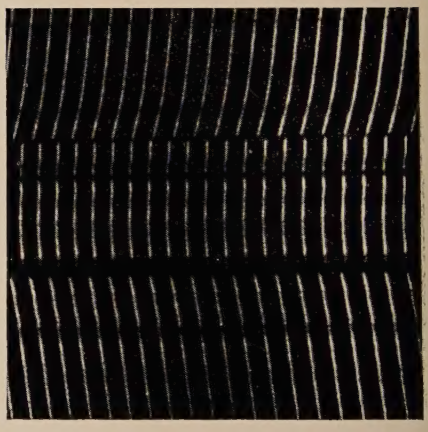

Fig. 7

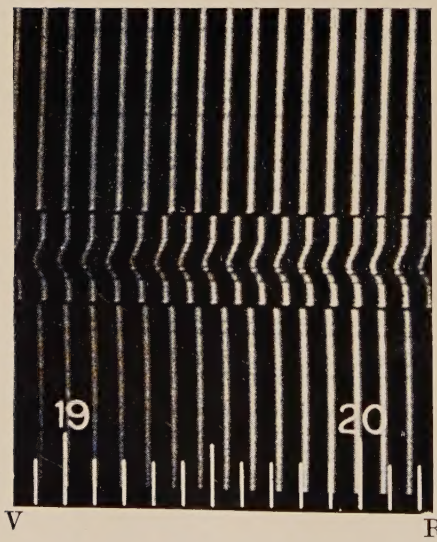

Figures 3, 4 and 5 show typical forms of white light fringes of equal chromatic order in the vicinity of the growing crystal. These fringes are always convex towards the shorter wave lengths. Figures 6 and 7 show interferograms for sections cutting the crystal. In fig. 7 the concentration is almost constant up to the boundary of the crystal.